2008-07-01

Development and Evaluation of a Sub-Grid Combustion Model for a Landscape Scale 3-D Wildland Fire Simulator

Michael M. Clark
Brigham Young University - Provo

DEVELOPMENT AND EVALUATION OF A SUB-GRID COMBUSTION MODEL FOR A LANDSCAPE SCALE 3-D WILDLAND FIRE SIMULATOR

by

Michael M. Clark

A dissertation submitted to the faculty of

Brigham Young University

in partial fulfillment of the requirements for the degree of

Doctor of Philosophy

Department of Chemical Engineering

Brigham Young University

August 2008

BRIGHAM YOUNG UNIVERSITY

GRADUATE COMMITTEE APPROVAL

of a dissertation submitted by

Michael M. Clark

This dissertation has been read by each member of the following graduate committee and by majority vote has been found to be satisfactory.

Date	Thomas H. Fletcher, Committee Chair
Date	Rodman R. Linn, Committee Member
Date	Larry L. Baxter, Committee Member
Date	Dean R. Wheeler, Committee Member
Date	John L. Oscarson, Committee Member

BRIGHAM YOUNG UNIVERSITY

As chair of the candidate's graduate committee, I have read the dissertation of Michael M. Clark in its final form and have found that (1) its format, citations, and bibliographical style are consistent and acceptable and fulfill university and department style requirements; (2) its illustrative materials including figures, tables, and charts are in place; and (3) the final manuscript is satisfactory to the graduate committee and is ready for submission to the university library.

Date

Thomas H. Fletcher
Chair, Graduate Committee

Accepted for the Department

Larry L. Baxter
Graduate Coordinator

Accepted for the College

Alan R. Parkinson
Dean, Ira A. Fulton College of Engineering and Technology

ABSTRACT

DEVELOPMENT AND EVALUATION OF A SUB-GRID COMBUSTION MODEL FOR A LANDSCAPE SCALE 3-D WILDLAND FIRE SIMULATOR

Michael M. Clark

Department of Chemical Engineering

Doctor of Philosophy

A mixture-fraction-based thermodynamic equilibrium approach for modeling gas-phase combustion was adapted and used in FIRETEC, a wildfire computational fluid dynamics model. The motivation behind this work was the desire to incorporate the features of complex chemistry calculations from the thermodynamic equilibrium model into FIRETEC without significantly increasing the computational burden of the program. In order to implement the mixture-fraction-based thermodynamic equilibrium approach, a sub-grid pocket model was developed to simulate the local mixture fraction of sub-grid flame sheets. Numerical simulations of wildfires were performed using FIRETEC with the new sub-grid, mixture-fraction-based pocket model to model gas-phase combustion. The thermodynamic equilibrium model was used to calculate flame temperatures and

combustion products, including CO_2 and CO, for sub-grid, gas-phase combustion in FIRETEC simulations. Fire spread rates from simulations using the new sub-grid combustion model were 25-100% higher than fire spread rates from previous FIRETEC simulations, but the successes of modeling propagating fire lines and calculating detailed equilibrium combustion products from simulated sub-grid flame sheets demonstrated the feasibility of this new approach. Future work into the fine-tuning of pocket model parameters and modifying the conservation equation for energy in FIRETEC was recommended.

ACKNOWLEDGMENTS

I would like to thank my academic advisor, Dr. Thomas H. Fletcher, for his support and encouragement throughout my graduate education. He offered me an opportunity that opened many other doors of opportunity for me and my family.

I thank Rod Linn for providing much advisement in this research and for his efforts in securing a large portion of the funding that supported this work. I am very grateful for the opportunity Rod gave me to spend one year working at Los Alamos National Laboratory. It was a privilege to work with the many fine students and staff in the Atmospheric, Climate, and Environmental Dynamics group.

I gratefully acknowledge the sources of funding for this work, which included the Institute of Geophysics and Planetary Physics at Los Alamos National Laboratory, the USDA Forest Service, and the Bill and Margaret Pope Professorship. I also gratefully acknowledge the computational resources and support for this work provided by the Los Alamos National Laboratory Institutional Computing Program and the Brigham Young University Fulton Supercomputing Laboratory.

I thank my wife Wendi and my family for their support and encouragement.

I am most grateful for the opportunity I had to study at Brigham Young University, where scholarship is fostered in an environment of faith and integrity.

TABLE OF CONTENTS

LIST OF TABLES

LIST OF FIGURES

NOMENCLATURE

Symbol	Units	Definition
a	-	flame-sheet thickness ratio
c_F	-	FIRETEC reaction rate coefficient
c_p	$J \cdot kg^{-1} \cdot K^{-1}$	heat capacity
F	$kg \cdot m^{-3} \cdot s^{-1}$	combined solid-gas reaction rate in FIRETEC
f_{air}	-	mixture fraction of air in a computational cell (excludes unreacted, combustible, hydrocarbon-like gas)
$\bar{f}_{cell}$	-	mean mixture fraction in a computational cell
F_{gas}	$kg \cdot m^{-3} \cdot s^{-1}$	gas reaction rate in FIRETEC
$f_{HCpocket}$	-	mixture fraction of spherical pockets composed of pure, unreacted, combustible, hydrocarbon-like gas; by definition equal to 1
f_r	-	mixture fraction of reacting mixture
F_{solid}	$kg \cdot m^{-3} \cdot s^{-1}$	solid reaction rate in FIRETEC
ΔH_{rxn}	$J \cdot kg^{-1}$	heat of reaction
$\Delta H_{sensible}$	$J \cdot kg^{-1}$	change in sensible heat
l	m	flame-sheet thickness parameter
M_{air}	$kg \cdot mol^{-1}$	molecular weight of air
M_{HC}	$kg \cdot mol^{-1}$	molecular weight of combustible, hydrocarbon-like gas
N_{HC}	-	mass ratio of reactive gas that reacts with oxygen
N_o	-	mass ratio of oxygen that reacts with a reactive gas
P	atm	pressure
r	m	radius of a spherical pocket of combustible, hydrocarbon-like gas
R	$m^3 \cdot atm \cdot K^{-1} \cdot mol^{-1}$	gas constant
s_x	m	turbulent length scale
T_{air}	K	temperature of reacting air
T_{flame}	K	flame temperature predicted by chemical equilibrium
$\overline{T}_{gas}$	K	average gas temperature
T_{HC}	K	temperature of reacting, combustible, hydrocarbon-like gas
$\hat{V}_{air}$	$m^3 \cdot kg^{-1}$	specific volume of reacting air

$V_{air,r}$	m^3	volume of reacting air
$\hat{V}_{HC}$	$m^3\ kg^{-1}$	specific volume of reacting, combustible, hydrocarbon-like gas
$V_{HC,r}$	m^3	volume of reacting combustible, hydrocarbon-like gas
A		constant for dissipation rate, dependent on flame structure and rate of reaction between fuel and oxygen OR area
$\overline{c_f}$	$m^3 \cdot kg^{-1}$	local time-mean concentration of fuel (kg/m^3)
c_F	-	a constant in FIRETEC reaction rate expression
$\overline{c_{O_2}}$	$m^3 \cdot kg^{-1}$	time-mean concentration of oxygen
C_p	$J \cdot kg^{-1} \cdot K^{-1}$	constant pressure heat capacity
C_v	$J \cdot kg^{-1} \cdot K^{-1}$	constant volume heat capacity
f	-	mixture fraction
F	$kg \cdot m^{-3} \cdot s^{-1}$	rate of reaction in FIRETEC
F_{gas}	$kg \cdot m^{-3} \cdot s^{-1}$	gas-phase reaction rate
F_{solid}	$kg \cdot m^{-3} \cdot s^{-1}$	solid-phase reaction rate
h		total enthalpy OR heat transfer coefficient
h_p		enthalpy of primary stream
h_r		residual enthalpy
h_s		enthalpy of secondary stream
ΔH_{rxn}	$J \cdot kg^{-1}$	heat of reaction
$(I_p)_o$	$J \cdot m^{-2} \cdot s^{-1}$	source of propagating flux without wind in units of energy/area/time
k		turbulent kinetic energy
L_f	m	flame length
$\dot{m}$		solid mass conversion rate
m_a	kg	mass of air mixing with combustible pyrolysis products
m_g	kg	mass of gas phase
m_p	kg	mass of combustible pyrolysis products
m_s	kg	mass of solid phase
N_{O2}	-	mass ratio of oxygen that reacts with a reactive gas
$N_{reactivegas}$	-	mass ratio of reactive gas that reacts with oxygen
p	Pa	pressure
p_s	Pa	standard pressure
$P(f)$	-	probability density function
$\overline{P}$	Pa	average pressure

Q_{ig}		energy required for ignition
Q_{conv}		heat addition due to convective heat transfer
Q_{mass}		energy loss due to mass exchange
Q_{rxn}		heat addition due to reaction
R	$m \cdot s^{-1}$ / $J \cdot K^{-1} \cdot mol^{-1}$	fire spread rate OR universal gas constant
r_f		stoichiometric coefficient
R_f		rate of combustion of fuel
s_x	m	turbulent length scale
t	s	time
Δt	s	change in time
T	K	temperature
T_{crit}	K	critical temperature, above which fuel can react
T_{flame}	K	flame temperature
T_g	K	gas temperature
T_{gas}	K	gas temperature
T_o	K	assumed initial temperature of reacting mixture
T_s	K	solid temperature
T_{solid}	K	solid temperature
$\overline{U}$	$m \cdot s^{-1}$	average velocity component
u	$m \cdot s^{-1}$	fluctuating velocity component
x	m	spatial coordinate
y	-	mole fraction
λ_{of}	-	stoichiometric coefficient
π	-	mathematical constant
$\overline{\rho}$	$kg \cdot m^{-3}$	total gas density
$\rho_{air,r}$	$kg \cdot m^{-3}$	bulk density of reacting air
$\overline{\hat{\rho}}_f$	$kg \cdot m^{-3}$	bulk density of vegetation
$\overline{\hat{\rho}}_{HC}$	$kg \cdot m^{-3}$	mean bulk density of combustible hydrocarbon-like vapors in the gas phase
$\rho_{HC,r}$	$kg \cdot m^{-3}$	bulk density of reacting, combustible, hydrocarbon-like gas
$\overline{\hat{\rho}}_o$	$kg \cdot m^{-3}$	mean bulk density of oxygen in the gas phase
$\overline{\hat{\rho}}_p$	$kg \cdot m^{-3}$	mean bulk density of primary mass in the gas phase
ρ_{ref}	$kg \cdot m^{-3}$	reference density, 1 kg m^{-3}
$\overline{\hat{\rho}}_s$	$kg \cdot m^{-3}$	mean bulk density of secondary mass in the gas phase
σ_{cm}	$m^2 \cdot s^{-1}$	turbulent mixing term

ϕ_r	-	volume fraction of reacting gas
χ	-	fraction of reacting mixture that consists of pure, combustible, hydrocarbon-like gas
Ψ_s	-	fraction of solid fuel that is above T_{crit}
Ψ_g	-	fraction of gaseous fuel that is above T_{crit}
α	-	probability of intermittency
β	-	scalar value, i.e. temperature, mole fraction
δ_{ij}	-	Kronecker delta
ε		dissipation of turbulent kinetic energy OR effective heating number
θ	K	potential temperature
θ_{solid}	K	fraction of reactive heat distributed to solid phase
λ_{of}	-	stoichiometric coefficient
μ		viscosity
ρ	$kg \cdot m^{-3}$	density
ρ_b	$kg \cdot m^{-3}$	bulk density of the fuel bed
$\bar{\hat{\rho}}_f$	$kg \cdot m^{-3}$	mean density of fuel
ρ_g	$kg \cdot m^{-3}$	gas density
$\bar{\hat{\rho}}_o$	$kg \cdot m^{-3}$	mean density of oxygen
ρ_{o2}	$kg \cdot m^{-3}$	bulk density of oxygen
$\rho_{reactivegas}$	$kg \cdot m^{-3}$	bulk density of reactive gas
σ_{cm}		turbulent mixing variable
ϕ_s	-	additive slope parameter
ϕ_w	-	additive wind parameter
Ψ_f	-	fraction of gaseous fuel that is above T_{crit}
Ψ_g	-	fraction of gaseous fuel that is above T_{crit}
Ψ_s	-	fraction of fuel that is above T_{crit}

1 Introduction

Each year wildland fires threaten human life and property, with significant costs resulting from fire suppression labor and equipment (2006a). Improved maintenance of forests, perhaps by properly prescribed burning and thinning, or by allowing natural fires to burn, may lead to a decrease in the intensity of future wildfires. Wildfires might then be more prone to burn through forest undergrowth at a much lower intensity, rather than exploding into the catastrophic, high-intensity, destructive fires that have occurred more frequently in recent years. An understanding of the nature, physics, and role of wildland fires is essential to improving fire management. Numerical models of wildland fires are powerful computational tools that contribute to the understanding of wildfire dynamics. Continued development of these models will provide improved prediction of fire behavior for planning prescribed burns, a tool for investigating past burns, and a means of risk analysis for properties located in areas prone to wildfires. However, all models have limitations that must be understood in order to judge the accuracy and validity of model results.

Perhaps the most difficult challenge to modeling large-scale fires in three dimensions is describing sub-grid combustion processes. Computational limitations on grid refinement, and deficiencies in atmospheric turbulence and fuels data, make it difficult or impossible to resolve important small-scale features of interest, such as flame

sheets and vegetation as well as temperature and wind fluctuations. As a result, simplified or heuristic expressions are used for numerical representations of physical processes, including convective and radiative heat transfer, solid-phase combustion, gas-phase combustion, and turbulence-driven mixing. However, this limitation should not curb development of models.

The purpose of this research is to develop and implement a new approach for the numerical representation of gas-phase combustion physics in FIRETEC, a wildland fire model developed at Los Alamos National Laboratory (LANL). This new approach for modeling gas-phase combustion in FIRETEC is based on an existing combustion modeling approach, namely the mixture fraction probability density function (PDF) model. By adapting and applying a thermodynamic equilibrium model, as in the mixture fraction approach, a gas-phase combustion model is developed for FIRETEC. The PDF of the mixture fraction is not used—just the assumptions of thermodynamic equilibrium and complete, instantaneous reaction. This new gas-phase combustion model produces predictions of flame temperature and product species compositions that are more detailed than previous combustion models implemented in FIRETEC.

Though combustion models based on the mixture fraction PDF approach have already been developed and are available, such as PCGC-3 (1999), the implementation of such a model into FIRETEC is not a trivial task. This is primarily due to grid resolution. Whereas most contemporary combustion computational fluid dynamics (CFD) modeling techniques resolve flame sheets at cm to mm scales, the FIRETEC grid resolution is on the order of one meter. In order to implement any concepts from the mixture fraction PDF approach, it becomes necessary to conceive and develop a sub-grid model. As stated

earlier, sub-grid modeling of combustion processes is one of the key challenges in the development and application of wildfire CFD. An awareness of and appreciation for this challenge is necessary in order to understand the nature and scope of this dissertation.

For this dissertation, a new sub-grid model was developed in order to apply a thermodynamic chemical equilibrium model into FIRETEC. The purpose was to provide a more detailed method for modeling gas-phase combustion in FIRETEC. This was to be accomplished by relying on some of the advantages of the mixture fraction concept. The dissertation is organized as follows. A background of CFD modeling approaches and published wildfire models and a detailed description of the FIRETEC model are given in Chapter 2. Research objectives are stated in Chapter 3. The implementation of the mixture fraction model is described in Chapter 4. Theoretical development and results for a constant radius sub-grid pocket model are then given in Chapter 5, followed by the presentation of limited development and results of a variable radius sub-grid pocket model in Chapter 6. Finally, conclusions and recommendations are given in Chapter 7.

2 Literature Review

Utilizing computational fluid dynamics (CFD) to model large-scale wildfire combustion is challenging, due in large part to the highly complex physics of turbulent fluid dynamics and chemical kinetics. The following review includes a brief discussion of general classifications of CFD models, and a review of chemistry models. Next, a review of models more specifically related to wildland fire sciences is included, followed by a brief description of other modeling techniques that can be utilized in wildfire CFD. Finally, a description is given of available experimental data for use in model evaluation.

2.1 Modeling Gas-phase Combustion: Treatment of the Navier-Stokes Equations

In most combustion applications of practical interest, the presence of turbulence significantly complicates the physics of fluid flow, and must be accounted for in the solution to the Navier-Stokes equations. It is no small task to predict the onset, transition, and development of turbulent flow. Beyond that, modeling fully developed turbulent flow still presents the closure problem – the task of describing unresolved physical quantities in a turbulence model – an active area of research in the fluid dynamics community. Coupled turbulence and combustion chemistry further complicate the task of modeling the flow due to additional species that may influence the nature of the turbulence, and

whose transport is strongly dependent on the turbulence. A few common classifications of CFD models for this type of flow are reviewed.

2.1.1 Reynolds Averaging

A common method of treating the Navier-Stokes equations in CFD is to perform a Reynolds decomposition on the momentum equations. This is simply a time average of the governing equations where the variables are expressed in mean and fluctuating components. The fluctuating components in the decomposition result in the so-called Reynolds stress terms in the momentum equations, and similar terms in the energy and species equations, all of which must be modeled. The resulting Reynolds-Averaged Navier-Stokes (RANS) equation for incompressible turbulent flow, neglecting body forces and any pressure fluctuations, in 3D Cartesian coordinates is (Bernard and Wallace, 2002):

$$\rho\left(\frac{\partial \overline{U}_i}{\partial t} + \overline{U}_j \frac{\partial \overline{U}_i}{\partial x_j}\right) = \frac{\partial}{\partial x_j}\left(-\overline{P}\delta_{ij} + \mu\frac{\partial \overline{U}_i}{\partial x_j} - \rho\overline{u_i u_j}\right) \qquad \textbf{(2-1)}$$

The Reynolds-averaged species conservation equations quickly become unmanageable once multiple reactions and fluctuations in composition and temperature are included, with three and four variable correlation terms arising from the Reynolds averaging (Turns, 2000). Any substantial kinetic mechanism would result in a system of equations that would be far too computationally expensive to solve while achieving appropriate temporal and spatial resolution. Additionally, such a system of equations would contain many terms associated with the composition and temperature fluctuations that cannot be reliably estimated.

2.1.2 Large Eddy Simulation

Large Eddy Simulation (LES) is used to model the transient nature of large-scale "eddies" in reacting flows. Without sufficient temporal and spatial resolution, RANS and other ensemble-averaged models fail to capture these transient features. In LES, these structures can be resolved as long as the computational mesh is sufficiently fine. The resolution of a range of scales in LES allows for the application of kinetics models for gas-phase combustion, as long as the temporal and spatial resolutions of the model are sufficient. Sub-grid scale turbulence must still be modeled, often by means of an effective diffusivity. However, if the computational mesh is sufficiently fine, at small-enough length scales this sub-grid scale turbulence becomes isotropic, in which case it is appropriate to use an effective diffusivity. Application of LES in combustion modeling is growing in popularity and has been reviewed by Janicka, et al. (2005) and Pitsch (2006).

2.1.3 Direct Numerical Simulation

The Navier-Stokes, energy and species continuity equations can be solved directly by discretizing the equations, applying a very fine mesh over the domain, and attempting to resolve all of the important length scales of the flow. This approach is termed direct numerical simulation (DNS), and has been used to model some simple, small-scale, non-reacting, boundary-layer flows of low Reynolds number (White, 2006), and more recently, some low-Reynolds number laboratory-jet-flame experiments (Mizobuchi et al., 2005; Westbrook et al., 2005). DNS is the most rigorous method of computational fluid dynamics, but it is extremely time-consuming. DNS simulations of turbulent reacting flows over complex domains of engineering interest are still well beyond the reach of current supercomputing power. However, this is an emerging field of computational

modeling and it will grow as computational resources and data collection and characterization techniques improve.

2.1.4 Summary

At the core of any computational fluid dynamics model is a method for solving the Navier-Stokes equations, which becomes complicated when turbulence is present. The challenge becomes finding an appropriate method to model unresolved temporal and spatial turbulence quantities. One approach is to improve temporal and spatial resolution as in DNS modeling. However, improved resolution limits the spatial dimensions of the computational domain and increases computational cost. Another approach is to improve the sub-grid turbulence models, which may save the computational cost of improved resolution. However, the sub-grid models may not properly account for all the physics in the flow field, resulting in questionable accuracy.

2.2 Modeling Gas-phase Combustion: Chemistry Models

The presence of turbulence in fluid flow significantly complicates the physics of any chemical reaction that occurs in the flow. The decomposition of model variables into mean and fluctuating components makes it impractical to apply kinetics models, due to the fluctuating temperature, where temperature is found in the exponential terms present in kinetics models (Turns, 2000). If however the fluid model temporally and spatially resolves these fluctuations, as in DNS and some LES models, then rigorous kinetics models can be applied. Otherwise approximations and assumptions must be made in the chemistry model. A few common approaches to chemistry modeling are now reviewed.

2.2.1 Eddy Breakup and Eddy Dissipation Concept

One way to simplify the turbulence-chemistry interaction problem is to assume that the chemistry is fast, and that the gas-phase reaction rates only depend on the mixing of fuel and oxidizer. Following this assumption, Spalding (1971), and later Magnussen and Hjertager (1976) proposed the eddy breakup, or eddy dissipation model. The reaction rate is modeled as the minimum of the mixing rate of oxidizer or the mixing rate of fuel, where fuel and oxidizer are assumed to reside in separate eddies. The rate at which these eddies mix is a function of the turbulence dissipation rate. The dissipation rate of fuel eddies is expressed by

$$R_f = A \cdot \overline{c_f} \left(\frac{\varepsilon}{k} \right) \left(kg / m^3 / s \right) \qquad \textbf{(2-2)}$$

where A is a constant, $\overline{c_f}$ is the time-mean concentration of fuel, ε is the dissipation of turbulent kinetic energy, and k is the turbulent kinetic energy. The dissipation rate of oxygen-rich eddies is expressed in similar form

$$R_f = A \cdot \frac{\overline{c_{O_2}}}{r_f} \left(\frac{\varepsilon}{k} \right) \left(kg / m^3 / s \right) \qquad \textbf{(2-3)}$$

in terms of the time mean concentration of oxygen, $\overline{C_{O_2}}$, and a stoichiometric coefficient for the amount of oxygen required to combust 1 kg of fuel, r_f.

The eddy dissipation model was later extended to include a check of kinetic rates of reaction to determine if the chemical kinetics are rate limiting. When the kinetics are rate limiting, then the kinetic rate is used as the rate of reaction, otherwise the minimum mixing rate is used. This model is frequently termed “the eddy dissipation concept” (Magnussen, 1989; Ertesvag and Magnussen, 2000), and may be more accurate than the strictly mixing-limited eddy dissipation models in predicting the formation of pollutants

such as CO and NO_x, where chemical kinetics become rate-limiting. For most wildfire modeling applications it is assumed that the kinetics are fast, in which case only the mixing rates are considered (Zhou and Pereira, 2000; Morvan and Dupuy, 2001, 2004; Zhou et al., 2005b).

2.2.2 Mixture Fraction PDF

A turbulent mixture fraction approach is sometimes used to describe gas-phase combustion reactions (Smoot and Smith, 1985). This approach was central to the research aims of this dissertation and will be discussed in more detail.

Turbulence-chemistry interactions can be modeled using averaged values of temperature, velocity, and the mixture fraction, where the mixture fraction, *f*, is the local fraction of mass that originated from a stream designated as the primary stream. These variables fluctuate about a mean value with a certain variance. A probability density function (PDF) is used to represent this variation, where *P* is a function of mixture fraction, *f*. The Gaussian distribution is a typical example of a PDF. Other examples include the clipped Gaussian, beta, and top hat distribution functions.

Variables that are conserved scalars, or that are derived from conserved scalars, can be represented as functions of the mixture fraction using equilibrium calculations or tabulated experimental data. With the PDF defined, and the functions of T and y_i known, the average value of T and y_i can be calculated by convoluting the scalar function over the PDF from $0 < f < 1$ as follows (Smoot and Smith, 1985):

$$\widetilde{\beta} = \alpha_p \beta_p + \alpha_s \beta_s + \int_0^1 \beta(f, h_r) P(\widetilde{f}) df \qquad \textbf{(2-4)}$$

where β is the temperature or species mole fraction, α is the probability of intermittency, the occurrence of pockets of pure primary- or pure secondary-stream material, and h_r is the residual enthalpy due to non-adiabatic conditions. The primary stream typically consists of fuel, such as methane in a methane burner, a coal-air mixture in a pulverized coal utility boiler, or pyrolysis products in a wildfire. The secondary stream usually consists of air. The tilde (~) indicates that the term has been Favre-averaged, which is a convenient method of weighting the variable with the instantaneous density before averaging, such that double-correlation terms containing density fluctuations do not result from the averaging (Smoot and Smith, 1985). The function $\beta(f, h_r)$ is obtained from equilibrium thermodynamics or from tabulated experimental data.

An example of this function is shown for species mole fraction and temperature in an adiabatic methane-air system. For this example, the equilibrium products of the methane-air system were calculated assuming adiabatic conditions (i.e. h_r = 0), with reactant properties calculated based on an initial temperature of 298.15 K. Therefore, the enthalpy of the system was determined by the mixture fraction. Species mole fractions for the equilibrium products of methane-air combustion, calculated using the NASA CEA2 equilibrium program (McBride and Gordon, 1996), are shown in Figure 2-1. The adiabatic equilibrium flame temperature for the same system is shown in Figure 2-2. Note that near the point where the mixture fraction is stoichiometric (f = 0.055,) the equilibrium flame temperature reaches a maximum value. Turns (2000) reports a maximum adiabatic flame temperature of 2226 K for the methane-air system. The maximum value of the CO_2 and H_2O equilibrium products also occurs near this point,

where the stoichiometry is such that the oxidation of carbon to CO_2 and hydrogen to H_2O is maximized. In fuel rich mixtures ($f > 0.055$) the products CO and H_2 become significant. On either side of the stoichiometric point the flame temperature is less than 2226 K. This occurs in fuel lean regimes, $f < 0.055$, where heating of excess air in the system consumes a portion of the heat of reaction, and in fuel rich regimes, $f > 0.055$, where there is insufficient oxygen to convert the carbon and hydrogen completely to CO_2 and H_2O.

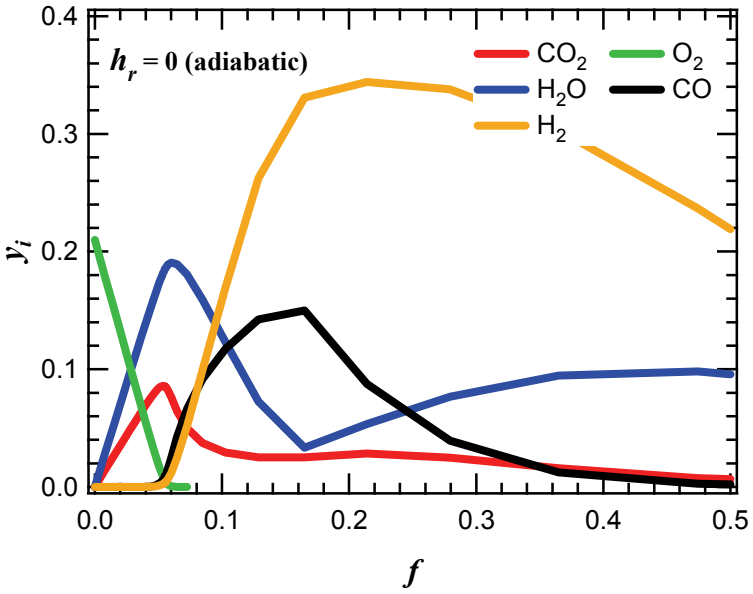

Figure 2-1. Species mole fraction as a function of mixture fraction calculated from chemical equilibrium under adiabatic conditions. For clarity, only five major species are shown in this graph.

This mixture fraction approach assumes that chemical reactions occur on a much faster time scale than mixing, i.e. reactions are mixing limited. In the previous example, adiabatic conditions ($h_r = 0$) were also assumed. Non-adiabatic conditions are accounted for by partitioning the total enthalpy into two parts. The total enthalpy consists of: (1) the

residual enthalpy, h_r, which results from non-adiabatic conditions (i.e. from heat losses due to radiative and convective heat transfer between the solid and gas phases), and (2) the enthalpy of the material in the computational cell, h_f.

$$h = h_f + h_r \tag{2-5}$$

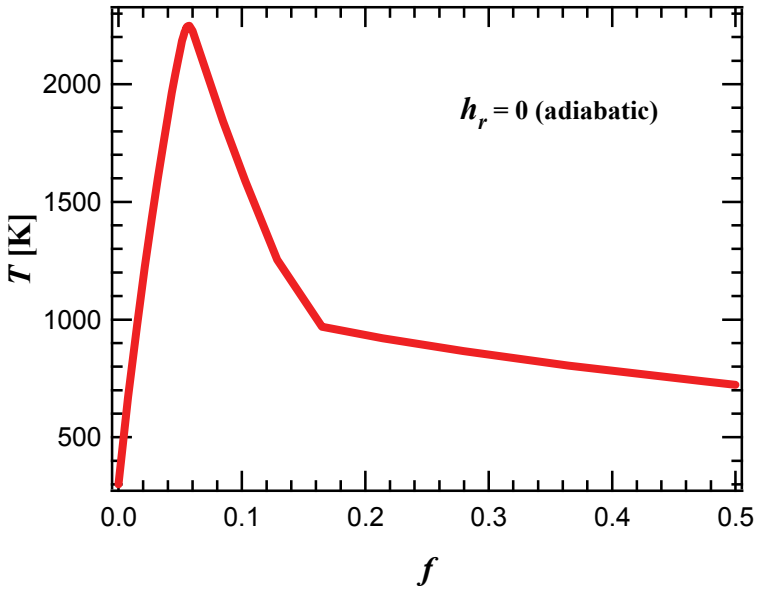

Figure 2-2. Temperature as a function of mixture fraction calculated from chemical equilibrium under adiabatic conditions.

The enthalpy of the material in the cell, h_f, is calculated from the enthalpies of the inlet primary (h_p) and secondary (h_s) streams using the mixture fraction. One assumes that all material in the cell originates from either the primary stream (fuel) or the secondary stream (oxidizer) (Smoot and Smith, 1985).

$$h_f = f h_p + (1 - f) h_s \tag{2-6}$$

Substituting equation (2-6) into (2-5) yields an equation for total enthalpy.

$$h = f h_p + (1 - f) h_s + h_r \tag{2-7}$$

Total enthalpy, h, and the mixture fraction, f, are conserved quantities, which can be obtained from the solution of the energy and mass conservation equations. The enthalpy of primary and secondary material, h_p and h_s, are properties of the material. Thus, equation (2-7) can be solved for the residual enthalpy, h_r.

$$h_r = h - fh_p - (1-f)h_s \qquad \textbf{(2-8)}$$

Just as the mixture fraction fluctuates, the enthalpy fluctuates as well. The PDF should then be a function of both f and h, since both fluctuate. However, it is assumed that fluctuations in h are highly correlated with fluctuations in f, and that h_r is usually small compared to h_f. Therefore, fluctuations in the total enthalpy are accounted for by only considering fluctuations in f, and the PDF remains a function of just the mixture fraction (Smoot and Smith, 1985).

2.2.3 Other Turbulence-Chemistry Approaches

Other approaches to modeling turbulence-chemistry interactions are available, including the PDF transport model (Pope, 1981, 1985), and the conditional moment closure model (Klimenko, 1990; Smith et al., 1992; Bilger, 1993). However, these models are deemed too complex for incorporation in this work.

2.2.4 Summary of Gas-phase Combustion Modeling

There has been significant progress in the development and use of CFD over the past decade. CFD has become a valuable tool for engineers, particularly for prediction and design, which improves efficiency in industrial manufacturing processes. Still, any modeling approach neglects some unresolved physics, or may include some empiricism

or approximation. All models are limited in predictive capabilities to geometries and flow conditions that are consistent with simplifying assumptions made during model development. This is particularly true if turbulence is involved, or if the modeling is performed over landscape-scale domains where sub-grid physics must be approximated. Finally, increased accuracy usually comes at the cost of increased computational costs, decreased size of the modeled domain, or both. One must understand these limitations when choosing and applying a specific type of model to use in CFD. This is arguably the most difficult challenge of wildfire CFD modeling.

2.3 Wildfire Models

A summary of published wildfire models is given in Table 2-1. Models are classified by scale (large or small) and by the level of detail in describing relevant physics (i.e., point-functional or physics-process-based). An empirical point-functional model is one in which fire physics are modeled at a single point using an experimental correlation based on properties and conditions locally at that point. In this way, fire spread rate is usually predicted as a function of variables such as wind speed, fuel loading, fuel moisture content, slope, etc. Current operational fire models simulate fire line propagation using point-functional models to predict the fire rate of spread at each of a series of points. A physics-process-based model is one in which fire physics are modeled over a domain using correlations or other mathematical expressions that represent the coupled physical processes of heat and mass transfer, fluid flow, and chemical reactions. The domains of small-scale models are on the order of the size of a small bush, with grid cell size dimensions at the centimeter scale. The domains of large-

scale models are on the order of hundreds of meters, with grid-cell size dimensions at the meter scale. These models are described in more detail in the next few sections.

Table 2-1. Summary of Fire Models

Classification	Benefits	Drawbacks	References
Empirical point-functional	-Models validated by controlled lab data -Spread rate predicted for a single location	-No dynamic link between fire and atmosphere -Correlated for specified conditions at a single point -Extrapolation made to fire conditions beyond the bounds of the conditions for which the empirical model was correlated	(Rothermel, 1972; Mardini and Lavine, 1995; Mardini et al., 1996; Vaz et al., 2004; Viegas, 2005)
Operational	-Use point-functional model over many points to mode fire line propagation -Run on desktop and/or laptop PCs; account for many conditions	-No modeling of dynamic fire/wind interaction -Based on point-functional models	**BEHAVEPLUS** (Andrews, 1986; Andrews and Bevins, 2003; Andrews et al., 2003; 2004) **FARSITE** (Finney, 1998; 2006b)
Physics-process-based small-scale	-Better grid refinement resolves vegetation, i.e. a single bush, tree, or bench-top scale fuel bed -Small scale fire features resolved -Centimeter scale	-Limited domain size; -Length scales of large fire features not covered	(Zhou and Pereira, 2000; Morvan and Dupuy, 2001; Zhou and Mahalingam, 2001; Morvan and Dupuy, 2004; Zhou et al., 2005a; Zhou et al., 2005b)
Physics-process-based large-scale	-May model large-scale fire features; -Captures dynamic interaction between fire and wind -Meter scale resolution	-High CPU costs; -Difficulties modeling sub-grid phenomena; -No resolution of sub-grid vegetation	**FIRETEC** (Linn, 1997; Linn and Harlow, 1998; Linn et al., 2003; Linn and Cunningham, 2005; Linn et al., 2005; Cunningham and Linn, 2007) **NIST FDS** (McGrattan, 2005; Mell et al., 2005; Mell et al., 2007)

2.3.1 Empirical Point-Functional Models

Empirical models are developed based on data recorded from laboratory-scale burns conducted in a controlled environment. These are usually point-functional models that use correlations fit to experimental data, often obtained from small-scale laboratory fires. A point-functional model predicts fire spread rate at a point, based on the given conditions for that point. Once such model that is widely used in wildfire modeling is the Rothermel model (1972):

$$R = \frac{(I_p)_o(1+\phi_w+\phi_s)}{\rho_b \varepsilon Q_{ig}}, \qquad \textbf{(2-9)}$$

where ϕ_w and ϕ_s are additive constants that account for increased propagating flux resulting from wind and slope. I_p is the heat flux from the flame front incident on the fuel bed in front of the fire. The fuel bed density is given by ρ_b, the heat of preignition is given by Q_{ig}, and ε is the effective heating number. The effective heating number, ε, is simply the ratio of the effective fuel bed bulk density to the actual fuel bed bulk density, implying that only a certain fraction of the fuel bed bulk density contributes to the spread of flaming combustion.

2.3.2 Operational Models

Operational models are used to predict fire propagation on a large scale. These models typically utilize a point-functional model to predict fire rate of spread, extending this model over a larger domain of interest to simulate line-fire propagation. The Rothermel model was originally implemented in the USDA Forest Service BEHAVE model (Rothermel, 1972). A more recent version of BEHAVE, called BEHAVEPLUS

(Andrews, 1986; Andrews and Bevins, 2003; Andrews et al., 2003; 2004) is still based on Rothermel's spread rate equation.

Another operational model developed by and used in the USDA Forest Service is FARSITE (Finney, 1998; 2006b). FARSITE is an extension of the Rothermel model in two dimensions to model a fire front. In FARSITE, the fire front is modeled by a series of ellipses. The shape of each individual ellipse is dependent on an effective wind speed, which combines the influence of wind and slope on fire spread rate. Rothermel's spread rate equation is used as the surface fire spread model in FARSITE.

Operational models developed by the forest service can be run on a typical laptop or desktop PC and are used by fire managers to predict fire perimeters in the field. Operational models may yield reasonable predictions for conditions relative to dead fuels. One limitation of these models is that the coupling of wind and fire is not dynamically treated. Therefore, the effects of fire plume fluid dynamics are not accounted for in operational models. Additionally, current models are based on empirical functions derived from experimental data for dead fuels, and may not accurately predict live fuels fire behavior for marginal burning conditions—"go, no go" conditions that fire managers strive to work under during prescribed burns.

2.3.3 Small-scale, Physics-process-based Models

Small-scale, physics-process-based models treat the coupled nature of fluid flow and combustion in a fire model. The small domain allows for grid refinement down to the centimeter scale, resolution of vegetation, and a more rigorous treatment of combustion chemistry. Gas-phase combustion chemistry is usually treated by applying a strictly mixing-limited Magnussen-Hjertager eddy dissipation model (Larini et al., 1998; Zhou

and Pereira, 2000; Morvan and Dupuy, 2001; Zhou and Mahalingam, 2001; Morvan and Dupuy, 2004; Zhou et al., 2005a). There is value to these small-scale models, particularly in using them in an effort to gain a mechanistic understanding of the rate of spread in line fires, or in studying fire behavior at the wildland-urban interface (i.e. where structures meet wildfire.) However, the small domains of these models usually do not cover length scales of large-scale effects such as ground-to-crown transition, topographic effects, and fire plume behavior.

2.3.4 Landscape-scale, Physics-process-based Models

Computational fluid dynamics techniques have also been applied to model wildfires numerically at landscape scales, with three-dimensional resolution at one-meter to tens-of-meters resolution for fully coupled hydrodynamics-combustion CFD models. Empirical fire spread algorithms from operational models have also been incorporated in a coupled wildfire-atmosphere mesoscale model (Clark et al., 2004).

NIST has developed the Wildland Fire Dynamics Simulator (WFDS) to model large-scale combustion on the so-called wildland-urban interface—where natural fuels are intermixed with structural fuels (Mell et al., 2005). WFDS is a coupled hydrodynamics-fire, physics-based model, and an extension of the NIST Fire Dynamics Simulator (FDS). WFDS has been used to model grassland fire experiments performed in Australia (Mell et al., 2007). The hydrodynamics are treated in FDS with LES, using the Smagorinsky model (1963) for the effective diffusivity.

The gas-phase combustion model in FDS is derived from a mixture-fraction, equilibrium-chemistry model, where it is assumed that combustion always occurs at the stoichiometric mixture fraction. Where there is a gradient in mixture fraction across

multiple computational cells, the model employs linear interpolation to find the spatial location between grid points where the mixture fraction is stoichiometric. Thus, the flame sheet may span multiple computational cells, and energy released over this flame sheet area is distributed to all cells which are cut by the flame sheet (McGrattan, 2005). Outside of this dissertation, the WFDS model is the only other known wildfire CFD model which uses the mixture fraction approach in any way.

FIRETEC is the other major wildfire CFD model currently under development and reported in the open literature. This model was developed at Los Alamos National Laboratory, and is a coupled wildfire physics hydrodynamics model. FIRETEC will be described in much greater detail in section 2.4. One main difference which sets FIRETEC apart from WFDS is that FIRETEC was developed from the ground up as a landscape-scale CFD wildfire model; whereas, WFDS is an off-shoot of the NIST FDS building fire computer model. It is important to understand that because of the differing origins of development between FIRETEC and WFDS, the approaches to modeling processes such as radiative heat transfer, combustion, and turbulence differ between the two computer models.

2.3.5 Summary

There are three common approaches to modeling wildfire found in the literature. One approach is to apply an empirical point-functional model to predict fire spread rates. This approach is computationally efficient, but does not account for the coupled effect of combustion on flow dynamics. A second approach is to use computational fluid dynamics to model wild fire at high resolution, as in small-scale physics-process-based models. This approach attempts to account for all the important physics, including the

implementation of common combustion modeling techniques such as the Magnussen and Hjertager eddy dissipation model. However, the high spatial and temporal resolution of the model limits the size of the computational domain, preventing full resolution of a large fire line or fire plume dynamics. A third approach is to model wildfire at landscape scales, and attempt to fully capture the flow dynamics of wildfires over a spatial domain that includes the entire fire line and plume. This approach is intriguing, with the ability to capture large features in the flow field that are coupled to the combustion processes of the wildfire. In modeling wildfire at landscape scales, the development and evaluation of sub-grid combustion models becomes a significant challenge to the landscape-scale physics-process-based approach to wildfire modeling.

2.4 FIRETEC

To understand the motivation behind this dissertation research, it is important to understand the current development state of the FIRETEC model. FIRETEC (Linn, 1997) is a computational fluid dynamics parallelized computer program developed to model the physical processes of fluid, energy, and species transport in wildfires. The FIRETEC computer code is coupled to a transient 3-dimensional, regional-scale, CFD atmospheric hydrodynamics code called HIGRAD, which uses a terrain-following coordinate system. In this dissertation, FIRETEC refers specifically to wildfire-physics subroutines, whereas HIGRAD refers to hydrodynamics subroutines. The HIGRAD/FIRETEC computer code includes programming subroutines to account for:

1. Momentum and energy transport.
2. Solid and gas phase combustion.

3. Convective and radiative heat transfer, both sub-grid and super-grid (meaning cell-to-cell over the computational domain.)
4. Unresolved turbulence.
5. Terrain of varied topography.

The primary goal of FIRETEC model development is to represent wildfire physics with the hope of having a tool that is useful for developing understanding of wildfire behavior and its interaction with environmental conditions including the fuels, atmosphere, and topography. Current efforts also focus on working to understand the implications of simplifying assumptions made in earlier model development. A fairly detailed overview of the combined HIGRAD/FIRETEC model is found in Smith, et al. (2007), a brief summary of which is included in this chapter.

2.4.1 HIGRAD Hydrodynamics Model

HIGRAD is an atmospheric CFD code that solves the fully compressible Navier-Stokes equations. The HIGRAD equations for conservation of momentum and energy, continuity, and conservation of any scalar in the gas phase are:

Momentum:
$$\frac{\partial \rho u_i}{\partial t} + \frac{\partial \rho u_j u_i}{\partial x_j} = -\frac{\partial P}{\partial x_i} + \rho g_i - 2(\varepsilon_{jk})_i \omega_j u_k + (S_m)_i \qquad \textbf{(2-10)}$$

Energy:
$$\frac{\partial \rho \theta}{\partial t} + \frac{\partial \rho u_j \theta}{\partial x_j} = S_\theta \qquad \textbf{(2-11)}$$

Overall Continuity:
$$\frac{\partial \rho}{\partial t} + \frac{\partial \rho u_j}{\partial x_j} = S_p \qquad \textbf{(2-12)}$$

Species Continuity:
$$\frac{\partial \rho \chi_i}{\partial t} + \frac{\partial \rho \chi_i u_j}{\partial x_j} = (S_\chi)_i \qquad i = 1.2,...., N_{species} \qquad \textbf{(2-13)}$$

The third term on the RHS of equation (2-10) accounts for the Coriolis effect, and this term is ignored in FIRETEC wildfire modeling applications (Smith et al., 2007).

The energy equation in HIGRAD is rather unique to the field of meteorology. The energy equation is cast in terms of potential temperature, which is "the temperature that an unsaturated parcel of dry air would have if brought adiabatically and reversibly from its initial state to a standard pressure" (Glickman, 2000). Potential temperature is defined as:

$$\theta = T\left(\frac{p_s}{p}\right)^{\frac{R}{C_p}} \qquad \textbf{(2-14)}$$

where T is the actual temperature, p_s is a standard pressure (usually 100 kPa), p is the actual pressure, R is the universal gas constant, and C_p is the gas heat capacity. The gas is assumed ideal ($C_p - C_v = R$). Potential temperature simply accounts for the change in temperature that occurs with increasing height in the atmosphere, and is related to the dry adiabatic lapse rate (Glickman, 2000).

The HIGRAD computer code uses a "non-oscillatory forward-in-time advection scheme" (Smith et al., 2007) to solve the Navier-Stokes equations. A "method of averaging" numerical technique is employed for numerical efficiency by integrating small-time-scale phenomena over smaller time steps, while integrating slower-time-scale phenomena over larger time steps while maintaining second-order accuracy (Reisner et al., 2000). Boundary conditions are imposed at the edges of the computational domain by relaxing transport variables to a prescribed constant or transient environmental (i.e. ambient) value (Smith et al., 2007).

2.4.2 FIRETEC Turbulence Model

FIRETEC models sub-grid turbulence at three different size scales (A, B, and C). These three size scales correspond respectively to the sub-grid spacing between bushes or trees, between branches, and between needles or leaves (Linn, 1997), thus the effort is to account for turbulence induced by flow in and through the vegetation within the computational domain. Conservation equations for A and B scale turbulence are:

$$\frac{\partial \rho K_A}{\partial t} = -R_{ij,A}\frac{\partial u_i}{\partial x_j} + \frac{2}{3}C_{DR}\frac{\partial}{\partial x_i}\left(s_A \frac{R_{ij}}{K^{1/2}}\frac{\partial K_A}{\partial x_j}\right), \\ -\frac{K^{1/2}}{s_A}K_A - \rho C_D a_v^B K^{1/2} K_A \qquad \textbf{(2-15)}$$

and

$$\frac{\partial \rho K_B}{\partial t} = -R_{ij,B}\frac{\partial u_i}{\partial x_j} + \frac{2}{3}C_{DR}\frac{\partial}{\partial x_i}\left(s_B \frac{R_{ij}}{K^{1/2}}\frac{\partial K_B}{\partial x_j}\right) \\ -\frac{K^{1/2}}{s_B}K_B - \rho C_D a_v^C K^{1/2} K_B + \rho C_D a_v^B \left(K^{1/2}K_A + |u|^3\right). \qquad \textbf{(2-16)}$$

Turbulence at the C scales is correlated to the B-scale turbulence, and a conservation equation for K_C is not solved. The reader is referred to Linn's thesis for a detailed description of the FIRETEC turbulence model (1997). Details are also found in Smith, et al. (2007). For purposes of this dissertation, it suffices to say that the FIRETEC turbulence model follows a fairly standard approach to the task of modeling unresolved turbulence, which includes accounting for turbulent production, dissipation, and the cascade of turbulent kinetic energy.

2.4.3 FIRETEC Combustion Models

A combustion model was formulated and implemented in HIGRAD to account for wildfire physics (Linn, 1997). During the initial development of FIRETEC, all gas-phase and solid-phase combustion reactions were lumped into one reaction rate expression by making simplifying assumptions. The reaction rate is given by

$$F = c_F \frac{\overline{\hat{\rho}}_f \overline{\hat{\rho}}_o \sigma_{cm} \Psi_s}{\rho_{ref} s_x^2} \lambda_{of}, \qquad \textbf{(2-17)}$$

where F is the reaction rate in units of mass per volume per time. The term $\overline{\hat{\rho}}_f$ represents the mass of available fuel for combustion per cell volume, and the term $\overline{\hat{\rho}}_o$, represents the mass of oxygen per cell volume. The caret indicates that the density quantity has been spatially averaged over the cell volume. The over bar indicates that the quantity is an ensemble average over many temporal realizations. These two types of averages are used in the development of the FIRETEC equations for modeling transport in the case of wildfires where both temporal fluctuations and spatial inhomogeneities may be present in the flow field. The reader is referred to Linn's thesis for more details on these forms of averaging (1997). The other terms in equation (2-17) are: c_F, a constant reaction rate coefficient; ρ_{ref}, a constant reference density; s_x, a constant turbulent size scale; σ_{cm}, a turbulent mixing variable; λ_{of}, a stoichiometric coefficient; and Ψ_s, the fraction of fuel that is above a specified critical temperature (Linn, 1997).

An assumed probability density function for temperature was employed to account for sub-grid combustion, since flame sheets are not resolved in HIGRAD/FIRETEC. It is assumed that reaction can occur in any portion of the cell that is above a specified critical temperature (T_{crit} = 600 K in FIRETEC.) An illustration of

this is given in Figures 2-3 through 2-5. In these figures, the PDF for temperature in a cell is assumed to be Gaussian. In each of the above-mentioned figures, the fraction of the area under the PDF that is shaded, where $T > T_{crit}$, represents the sub-grid fraction of reactive mass in a computational cell that is hot enough to combust. This sequence of figures shows that as the mean value of the temperature in the cell increases, a greater fraction of mass in the cell is assumed to be hot enough to react.

Figure 2-6 shows the fraction of mass in a computational cell, Ψ, which is hot enough to combust, as a function of average temperature in a computational cell. For the Gaussian distribution, this integrated function is the error function, and it scales with an assumed variance and critical temperature. In FIRETEC, a function similar to the error

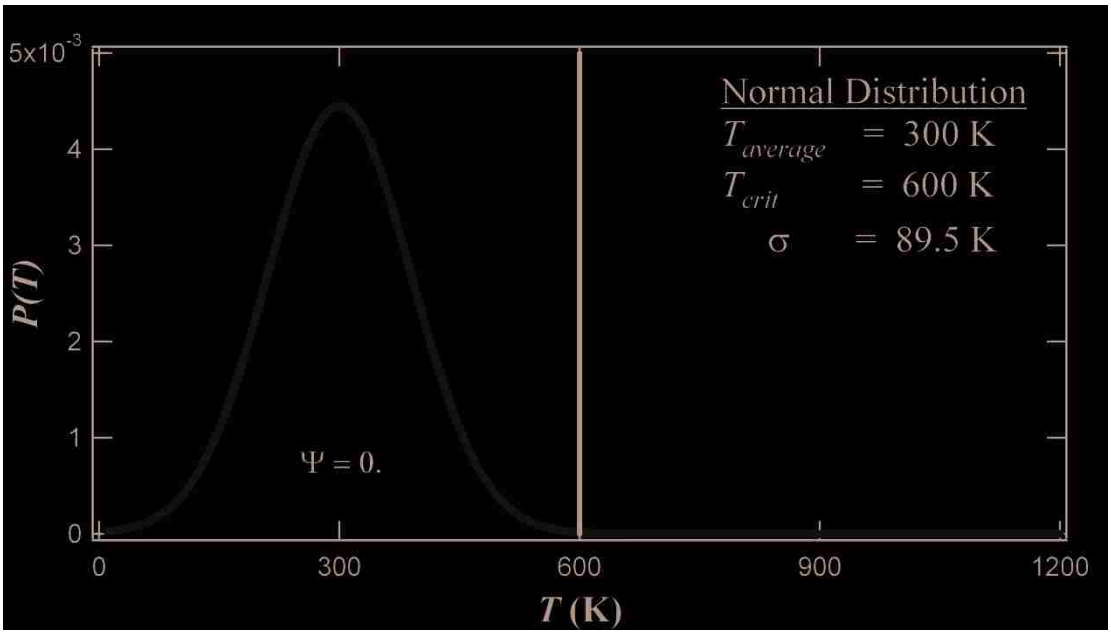

Figure 2-3. A probability density function for temperature with an average temperature of 300 K, where Ψ ≈ 0.

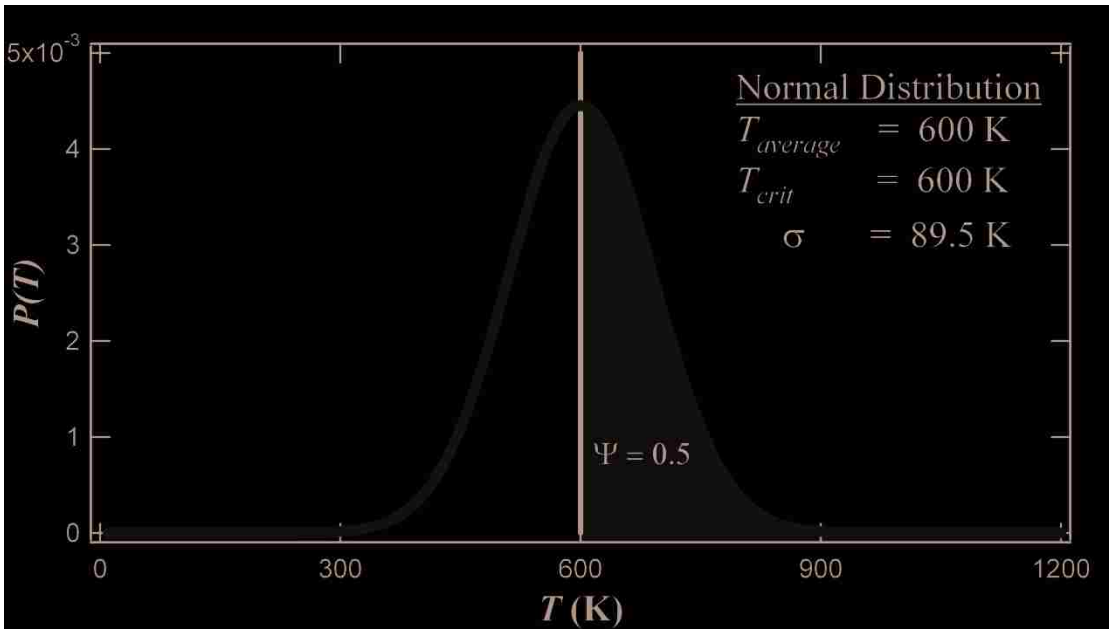

Figure 2-4. A probability density function for temperature with an average temperature of 600 K, where $\Psi \approx 0.5$.

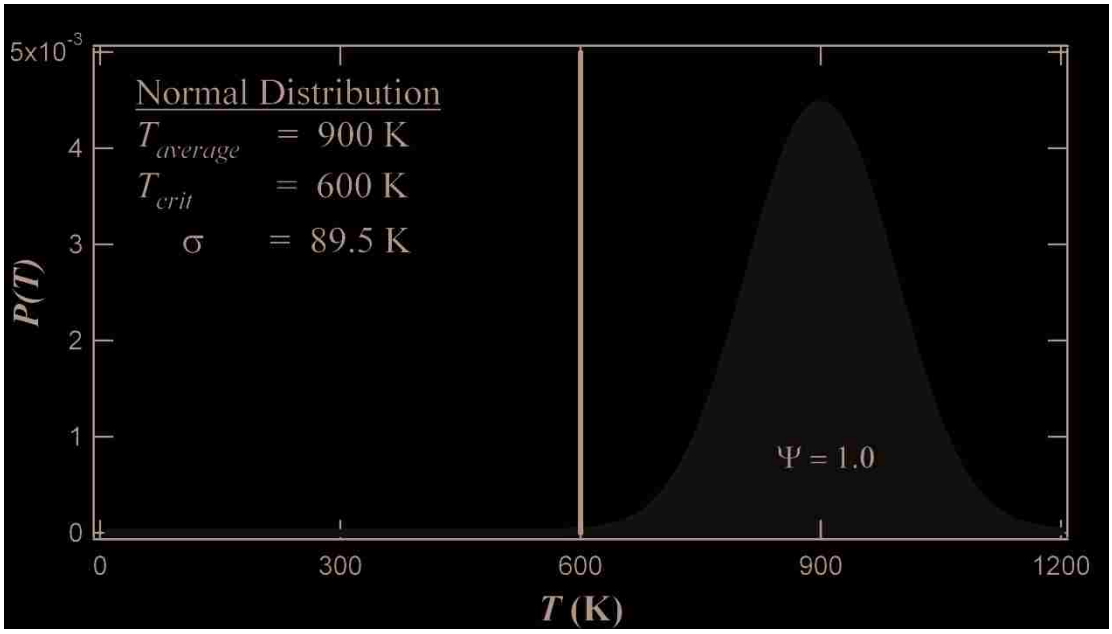

Figure 2-5. A probability density function for temperature with an average temperature of 900 K, where $\Psi \approx 1.0$.

function was implemented. The comparison of the error function to the FIRETEC function for Ψ is shown in Figure 2-6. The variance and critical temperature of the FIRETEC function for Ψ were tuned during development, thereafter remaining constant parameters. This PDF approach to combustion modeling in FIRETEC is heuristic and could be improved. However, an improvement would have to account for sub-grid variations in temperature, composition, and reaction rates. Despite the fact that the FIRETEC PDF approach is heuristic, it has thus far proven to be a functional method for approaching this problem in wildfire modeling.

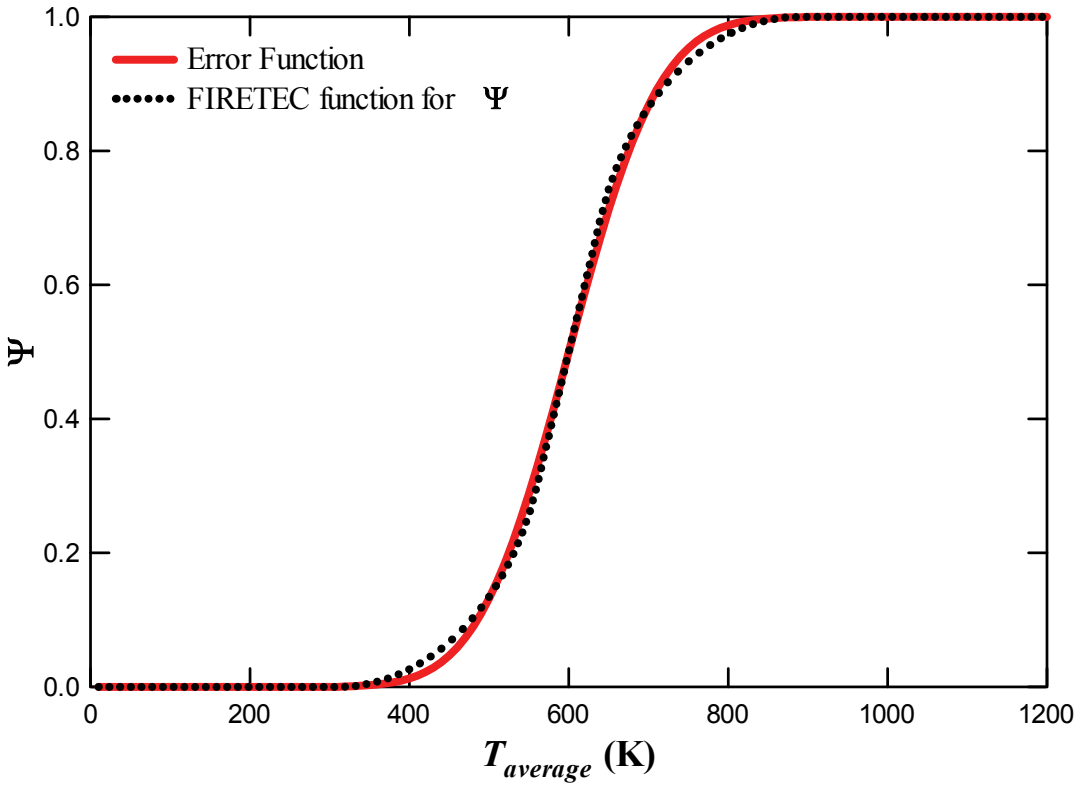

Figure 2-6. Ψ, or the sub-grid fraction of a cell that is burning. This function scales with T_{crit}, and the assumed variance of the PDF.

Source and sink terms for both gas-phase energy and solid-phase energy are accounted for in FIRETEC. These include terms for: (1) the radiative heat transfer, calculated in a separate diffusional submodel; (2) the convective heat transfer based on an approximate heat transfer coefficient that is a function of fuel size and fuel type, $Q_{conv} = hA(T_{solid} - T_{gas})$; (3) the heat of reaction from combustion, $Q_{rxn} = \Delta H_{rxn} F \Delta t (1 - \theta_{solid})$, where θ_{solid} is a fractional variable used to distribute a portion of the reactive heat to the solid phase, and the balance to the gas phase (details or this are described in Colman and Linn (2007)); and (4) the energy transport due to mass exchange from the solid phase to the gas phase, $Q_{mass,i} = FC_{p,i}T_i$, where it is assumed that the heat capacities of the species are constant, and the reference temperature is 0 Kelvin.

Subsequent development of the FIRETEC model treated the gas-phase reactions separately from the solid-phase reactions (Colman and Linn, 2005). A combustible, hydrocarbon-like gas species variable was added to the model to track it as a transportable gas. This implementation is referred to as the non-local model, since the combustible gas species produced during pyrolysis are allowed to be transported and to react in computational cells beyond the cell from which these species originated. An initial source term for the combustible gas is the solid reaction rate, given by

$$F_{solid} = \frac{c_F \rho_f \sigma_{cm} \Psi_f}{s_x^2}, \qquad \textbf{(2-18)}$$

which is essentially the same form as the combined reaction rate from the initial development of FIRETEC given by equation (2-17), except that the stoichiometric coefficient and reference density have been lumped into the constant c_F. Significant

reformulation of this source term is currently in progress, which is meant to describe in improved detail the pyrolysis process.

Gas-phase reactions were treated following the formulation for reactions involving two gases, originally proposed by Linn (1997), and the form of the gas-phase rate equation was given by

$$F_{gas} = \frac{\rho_{reactivegas}\rho_{O_2}\sigma_{cm}\Psi_g}{2(N_{O_2}\rho_{reactivegas} + N_{reactivegas}\rho_{O_2})} \qquad \textbf{(2-19)}$$

where N_{O_2} and $N_{reactivegas}$ are constants that account for the ratio of the mass of oxygen that reacts with a mass of reactive gas.

Node spacing in HIGRAD is typically on the order of two meters—a scale too large to allow for resolution of the fine detailed processes that occur in the combustion environment, but sufficient for a large-scale model used for atmospheric modeling and research. Grid refinement would improve combustion resolution, but prohibitively increase the computational cost of the model.

2.4.4 FIRETEC Heat Transfer Models

Radiative Heat Transfer

A radiative heat transfer model, diffusive in form and tailored to an optically thin media, was developed for FIRETEC with consideration for modeling wildfires on a parallel computing platform. The pseudo-steady-state equation for three-dimensional radiative heat transfer in FIRETEC is:

$$0 \cong 4(\varepsilon n A)\sigma T^4 - (\varepsilon n A)^2 k_{eff} u + \nabla \cdot \xi k_{eff} \nabla u \,, \qquad \textbf{(2-20)}$$

where u is the energy density, and the RHS of the equation includes a source term from the vegetative canopy and hot gases, a sink term to the vegetative canopy, and a diffusive term. The diffusive term arises from making a diffusion approximation, which greatly simplifies the integration of the radiative transfer equation. An iterative solution technique is used to solve for the radiative heat transfer field over the computational domain, assuming that the radiative heat transfer rapidly arrives at a pseudo-steady-state (Smith et al., 2007). This method is scalable and lends itself well for use in FIRETEC parallel computational fluid dynamics.

Convective Heat Transfer

FIRETEC also includes a convective heat transfer model to account for heat exchange between the vegetation and the gas phase. A simple correlation is used to estimate a heat transfer coefficient (Incorpera and DeWitt, 1985):

$$h = 0.683 \frac{33.8 \times 10^{-3} \, \mathrm{Re}_{s_s}^{\,0.466}}{s_s}. \qquad \textbf{(2-21)}$$

The Reynolds number is calculated from the root mean square average of all three velocity components, and the characteristic length, s_s, is a specified sub-grid length scale that is characteristic of the vegetation (Linn, 1997). In the version of FIRETEC used in this research the value of s_s was 0.5 mm.

2.4.5 FIRETEC Fuel Bed Description

Fuel beds modeled in FIRETEC are user-defined, meaning any number of fuels can be modeled in FIRETEC as long as the user inputs this information correctly. The fuel bed description that follows is typical of most current FIRETEC modeling work, and is the fuel bed description that was used in this dissertation work.

Solid fuels in FIRETEC are composed only of fine vegetation, i.e., leaves, needles, and small branches or twigs. Thermally thick fuels such as tree trunks are not currently modeled in FIRETEC. Although thermally thick fuels can smolder over long periods of time after a firefront passes over them, these fuels are not thought to contribute significantly to combustion in a moving firefront, and are therefore neglected in FIRETEC.

Grass fuel beds typically consist of evenly distributed grass at a height of 0.7 m, covering the entire ground-layer surface of the domain. The height and distribution of the fuel can be adjusted as desired by the user. The fuel loading for grass is typically 0.7 $kg \cdot m^{-2}$, and the initial moisture content of the grass is specified. Moisture contents are given on a dry-fuel basis (i.e., kg of moisture/kg of dry fuel), since this is customary in the field of forestry research and management.

Ponderosa pine fuel beds are modeled similarly to a previously reported method (Linn et al., 2005). Pine fuel beds consist of a Ponderosa pine canopy distributed across the fuel layer based on measurements that include detailed tree location data from a plot surveyed by the USDA Forest Service Rocky Mountain Research Station. In these survey data, the maximum canopy height was 19.9 m, and the average canopy bulk density was ~0.12 $kg \cdot m^{-3}$. The initial moisture content of the canopy can be specified. Ground layer fuels, both litter and grass (each with a specified moisture content,) are distributed below the canopy. The distribution of ground layer fuels scales with the openness of the canopy above the ground, i.e., the more open the canopy, the more mass of ground layer fuels found at the surface.

The fuel beds for chaparral simulations are modeled using the same routine used for Ponderosa pine simulations. However, in the case of the chaparral fuel beds, the fuel distribution is not based on data from specific field surveys. The average crown diameter is assumed to be 2.5 m, with 60% coverage, and shrub heights between 1 and 2 m. The initial fuel moisture content for the canopy is user-specified, and ground layer fuels are distributed depending on the openness of the canopy above the surface (as in Ponderosa pine fuel beds).

2.4.6 Ignition

Fire line ignition in FIRETEC simulations usually occurs along a strip of surface-layer cells, typically between 20 to 100 m long and 4 m wide. Figure 2-7 provides a graphical illustration of the location of the ignited fire line in the computational domain. The location of the initial fire line can be placed anywhere in the domain, but it is usually placed 50 to 60 meters downwind from the wind inlet boundary, and centered in the crosswind direction of the domain. To 'ignite' the solid fuels in FIRETEC simulations, the temperature of the fuels is artificially ramped up from 300 K to 1000 K over 2 seconds of simulated time (Colman and Linn, 2005; Linn and Cunningham, 2005).

Another optional ignition function exists within FIRETEC that simulates an ignition caused by running a drip-torch run along the length of the initial fire line. Instead of igniting the entire fire line at the same time, the fire line is ignited from one end of the line to the other end, which is usually how ignition is initiated in field experiments or controlled burns. This optional FIRETEC ignition function still uses the technique of artificially increasing the solid temperature.

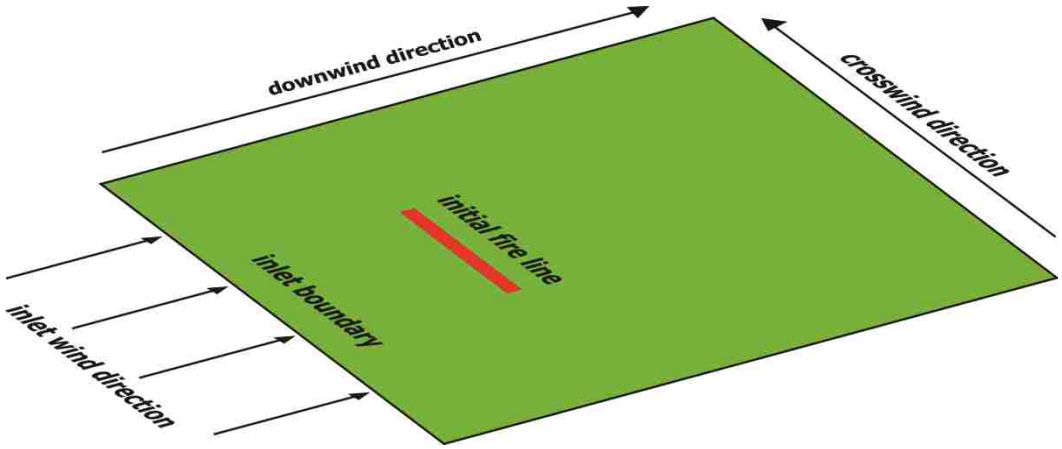

Figure 2-7. Diagram of a typical fire line location upon ignition in FIRETEC.

2.4.7 Summary

Currently, active development of the model includes work on firebrand transport, modeling of radiative heat transfer via the Monte-Carlo approach, a multiple-fuels-type representation of the solid fuels, the implementation of cyclic boundary conditions, the use of well-developed wind profiles as boundary conditions, and the work of this dissertation in implementing a mixture fraction approach to gas phase combustion. These examples of current development illustrate the value of HIGRAD/FIRETEC, which lies in the fact that it includes numerical representations of critical physical processes. Since these representations are based on fundamental theory, rather than being implicitly lumped into empirical expressions as is done in operational models, one can explore a variety of numerical approaches to modeling wildfire physics. Still, there are significant approximations made in FIRETEC, particularly in the chemistry submodels. However, with a foundation on fundamental physics, improvements to the chemistry submodels can be made, which is the purpose of this research.

The obvious drawback of HIGRAD/FIRETEC is computational cost, which is currently high—requiring a parallel computing platform and significant CPU time. Another weakness is that the limits of the predictive capability of the model have not been fully explored, which requires justification of model approximations and evaluation by comparison to experimental data over a range of conditions. A number of experimental data sets can be used to compare overall spread rates and fire perimeter behavior. However, these data are not sufficient to fully validate a CFD computer model, because they do not fully characterize the flow field of a wildfire. In particular, the local variability in measured ambient wind could have a profound impact on fire behavior, but this detail is not available in current input data sets.

2.5 Other Modeling Techniques

2.5.1 Flame Length Correlations

Correlations can be developed for flame lengths of combustion for different fuels. Recent experiments have been performed on live fuels including California chaparral and Utah fuels. Observed flame heights have been correlated with measured mass loss rates for these fuels. For live fuels a suggested correlation is (Weise et al., 2005):

$$\log(L_f) = -0.38 + 0.5\log(\dot{m}) \qquad \textbf{(2-22)}$$

where L_f is the flame length in units of meters and $\dot{m}$ is the mass loss rate of the vegetation in units of grams/second. A flame length correlation may be applicable to wildfire model development.

2.5.2 Adaptive Grid Refinement

As mentioned previously, computational limitations restrict grid refinement, preventing detailed resolution of small-scale fuels and processes. As a result, in the development of large-scale wildfire models, it becomes necessary to approximate the physics of sub-grid phenomena like gas-phase and solid-phase combustion. One way to relax these approximations and incorporate more rigorous descriptions of fire physics is to employ adaptive grid refinement, where the computational mesh in and around the fire location within the domain is more finely resolved. Away from the fire, where grid refinement is not needed, the grid cells are larger. As the fire moves through the computational domain, algorithms in the numerical model adapt the computational mesh accordingly by cutting larger grid cells into smaller cells, or by combining smaller cells into larger cells. Along the way the current values of the temperature, velocities, species concentrations, etc. are remapped onto the "adapted" mesh by interpolation.

Adaptive grid refinement improves (or makes possible) resolution of fire physics, which allows for the application of more complex models. This technique would be useful in any fire model where important sub-grid combustion physics are not resolved. For this reason, it is mentioned in this review; however, the complexity of implementing this technique in an existing model is beyond the scope of this work.

2.5.3 Decoupled Wind and Fire Model

One unique approach to fire modeling combined the use of computational fluid dynamics software with an operational fire model to simulate fire propagation over mountainous terrain. Wind maps were generated by using commercial CFD software, then used as input conditions for an operational model, FARSITE, to predict fire spread

rate. The use of these wind maps resulted in improved accuracy of FARSITE predictions. The improvement in accuracy was reportedly a direct result of the CFD-generated wind maps, which provided more accurate input for the operational model than just a single point wind measurement due to the effect of terrain on the airflow (Butler et al., 2005). This approach did not include any fire-induced effects in the flow field. However, it is known that wildfires induce local air currents in the vicinity of the flame front through large buoyancy-induced drafts. Therefore by neglecting the coupling of flow dynamics and combustion, this modeling approach did not account for these effects.

2.6 Experimental Data

High-quality experimental data are invaluable to modeling efforts for use in comparing model results to real observations. However, physical and cost limitations impact the availability and quality of experimental data, particularly for large-scale wildfires. Two primary datasets are available, and have been used for evaluation of the HIGRAD/FIRETEC model: the Australian grass-fire experiment (Cheney and Gould, 1995; Cheney et al., 1998), and the International Crown Fire Modeling Experiment (ICFME) (Stocks et al., 2004). Measured fire rates of spread and fire perimeters are data available from these two experimental projects, and can be used for purposes of evaluating results from a transient, large-scale, three-dimensional wildfire CFD model.

Additionally, there are some local point-measurement data available on velocity, temperature, and incident heat flux in the ICFME data. However, it is not possible to truly validate a three-dimensional model based on a few point measurements for two reasons: first, an unknown number of numerical solutions may yield the same value as

the measurement; second, large-scale, three-dimensional, transient structures in the initial and boundary conditions may become significant, and are not well-characterized by limited point-measurement data. This is a significant challenge to the wildfire modeling community. While computing resources make feasible more complex physics-based CFD models, the current costs of measurement devices and controlled-burn experiments render any kind of thorough model validation impossible at large scales. Currently available experimental data are valuable and useful for comparison with simulation results. Nevertheless, this type of comparison for evaluation purposes must not be viewed as a rigorous validation of the model.

2.7 Summary and Motivations for Development

Modeling wildfire is not a trivial task, especially on a large scale where coarse grid resolution prevents resolution of flame sheets, and direct application of existing combustion modeling approaches. This work focuses on continued improvement of one particular numerical fire model, FIRETEC. Since FIRETEC is coupled to a hydrodynamics model, and based on models of physical processes, it is amenable to incorporating improved descriptions of gas-phase combustion chemistry. However, since flame sheets are not resolved in FIRETEC, existing ideas from combustion modeling must be adapted, and incorporated in a sub-grid model to accomplish this task. While the primary task of this research is to improve the gas-phase chemistry model, parallel efforts are in progress to also improve the solid-phase chemistry model. Finally, comparison with experimental data is needed for model evaluation, although limitations in the available experimental data are recognized.

As the availability of high-performance parallel computing resources expanded over the last decade, there arose interest in the wildfire modeling community to develop CFD computer programs to try to model wildfire behavior. CFD wildfire models are not being developed to become real-time predictors of fire behavior for use in the field; the computational cost negates use in the field and real-time prediction. However, it is hoped that CFD models can be tools that are used to gain insight into fire dynamics to somehow improve upon the existing, faster-than-real-time, operational models for fire behavior prediction.

Here are some of the key motivations behind this dissertation work:

- Desire to improve upon a simplified one-equation model (the 'local' model developed by Rod Linn) and a simplified two-equation model (The 'nonlocal' model implemented by Jonah Colman).
- Desire to bring to FIRETEC the benefits of the mixture fraction thermodynamic equilibrium approach: computational efficiency, and complex chemistry modeling capability.
- Desire to be able to then look more objectively at the performance of the simpler local & nonlocal models to answer questions such as:
    - Do the simpler models work well enough already?
    - What overall impact does the gas-phase chemistry model have on simulated fire behavior?
- Desire to 'improve' the gas-phase combustion model:
    - Opening avenues for more complex models to be incorporated, such as soot production and transport

- Prediction of an increased number of chemical species (i.e., CO, CO_2, etc.), in addition to merely oxygen and fuel.

3 Research Objectives

The objective of this research was to improve the gas-phase combustion model in FIRETEC by incorporating concepts from the mixture fraction combustion model. This objective was broken down into a few smaller tasks, as follows:

(1) Implement a thermodynamic equilibrium solver for use in a FIRETEC mixture fraction combustion model

Incorporation of a mixture fraction approach in a sub-grid model requires dynamically solving for temperature and product species mole fractions. Existing Fortran code from a recent version of NASA Chemical Equilibrium with Applications (CEA2) software was implemented for this purpose. CEA2 is used to generate a look-up table of thermodynamic equilibrium solutions, which are then be used in the mixture-fraction-based gas phase combustion model in FIRETEC. To generate the look-up table, the CEA2 Fortran code was modified to produce thermodynamic equilibrium solutions to gas mixtures with mixture fractions from 0 to 1 at increments of 0.01.

(2) Develop and implement a simple sub-grid gas-phase combustion model

A simple sub-grid model was developed based on an assumed constant value of flame temperature. This was intended to be a first-generation gas-phase model to incorporate the mixture fraction approach into FIRETEC. The mixture fraction of the

sub-grid gas-phase combustion zone was assumed to be at the stoichiometric conditions that would yield this adiabatic flame temperature at chemical equilibrium.

(3) Develop and implement an improved sub-grid gas-phase combustion model

A second-generation sub-grid gas-phase combustion model was developed based on variables that would impact sub-grid flame sheet area, such as solid mass conversion rate, wind velocities, turbulent mixing, surface area to volume ratio of the solid fuel, flame length (using an appropriate correlation), and oxygen concentration.

(4) Evaluate the new models

The new sub-grid combustion model was implemented in FIRETEC, and results from this revision of FIRETEC were compared to an empirical function for fire spread in grasslands, obtained from experimental burns conducted in Australian grasslands. Simulation results were also compared to results from previous revisions of the FIRETEC code. These comparisons were performed to evaluate the impacts of simplifying assumptions made in the new sub-grid model, as well as the costs and benefits associated with implementing the new sub-grid gas-phase combustion model.

Final test simulations included:

- Four grassfire cases, four California chaparral cases, and four Ponderosa pine cases using the first-generation constant radius sub-grid pocket model for gas phase combustion.
- Eight more grassfire cases using the first-generation constant radius sub-grid pocket model. However, these eight cases were performed using an updated

version of the HIGRAD/FIRETEC computer code, which included corrections to the FIRETEC radiative heat transfer model.

- Four grassfire cases using the second-generation sub-grid gas-phase combustion model.
- Four grassfire cases using the 'local' model' for comparison purposes, and using the most recently developed version of FIRETEC.

4 Implementation of a Thermodynamic Equilibrium Model

The gas phase, mixture-fraction-based combustion model developed for this dissertation work relies on thermodynamic equilibrium to calculate flame temperatures and product species compositions. Thermodynamic equilibrium solution values for flame temperatures and product species compositions are stored in a look-up reference table generated by using an equilibrium chemistry solver. Tabulated experimental data could be used instead of tabulated equilibrium calculations, but for this dissertation work a chemical equilibrium solver was employed to generate a look-up reference table.

4.1 Mixture Fraction Definitions and Equations

The mixture fraction, f, is defined as the fraction of mass that originated from a primary source.

$$f = \frac{m_p}{m_p + m_s} \tag{4-1}$$

The primary source could be the fuel inlet port of a methane burner, for example. Mass from the primary source, m_p, is referred to as primary material. Though the primary source is often chosen to be a fuel inlet source to the system, the choice of primary source is arbitrary. The only requirement is that the properties of the primary source be known. These properties include the elemental composition and the enthalpy evaluated at the

source temperature. The remaining mass in the system originates from a secondary source and is referred to as secondary material, m_s. The properties of the secondary material must also be known (Smoot and Smith, 1985).

When the properties of the primary and secondary material are known, the properties of any mixture of primary and secondary material can be calculated as a simple linear combination of the source material properties. For example, the enthalpy of the mixture can be calculated by

$$h = f\, h_p + (1 - f)\, h_s \,, \qquad \textbf{(4-2)}$$

where h_p is the enthalpy of the primary material, and h_s is the enthalpy of the secondary material. Note that in equation (4-2), the system is assumed to be adiabatic. When the system is not adiabatic, the enthalpy of the reacting mixture would be calculated as follows:

$$h = f\, h_p + (1 - f)\, h_s + h_r \qquad \textbf{(4-3)}$$

where h_r is defined as the residual enthalpy (Smoot and Smith, 1985).

With the properties of a reacting mixture determined, namely the mixture enthalpy, pressure and the mixture elemental composition, the equilibrium product temperature and composition can be calculated by a minimization of the Gibbs energy for the mixture (Gordon and McBride, 1994). The reference look-up table is generated by making a sequence of equilibrium calculations over a range of the mixture fraction, f.

4.2 Chemical Equilibrium

The NASA Chemical Equilibrium with Applications program (McBride and Gordon, 1996) was adapted and used to generate a look-up table of thermodynamic

equilibrium solutions covering the range of mixture fractions, $0 \leq f_r \leq 1$, where f_r is the mixture fraction of the reacting mixture. The input primary material was specified by weight percent of species as listed in Table 4-1 at an initial temperature of 700 K. This gas composition given in Table 4-1 was based on analyses of rapid pyrolysis products for dried samples of cellulose and lignin by previous researchers (Hajaligol et al., 1982; Nunn et al., 1985). It is assumed that the pyrolysis of the solid vegetation results in this same gas composition.

The input secondary material was specified as air (76.7 wt% N_2, 23.3 wt% O_2), also at a temperature of 700 K. This initial temperature of 700 K was chosen to roughly approximate the thermodynamic conditions of pre-heated reactants within the vicinity of gas-phase wildland fire combustion. This does not mean that the gases will necessarily be at a temperature of 700 K prior to reaction in the model. The temperature of 700 K is only used in the calculation of the initial enthalpy of the gas mixture. Combustion of the mixture in the model is then assumed to occur under locally adiabatic conditions, such that any residual enthalpy, h_r, is always neglected. These assumptions of an initial temperature and locally adiabatic conditions were necessary due to the form of the energy equation in HIGRAD.

The energy equation in FIRETEC was cast in terms of potential temperature, which is a conventional form of the energy equation for fluid dynamics models that are developed by the atmospheric science community. The conversion from the gas potential temperature to the actual gas temperature is trivial, but to calculate the enthalpy of any particular gas mixture, one must specify the temperature, pressure, and composition of the gas. Given temperature, pressure, and composition, the gas enthalpy can be calculated

easily with reference to an appropriate thermodynamic table. Unfortunately, information on the exact gas composition was not available in FIRETEC, because it was not feasible to explicitly model the transport of a large number of distinct gas species. For this reason, the gas enthalpy could not be accurately determined in the FIRETEC model, and the development of the equilibrium mixture-fraction-based model for FIRETEC required a method of estimating the enthalpy of the reacting gas mixture.

With the energy equation cast in terms of potential temperature, it is possible to convert potential temperature to enthalpy by assuming that the heat capacities of all species are a constant average value, and that the heats of formation of all species are 0 J/kg at 0 K. Making these two assumptions does not seem any more justifiable than assuming locally adiabatic combustion and material properties evaluated at 700 K, which was the method chosen to estimate the enthalpy of the reacting gas mixture in this work. Otherwise, it would become necessary to track all species mass fractions globally throughout the model, a computational task that would be beyond reason and eliminate the efficiency benefits gained by applying the thermodynamic equilibrium assumption in a gas-phase combustion model.

Product species considered in the equilibrium solution routine in this study were limited to CH_4, CO_2, H_2, NH_3, N_2, OH, C(solid), CO, H, H_2O, NO, O, and O_2. The reason for the limitation is simply to avoid creating an overly-large look-up reference table. However, it is possible to consider any chemical species by either using the extensive NASA library of thermodynamic properties, or manually specifying the thermodynamic properties of the species. For this dissertation work, detailed equilibrium solutions were made over the range of mixture fractions, $0 \leq f_r \leq 1$. These detailed equilibrium solutions

considered all possible chemical species in the NASA thermodynamic property library, and they were examined to determine which product species were present in significant quantities.

Table 4-1. Composition of hydrocarbon-like combustible gas used in mixture fraction model simulations (Colman and Linn, 2005).

Species	wt%	Species	wt%
CO_2	16.04%	C_2H_4	3.49%
H_2O	15.97%	C_2H_6	0.50%
CO	46.87%	C_3H_6	1.05%
H_2	2.49%	CH_3OH	3.98%
CH_4	5.98%	CH_3CHO	3.65%

From the generated look-up table of thermodynamic equilibrium solutions, values of combustion flame temperatures as a function of mixture fraction are shown in Figure 4-1. Note that the peak flame temperature occurs at or near the stoichiometric value of the mixture fraction, which is 0.188 in this case. The peak flame temperature is high due to the enthalpy of the mixture being calculated for an assumed initial temperature of 700 K. Also note that at a mixture fraction of 1.0, the reaction of pure fuel would result in an equilibrium product temperature that would be higher than the initial temperature of 700 K. This is due to presence of oxygen within the fuel, which could theoretically react with the carbon and hydrogen in the fuel to produce heat.

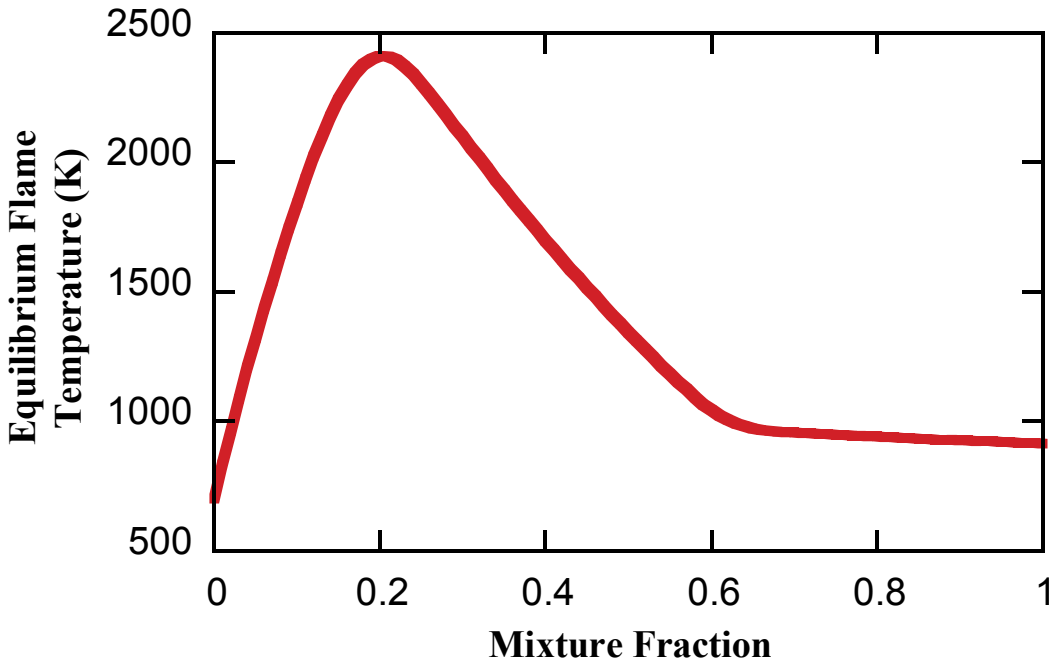

Figure 4-1. Equilibrium flame temperature as a function of mixture fraction for the combustion of 'hydrocarbons' with air.

Values of product species mole fractions corresponding to Figure 4-1 are shown in Figure 4-2, with major species plotted in Figure 4-2*a* and minor species plotted in Figure 4-2*b*. Near the stoichiometric mixture fraction, the primary products of combustion are CO_2 and H_2O. However, at more fuel rich mixture fractions greater than 0.2, CO and H_2 become significant combustion products. At very fuel rich mixture fractions greater than 0.6, CH_4 and C(solid) are predicted equilibrium products. C(solid) can be thought of as a driving force for soot, and the prediction of C(solid) production using the mixture fraction equilibrium model may provide an avenue to incorporation of a simple soot production and transport model.

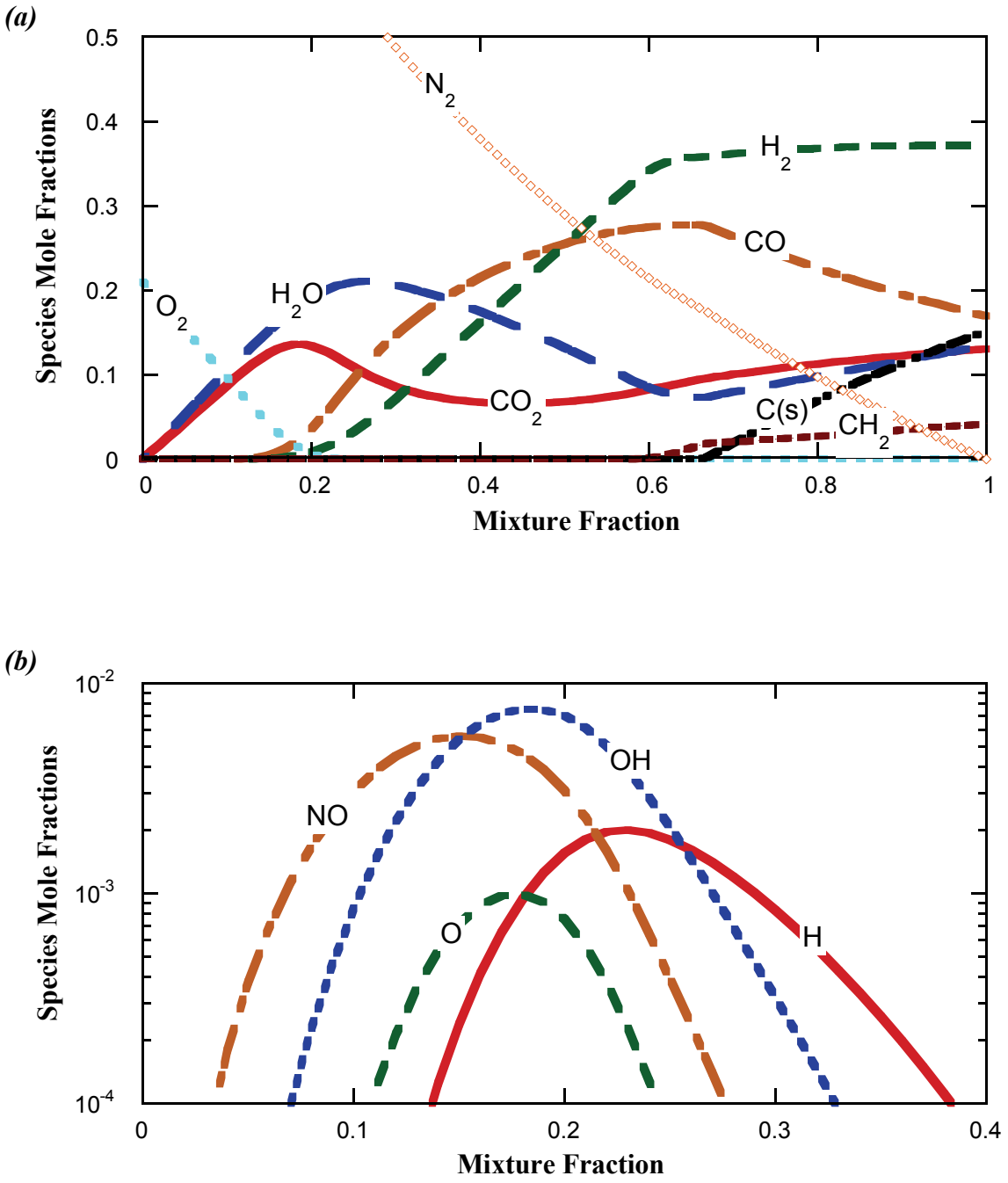

Figure 4-2. **Equilibrium product species mole fractions as a function of mixture fraction for the combustion of the selected hydrocarbon mixture with air. *(a)* Major species. *(b)* Minor species with NH_3 excluded, because its mole fraction was less than 10^{-4}.**

In order to illustrate the versatility of using a chemical equilibrium model, equilibrium flame temperature predictions were generated for three different types of fuel-air systems. The three types of fuels were:

- The selected hydrocarbon mixture given in Table 4-1
- Methane
- A fuel of elemental composition based on standard ultimate analysis of the foliage of four California chaparral species (Pickett, 2007), which had an average elemental composition of 52.17% carbon, 6.43% hydrogen, 1.29% nitrogen, and 40.11% oxygen (wt%, dry ash free basis.)

Initial reactant temperatures in this comparison were 700 K, and the species considered at chemical equilibrium were limited to CO, CO_2, H, H_2, H_2O, NO, N_2, O, OH, O_2, NH_3, CH_4, C(solid), HCN, HNC, NO_2, and C_2H_2. Note that four additional species were considered in this comparison (HCN, HNC, NO_2, and C_2H_2) since the presence of these species became significant in the converged equilibrium solutions for the methane and California chaparral fuel types. A comparison of flame temperatures for three different primary streams is shown in Figure 4-3, which is shown to illustrate that thermodynamic equilibrium solutions can be generated for a variety of possible reactive gas mixtures. This allows for a certain amount of flexibility in choosing fuel properties, without adding significant computational burden to the modeling task.

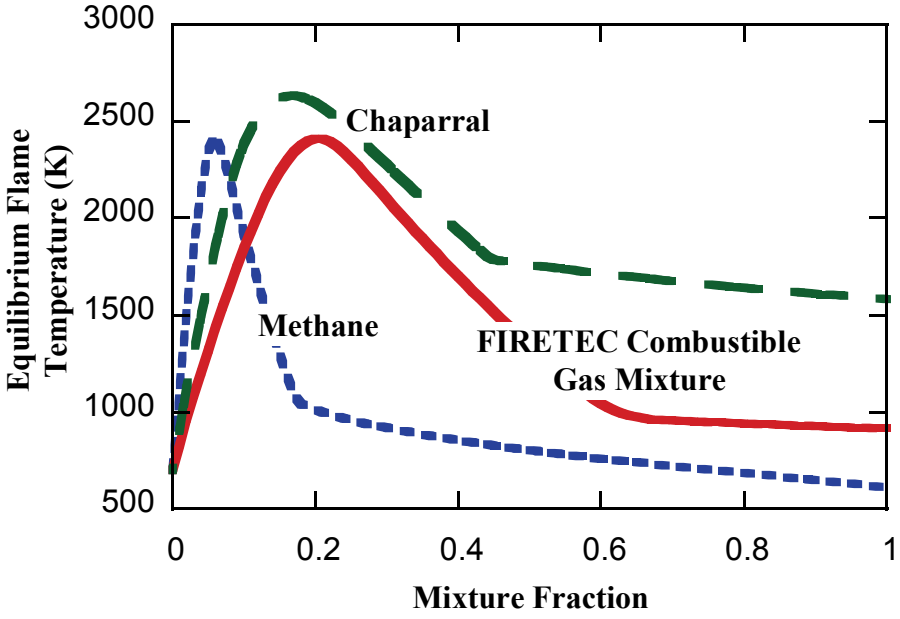

Figure 4-3. **Comparison of predicted equilibrium flame temperatures for (1) the combustible gas mixture used in the 'nonlocal' and sub-grid pocket models, (2) methane, and (3) a combustible gas mixture from chaparral, assuming the same elemental composition as the unburned foliage.**

5 First-Generation Sub-Grid Mixture Fraction Model

Computational costs constrain grid refinement in HIGRAD/FIRETEC, limiting resolution to length scales on the order of 1 m. Since the physics and chemistry of combustion are impossible to resolve with the grid resolution on the order of meters in HIGRAD/FIRETEC, it becomes necessary to utilize sub-grid models to account for these phenomena. To facilitate the application of the mixture fraction model to HIGRAD/FIRETEC, a new sub-grid model was conceived and developed in order to account for the fact that volatiles and oxygen are not homogeneously distributed within the cells. This new sub-grid model is described in detail in this chapter. A discussion of simulation results from the new model is included as well.

5.1 Constant Radius Pocket Model Development

Gas phase combustion in wildfire consists primarily of the oxidation of carbon-based molecules pyrolyzed from solid vegetation. In wildfire combustion, the products of solid pyrolysis are a mixture of combustible hydrocarbon-like gases. For purposes of the first-generation sub-grid mixture fraction model, it is assumed that in wildfires, combustible hydrocarbon-like gases reside within spherical pockets. These spherical hydrocarbon pockets are represented in 2-D by the solid circle in Figure 5-1, which is a simplified cartoon shown to illustrate the first-generation sub-grid mixture fraction

model. The circle on the left is the unreacted hydrocarbon volume. Assuming that unburned hydrocarbons reside within spherical pockets, mixing and reaction of hydrocarbons and oxygen molecules occurs in the boundary region between the pocket and the surrounding air. A certain volume of air surrounding these pockets and unburned hydrocarbons within these pockets mixes and reacts, forming product chemical species and producing heat. This mixed volume is illustrated in the right-hand figure in Figure 5-1 by the shaded region between the dashed boundaries, and is labeled 'hydrocarbon-air mixture.'

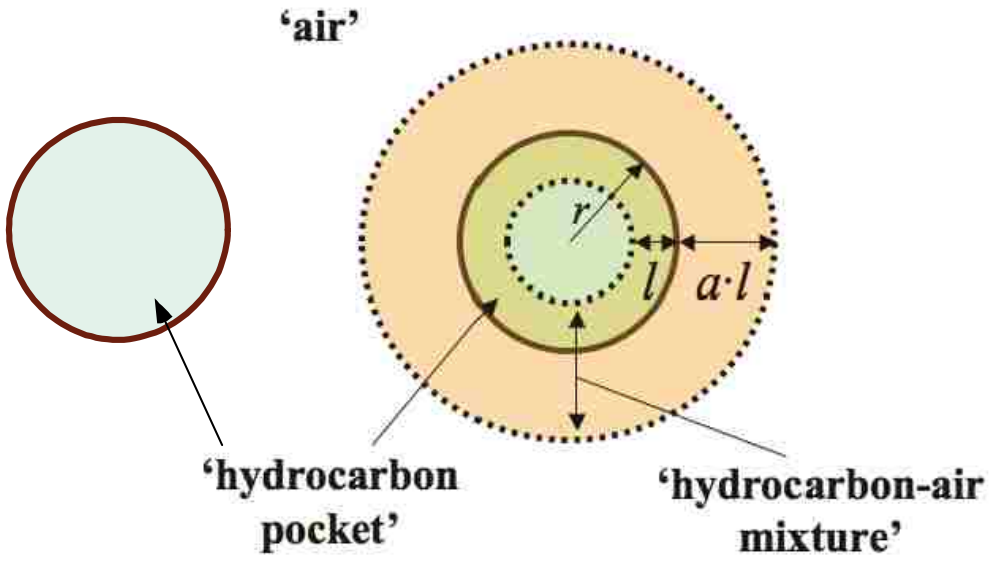

Figure 5-1. Illustration of a sub-grid spherical 'pocket' of combustible gas mixing with surrounding air.

The mixing of air and hydrocarbons is assumed to occur in the boundary layers on both the inside ($r - l$) and the outside ($r + l \cdot a$) of the hydrocarbon pocket. The length over which air and combustible gases mix is then $l + l \cdot a$, as depicted in Figure 5-1 by the lightly shaded region. These parameters are meant to help describe the area and thickness

of a mixing zone at the interface of the volatiles-rich and oxygen-rich zones. The parameters *r*, *l*, and *a* are not defined as functions of any specific resolved quantities in the hydrodynamics model; however, future research could investigate how these parameters depend on resolved quantities such as pyrolysis rate, inhomogeneity of fuels, and turbulence. It is also anticipated that these parameters might evolve with time and space as volatiles are transported and react in the flow field (i.e., the pocket radius decreases as volatiles combust). In this model, the pocket radius is held constant in time and space; instead of tracking the changes that would occur in the pocket radius with shrinking pockets, it is assumed that the number of pockets decreases as gases react. By specifying *r*, *l*, and *a*, and solving for both the density of unreacted combustible gas (i.e. the number of pockets of combustible gas in a cell) and the mixture fraction within a computational cell from transport equations, the local mixture fraction of the reacting 'hydrocarbon-air mixture' can be calculated. This is shown in the following sequence of equations.

For each hydrocarbon pocket, the volume $V_{HC,r}$ of combustible gas (hereafter referred to as hydrocarbons) that mixes and reacts between *r* and (*r*–*l*) is determined by calculating the difference between the volume of one sphere inside another as shown:

$$V_{HC,r} = \frac{4}{3}\pi r^3 - \frac{4}{3}\pi (r-l)^3 \qquad \textbf{(5-1)}$$

which simplifies to:

$$V_{HC,r} = \frac{4}{3}\pi\left(3lr^2 - 3l^2 r + l^3\right) \qquad \textbf{(5-2)}$$

Likewise, the volume $V_{air,r}$ of air that mixes and reacts between *r* and $r + l \cdot a$, is calculated as follows:

$$V_{air,r} = \frac{4}{3}\pi\left(r + a\,l\right)^3 - \frac{4}{3}\pi\, r^3 \qquad \textbf{(5-3)}$$

which simplifies to:

$$V_{air,r} = \frac{4}{3}\pi\left(3alr^2 + 3a^2l^2r + a^3l^3\right) \qquad \textbf{(5-4)}$$

The volume of reacting mixture is the sum of the volumes of reacting hydrocarbons and air, which were calculated by equations (5-2) and (5-4). This sum is given by:

$$V_{HC,r} + V_{air,r} = \frac{4}{3}\pi\left[\left(3l + 3al\right)r^2 + \left(3a^2l^2 - 3l^2\right)r + a^3l^3 + l^3\right] \qquad \textbf{(5-5)}$$

The volume fraction of the reacting mixture in a pocket that consists of pure hydrocarbons (χ) is then calculated.

$$\chi = \frac{V_{HC,r}}{V_{HC,r} + V_{air,r}} = \frac{3r^2 - 3lr + l^2}{\left(3 + 3a\right)r^2 + \left(3a^2l - 3l\right)r + a^3l^2 + l^2} \qquad \textbf{(5-6)}$$

Next, the volume fraction of reacting gases within a computational cell (ϕ_r) is calculated.

$$\phi_r = \frac{N_{pockets}\left(V_{HC,r} + V_{air,r}\right)}{V_{cell}} \qquad \textbf{(5-7)}$$

The number of reacting pockets is calculated by dividing the total volume of hydrocarbons in a computational cell by the volume of one pocket, i.e.,

$$N_{pockets} = \frac{m_{HC}\hat{V}_{HC}}{\frac{4}{3}\pi r^3} \qquad \textbf{(5-8)}$$

.

Substituting equations (5-5) and (5-8) into equation (5-7) one obtains:

$$\phi_r = \frac{m_{HC}\hat{V}_{HC}}{\frac{4}{3}\pi r^3}\,\frac{\frac{4}{3}\pi\left[\left(3l + 3al\right)r^2 + \left(3a^2l^2 - 3l^2\right)r + a^3l^3 + l^3\right]}{V_{cell}} \qquad \textbf{(5-9)}$$

.

Equation (5-9) can then be simplified to:

$$\phi_r = \frac{\overline{\hat{\rho}}_{HC}\hat{V}_{HC}}{r^3}\left[(3l+3al)r^2+\left(3a^2l^2-3l^2\right)r+a^3l^3+l^3\right], \qquad \textbf{(5-10)}$$

where the mass of hydrocarbons per volume of cell is now given by the density, $\overline{\hat{\rho}}_{HC}$. Recall that the caret above a density (i.e. $\overline{\hat{\rho}}_{HC}$) indicates that the quantity has been spatially averaged over the cell volume. The over bar indicates that the density quantity is an ensemble average over many temporal realizations. These are two types of averaging used in the development of the FIRETEC equations for modeling transport for wildfires, in which both temporal fluctuations and spatial inhomogeneities may be present in the flow field.

The specific volume term in equation (5-10) for the reacting hydrocarbons, $\hat{V}_{HC}$, is calculated assuming ideal gas, i.e.,

$$\hat{V}_{HC} = \frac{RT_{HC}}{M_{HC}P}. \qquad \textbf{(5-11)}$$

Next, the mass of reacting hydrocarbons and air per computational cell volume are calculated. These masses per cell volume are represented by the density terms shown as follows.

$$\rho_{HC,r} = \frac{\chi\phi_r}{\hat{V}_{HC}} = \frac{\chi\overline{\hat{\rho}}_{HC}\left[(3l+3al)r^2+\left(3a^2l^2-3l^2\right)r+a^3l^3+l^3\right]}{r^3}, \qquad \textbf{(5-12)}$$

and

$$\rho_{air,r} = \frac{(1-\chi)\phi_r}{\hat{V}_{air}} = \frac{(1-\chi)\overline{\hat{\rho}}_{HC}\left[(3l+3al)r^2+\left(3a^2l^2-3l^2\right)r+a^3l^3+l^3\right]}{r^3}\frac{\hat{V}_{HC}}{\hat{V}_{air}}. \qquad \textbf{(5-13)}$$

The ratio of the specific volume of hydrocarbons to that of air is assumed to be approximately one, since gases are assumed ideal and the temperatures and molecular weights of the hydrocarbons and air are similar.

$$\frac{\hat{V}_{HC}}{\hat{V}_{air}} = \frac{T_{HC}}{T_{air}} \frac{M_{air}}{M_{HC}} \approx 1 \qquad \textbf{(5-14)}$$

This approximation simplifies the equation for the density of reacting air to quantities in the model that are either resolved or specified, yielding

$$\rho_{air,r} = \frac{(1-\chi)\bar{\hat{\rho}}_{HC}\left[(3l+3al)r^2 + \left(3a^2l^2 - 3l^2\right)r + a^3l^3 + l^3\right]}{r^3}. \qquad \textbf{(5-15)}$$

Since it is more convenient to operate in terms of bulk density, rather than mass, the mixture fraction is computed from the bulk densities in the model. The overall mixture fraction in a computational cell is defined as the fraction of elemental mass in the cell that originated from a primary source:

$$\bar{f}_{cell} \equiv \frac{\bar{\hat{\rho}}_p}{\bar{\hat{\rho}}_p + \bar{\hat{\rho}}_s}. \qquad \textbf{(5-16)}$$

For wildfires, the primary source is chosen as the production of hydrocarbons from pyrolysis. The chemical and physical properties of this primary material are calculated at 700 K for the gas mixture described in Colman and Linn (2005), listed earlier in Table 4-1. It is assumed that the spherical pockets contain only pure, *unreacted* primary material; therefore, the mixture fraction of these pockets, $f_{HCpocket} = 1$. Primary material which has already *reacted* no longer resides within the spherical pockets, but is assumed to be evenly mixed in the air surrounding the pockets. Therefore, a mass fraction of primary material (a mixture fraction) in air can also be computed. The mixture fraction of the air in the cell (i.e. the mass fraction of *reacted* primary material in air) is

$$f_{air} = \frac{\rho_{p,air}}{\overline{\rho} - \overline{\hat{\rho}}_{HC}}, \tag{5-17}$$

where the density of primary material in the air, $\rho_{p,air}$, is the mass of primary material per cell volume that have already reacted and no longer reside within spherical pockets. The density of primary material in the air can be computed as the difference between the total density of primary material in the cell and the density of unburned primary material located in hydrocarbon pockets, i.e.,

$$\rho_{p,air} = \bar{f}_{cell}\overline{\rho} - \overline{\hat{\rho}}_{HC}. \tag{5-18}$$

Substituting Equation (5-18) into Equation (5-17), the expression for the mixture fraction of the air in the cell becomes:

$$f_{air} = \frac{\rho_{p,air}}{\overline{\rho} - \overline{\hat{\rho}}_{HC}} = \frac{\bar{f}_{cell}\overline{\rho} - \overline{\hat{\rho}}_{HC}}{\overline{\rho} - \overline{\hat{\rho}}_{HC}}. \tag{5-19}$$

Finally, the mixture fraction of the reacting mixture can be calculated:

$$f_r = \frac{f_{HCpocket}\rho_{HC,r} + f_{air}\rho_{air,r}}{\rho_{HC,r} + \rho_{air,r}}. \tag{5-20}$$

The flame temperature and mole fractions of combustion products are obtained by interpolation from a look-up table of stored thermodynamic equilibrium calculations. The look-up table covers the entire range of possible mixture fractions, $0 \le f_r \le 1$, and is generated prior to running the simulation. The heat of reaction is not calculated explicitly; rather, it is approximated using an energy balance. Assuming that all species have constant heat capacities equal to that of air and that conditions are adiabatic, the heat of reaction is approximately equal to the change in sensible heat that results from the

reaction. The flame temperature is used to estimate the change in sensible heat, calculated by multiplying the heat capacity of air by the difference between the flame temperature and the average gas temperature in the cell prior to reaction.

$$\Delta H_{rxn} \approx \Delta H_{sensible} \approx c_p \left(T_{flame} - \overline{T}_{gas} \right) \qquad \textbf{(5-21)}$$

Equation (5-21) might seem like an oversimplification in modeling the energy produced during the gas-phase combustion processes. However, as was previously mentioned, the formulation of the energy equation in HIGRAD is cast in terms of potential temperature. The enthalpy of the total gas mixture could be calculated if the concentrations of all gas-phase chemical species were explicitly tracked. Lacking the necessary detail for a thermodynamically consistent method of converting from potential temperature to enthalpy, equation (5-21) is used to approximate the change in energy due to gas-phase combustion. The other option is to assume a standard enthalpy of the gas mixture at 0 K, assume a constant heat capacity, and calculate the enthalpy at any temperature, i.e.;

$$h(T) = c_p T \,. \qquad \textbf{(5-22)}$$

However, considering the huge temperature ranges and wide variety of gas mixtures to be encountered in a wildfire scenario, equation (5-22) does not provide a reliable means to estimate the enthalpy of the reacting mixture. This is the primary justification for choosing to use equation (5-21) to estimate the heat of reaction, working within the framework of the existing HIGRAD/FIRETEC model.

Two features of the mixture fraction PDF model are not applied to this sub-grid mixture fraction wildfire combustion model. First, the concept of residual enthalpy, h_r, is not used. The implication of not being able to calculate the total enthalpy is that it is not

possible to determine the residual enthalpy, h_r, for the reacting mixture. In this model the enthalpies of the primary and secondary material are calculated at a specified temperature, and the combustion of the mixture is assumed to be locally adiabatic. Thus, the adiabatic equilibrium flame temperature determines the product temperature in the portion of the grid cell that is reacting at a given time. The other feature from the mixture fraction probability density function (PDF) model that is not used is the PDF itself. The local variance in the mixture fraction is not treated in this first-generation sub-grid mixture fraction model. Therefore, no attempt is made at this point to apply a PDF in the gas-phase equilibrium combustion calculation as is commonly utilized in the standard mixture fraction PDF model.

5.2 Numerical Simulations

A suite of HIGRAD/FIRETEC simulations was performed using the implemented mixture fraction model for gas-phase combustion. Fire spread was simulated in three fuel beds: grass, California chaparral, and Ponderosa pine. Four simulations were performed for each fuel bed with inlet wind velocities of 1, 3, 6, and 12 $m \cdot s^{-1}$, for a total of 12 simulations. The domain for all simulations was 320 m x 320 m x ~600 m. The grid was uniform in the horizontal dimensions nodes spaced at 2 m intervals. In the vertical dimension the grid was not uniform; the grid was stretched with the vertical spacing of the nodes at ~1.5 m in the ground layer, and further apart with increasing vertical elevation. All fuel beds covered the entire surface of the domain, the topography was flat, and a neutral atmospheric stability was assumed.

A parametric study was performed on a smaller 80 m x 80 m x ~600 m domain to determine appropriate values for r, l, and a. Many values of the parameter values which were tested in this initial parametric study failed to produce a successful simulation of a propagating wildfire. The best values of the pocket parameter from this parametric study were: r = 0.01 m, $l = 0.67 \cdot r$, and a = 2.5. These specified values for pocket model parameters were used in the simulations described in this chapter.

5.2.1 Description of Fuel Bed Properties Used in Simulations

Grass fuel beds were defined to consist of evenly distributed grass at a height of 0.7 m, covering the entire ground-layer surface of the domain. As mentioned previously, the height of the fuel bed can be specified arbitrarily by the user. For this work, the height of grass, and all other fuel properties and conditions were chosen so as to be consistent with previous FIRETEC simulations (Colman and Linn, 2005; Linn and Cunningham, 2005; Linn et al., 2005). The fuel loading for grass was 0.7 $kg \cdot m^{-2}$, and the initial moisture content of the grass was 5%. Moisture contents were given on a dry-fuel basis, meaning the mass of moisture in the vegetation per mass of dry vegetation. Since moisture contents are given on a dry basis, it is possible to have moisture contents greater than 100%, meaning that more than one half of the mass of vegetation is moisture.

The fuel bed for Ponderosa pine simulations was modeled similarly to a previously reported method (Linn et al., 2005). The fuel bed consisted of a Ponderosa pine canopy distributed across the fuel layer based on measurements that included detailed tree location data from a plot surveyed by the USDA Forest Service Rocky Mountain Research Station. The maximum canopy height was 19.9 m, the average canopy bulk density was ~0.12 $kg \cdot m^{-3}$, and the initial moisture content of the canopy was

specified as 130% (kg moisture/kg dry fuel). Ground layer fuels were distributed as follows: solid fuel representative of pine needle litter with a moisture content of 10% in areas underneath the canopy, and grass with a moisture content of 5% in areas where the canopy was thinner, or open. The maximum bulk density of both grass and litter was 1.0 $kg \cdot m^{-3}$.

The fuel bed for chaparral simulations was modeled using the same routine used for Ponderosa pine simulations. However, in the case of the chaparral fuel beds, the fuel distribution was not based on data from specific field surveys. The average crown diameter was 2.5 m, with 60% coverage, and shrub heights between 1-2 m. The initial fuel moisture content for the canopy was specified as 130%. For the ground layer fuels the specified moisture contents were 5% for grass and 10% for litter, with the maximum bulk density of both the grass and litter being 1.0 $kg \cdot m^{-3}$.

Ignition for all simulations began along a strip 100 m long and 4 m wide, at a location 60 m downwind from the wind inlet boundary, and centered in the crosswind direction of the domain. Within this strip of the computational domain, the solid temperature was artificially increased from 300 K to 1000 K over 2 seconds of simulated time. This ignition method was consistent with previous simulations performed using the 'local' and 'nonlocal' models (Colman and Linn, 2005; Linn and Cunningham, 2005).

5.2.2 Combustible Gas Properties

The properties of the combustible gas were specified based on the composition of the hydrocarbon-like gas mixture used in the 'nonlocal' model (Colman and Linn, 2005). This gas composition was based on analyses of rapid pyrolysis products for both cellulose and lignin by previous researchers (Hajaligol et al., 1982; Nunn et al., 1985).

The elemental composition of the pyrolysis products was specified based on these studies of cellulose and lignin pyrolysis. The elemental composition is given in Table 5-1.

Table 5-1. Assumed elemental composition of pyrolysis products

Element	*Weight %*
Carbon	37
Hydrogen	7
Oxygen	56

The species compositions of the primary material stream used in the mixture fraction model are shown in Table 5-2. The species compositions in Table 5-2 match the elemental composition shown above. The same primary stream properties were used for grass, chaparral, and Ponderosa simulations in this work. However, with the sub-grid gas-phase combustion model developed in this work, it becomes possible for one to specify primary stream properties that are unique to specific individual fuel types as long as the elemental composition of each fuel type is known. This is one feature that opens possible avenues for future model development, adding value to the FIRETEC model.

Table 5-2. Composition of hydrocarbon-like combustible gas used in mixture fraction model simulations (Colman and Linn, 2005).

Species	**wt%**	**Species**	**wt%**
CO_2	16.04%	C_2H_4	3.49%
H_2O	15.97%	C_2H_6	0.50%
CO	46.87%	C_3H_6	1.05%
H_2	2.49%	CH_3OH	3.98%
CH_4	5.98%	CH_3CHO	3.65%

5.2.3 Computational Cost

One motivation behind the implementation of a mixture-fraction-based equilibrium model was to obtain more detailed model predictions without adding significant computational burden to the overall FIRETEC computer program. Instead of solving a number of species continuity equations containing kinetic rate expressions as source and sink terms, the mixture fraction model accesses tabulated thermodynamic equilibrium solutions, in other words a numerical look-up table. Accessing the look-up table for equilibrium solutions is more efficient than computing kinetic rates while solving a complex kinetic mechanism. Nevertheless, there is still some computational cost associated with solving the continuity equation for the mixture fraction, as well as the numerical interpolation to find solutions between tabulated points on the equilibrium look-up table.

Simulations for this dissertation were performed on parallel supercomputing clusters at Los Alamos National Laboratory and Brigham Young University. The Los Alamos National Laboratory Coyote cluster was composed of AMD Opteron 2.6 GHz processors with 1 MB secondary cache, 2 processors per computational node with each node sharing 8 GB of RAM, Voltaire InfiniBand interconnects for low-latency networking, and a large Panasas file system for scratch disk storage. The Brigham Young University Marylou4 cluster was composed of Dual-core Intel Xeon EM64T 2.6 GHz processors, 2 processors per computational node with each node sharing 8 GB of RAM, Ethernet networking between nodes, and a large Ibrix file system for scratch disk storage. Intel Fortran compilers with compatible Message Passing Interface libraries were used on both clusters to compile the FIRETEC Fortran computer code.

Data storage requirements for FIRETEC simulations were quite high depending upon the frequency of data output from the simulation and the size of the computational domain. For example, simulations in this dissertation were performed with a computational domain of 160x160x41 nodes. These simulations produced data output files which were ~140 MB each. With data output files stored at intervals of 100 time steps, each simulation in this dissertation required between 20 and 40 GB of storage space. The effort to extract data from these output files and visualize these data was not trivial.

Three runs were performed on the Los Alamos National Laboratory Coyote cluster to compare the computational costs associated with the three different combustion models in the FIRETEC code: the 'local' model, the 'nonlocal' model, and the mixture fraction pocket model. The Intel Fortran compiler with associated MPI libraries were used to compile the code with a level -02 optimization for all three runs. The simulation scenario was a grass fuel bed having the same characteristics as described previously, ambient wind at 6 $m \cdot s^{-1}$, and a 4 meter by 100 meter fire line ignition. All three simulations were run on 64 processors for 100 seconds of simulated time. In Table 5-3 the total CPU times are given for each simulation run. The total CPU times were reported by the Coyote cluster batch scheduler, and represent the number of seconds of compute time the simulation consumed on each processor, summed over all 64 processors. To clarify this definition with an example, a run which consumed 1000 seconds on each of 10 processors would have a reported total CPU time of 10000 seconds.

For this particular simulation scenario (grassfire, 6 $m \cdot s^{-1}$ ambient wind, 4 meter by 10 meter ignition line), the use of the mixture fraction pocket model in FIRETEC only

consumed 7% more compute time than the use of the 'local' model in FIRETEC. This minimal addition in computational time is quite acceptable considering the potential avenues for future development that the mixture fraction pocket model provides by producing more detailed predictions of combustion product chemical species. In addition, future work could be done to optimize the FIRETEC computer code in order to improve the overall numerical efficiency of the program.

Table 5-3. Compute times for the three FIRETEC combustion models: local, nonlocal, and sub-grid mixture fraction pocket models.

Model	*Local*	*Nonlocal*	*Mixture Fraction Pocket Model*
Total Simulated Time (s)	100	100	100
Number of processors	64	64	64
Total CPU time (s)	8.351×10^5	8.636×10^5	8.934×10^5
CPU Time/Simulated Time	8351	8636	8934
% increase over Local model		3.41%	6.98%

5.2.4 Grassfire Simulations

Fire downwind spread distance was defined as the distance to the point farthest downwind where the solid temperature was above 500 K. Lateral spread distance was defined likewise for spread in the crosswind direction. The downwind spread distance and lateral spread distance are illustrated in Figure 5-2. Overall fire spread rates were determined by taking the time derivative of the downwind spread distance using simple linear regression. The downwind spread distance is plotted for four grass fire simulations, shown in Figure 5-3*a*. Lateral spread distance is shown in Figure 5-3*b*. The simulations yielded a trend of more rapid fire spread at higher ambient wind velocities. In the 1 $m\cdot s^{-1}$

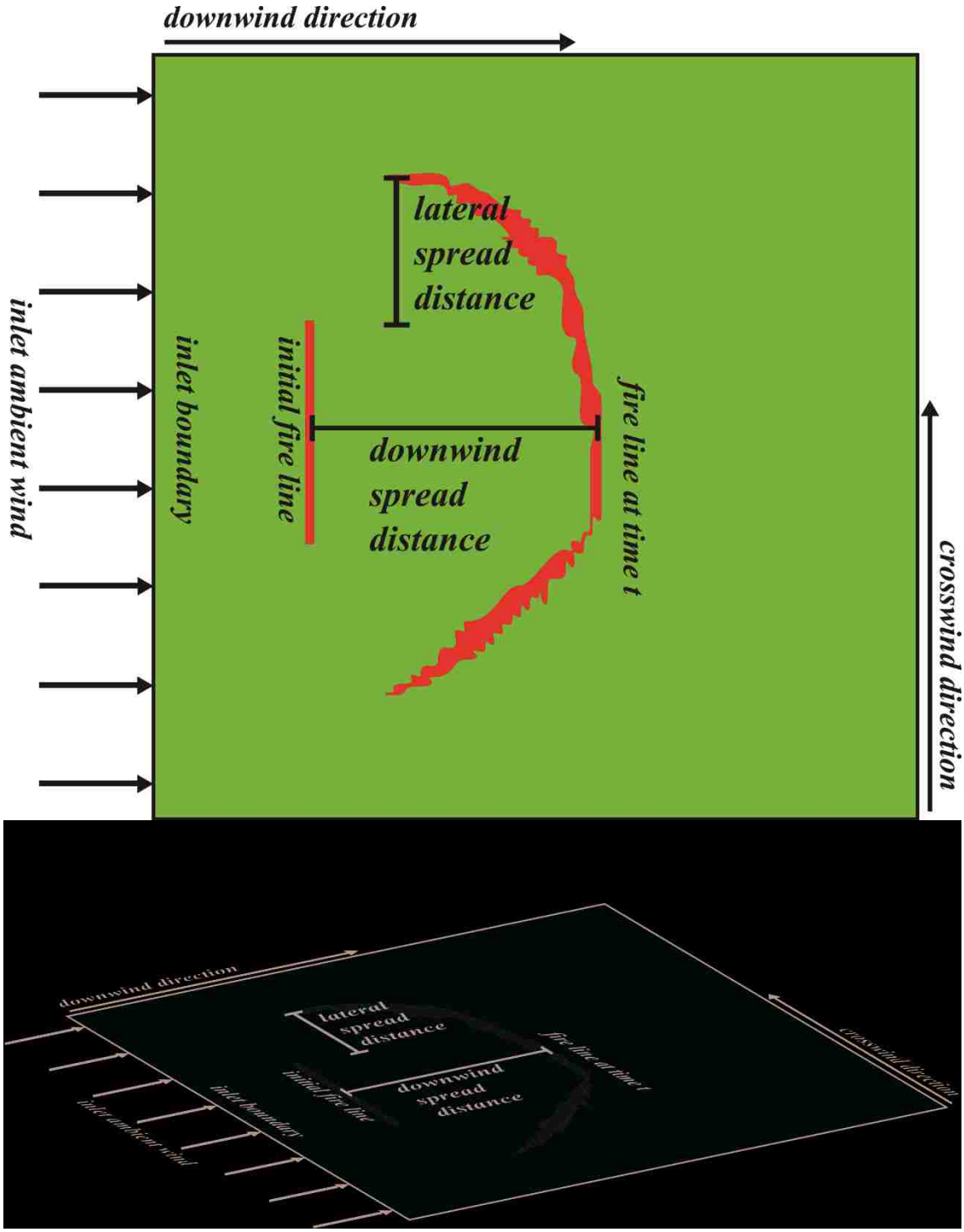

Figure 5-2. Illustration of downwind and lateral spread distances for simulated line fires.

(a)

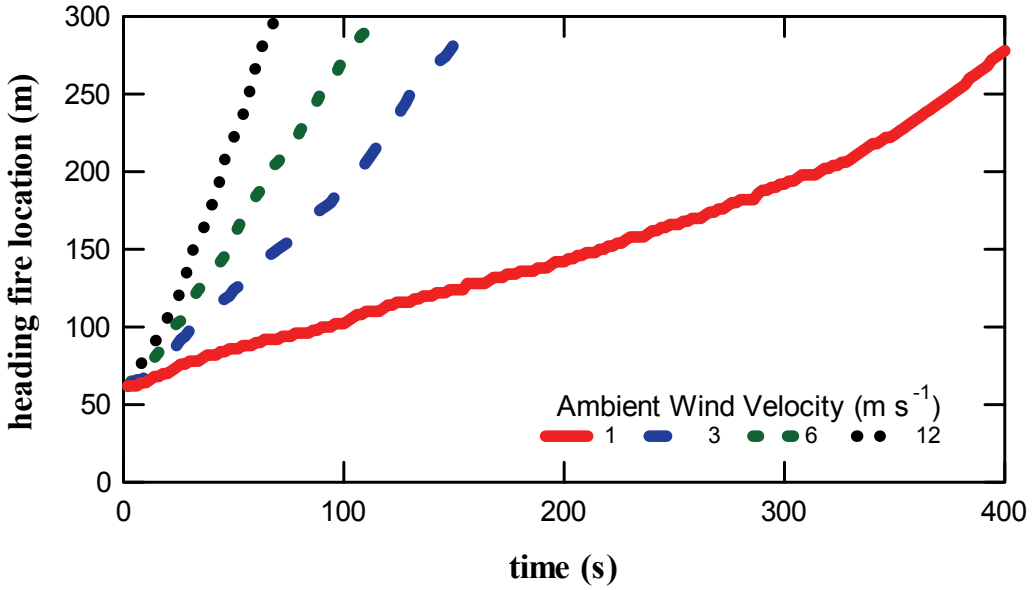

(b)

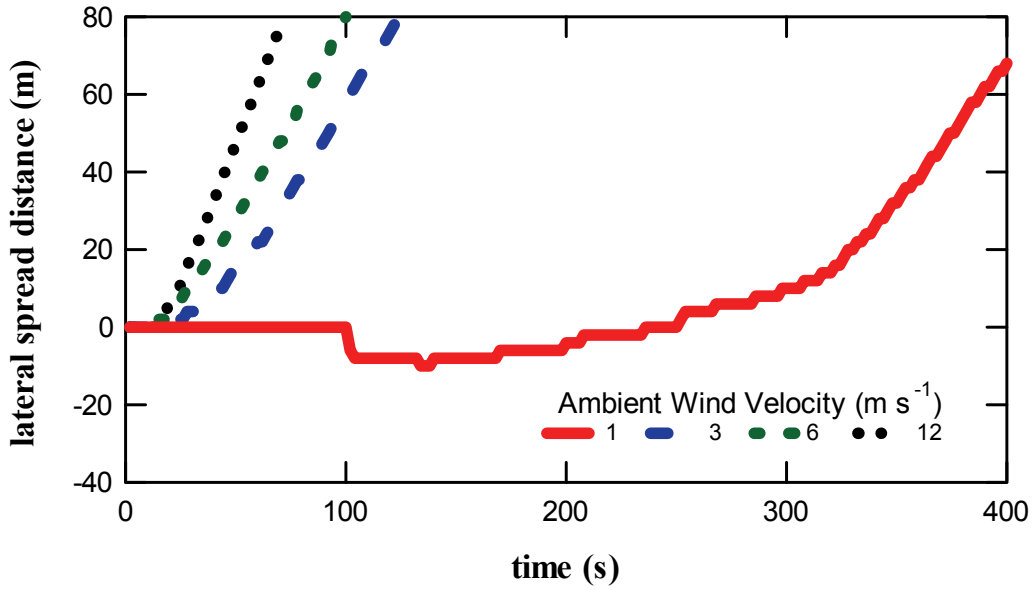

Figure 5-3. **Results from the new sub-grid pocket model. *(a)* Downwind spread distance vs. time from simulated grass fires. *(b)* Lateral spread distance vs. time from simulated grass fires.**

simulation, the fire line narrowed initially, indicated by the negative lateral spread distance. After this initial narrowing, the fire began to propagate with positive lateral spread, and continued to spread laterally throughout the remainder of the simulation.

Overall fire spread rates from the mixture-fraction-based FIRETEC simulations are compared in Figure 5-4 to previously reported spread rates from FIRETEC simulations (labeled in the figure as 'local' and 'nonlocal' as reported by Colman and Linn (2005), and to an empirical correlation for fire spread in undisturbed, 100% cured, natural pasture grasslands (Cheney et al., 1998). In all cases, the mixture fraction-based model produced simulated fire spread rates that were 25-100% higher than the fire spread rates from the 'local,' 'nonlocal,' and empirical models. However, the mixture fraction-based model was not tuned to any specific data, nor to any previous model. Tuning of the a and l parameters could be performed in future work in order to obtain better agreement, if desired. However, this tuning would be complex, since it could involve adjusting parameters, such as c_F, which were already tuned for the 'local' and 'nonlocal' models.

The observation that the fire spread rate results from the mixture-fraction-based FIRETEC model is always higher than the Cheney correlation and previous models is an indication that the model over-predicts the overall heat release to the system generated by gas phase combustion. The overall heat release was not a parameter tracked in FIRETEC, so unfortunately this could not be verified. However, this explanation seems logical, considering two of the assumptions made in the sub-grid mixture fraction model. One assumption was that the heat of reaction was approximately equal to the change in sensible heat as the gas temperature rises from its average value prior to reaction to the flame temperature value after reaction. The other assumption was that the enthalpy of the

gas mixture was only a function of the mixture fraction of the mixture, with gas mixture properties calculated at an assumed temperature (T_o) of 700 K. The sensitivity of the model to this assumed temperature of 700 K could be explored in future work, however to provide a more substantial analysis of the effect of the choice of T_o, a plot of calculated

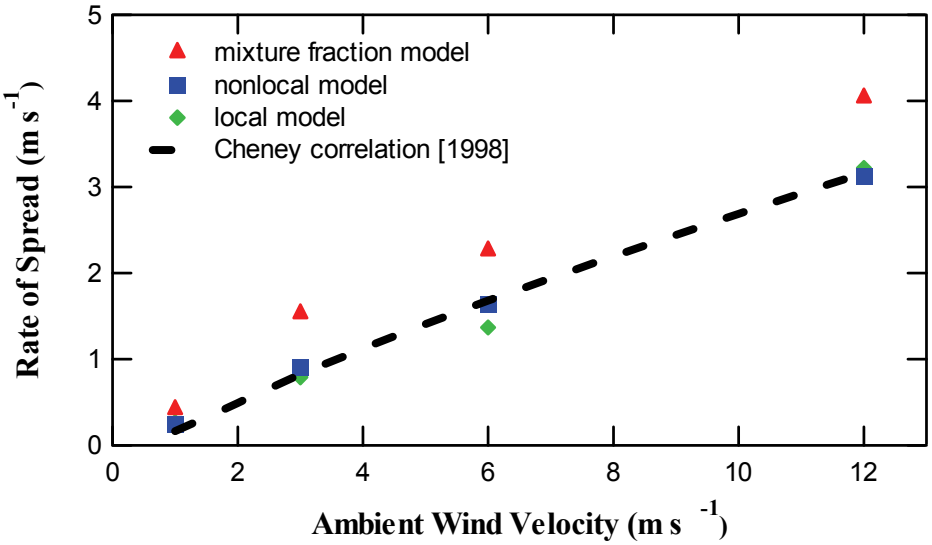

Figure 5-4. Comparison of downwind spread rates in simulated grass fires. Results are shown from simulations of the three FIRETEC chemistry models: 'local,' 'nonlocal,' and the mixture fraction models with a comparison to Cheney, *et al.* (1998).

equilibrium flame temperatures versus mixture fraction for a range of T_o is given in Figure 5-5. The simplest observation that can be made from Figure 5-5 is that equilibrium flame temperature increases with increasing T_o, as expected since a higher initial temperature of the reactants indicates a higher initial reactant enthalpy. Thus there is significant sensitivity of ΔH to T_o in this sub-grid pocket model. Assuming a mixture fraction of 0.20 for the reacting gas mixture and initial gas mixture temperature of 500 K, the estimated heat of reaction (ΔH) would decrease by 10% by changing T_o from 700 K to 300 K.

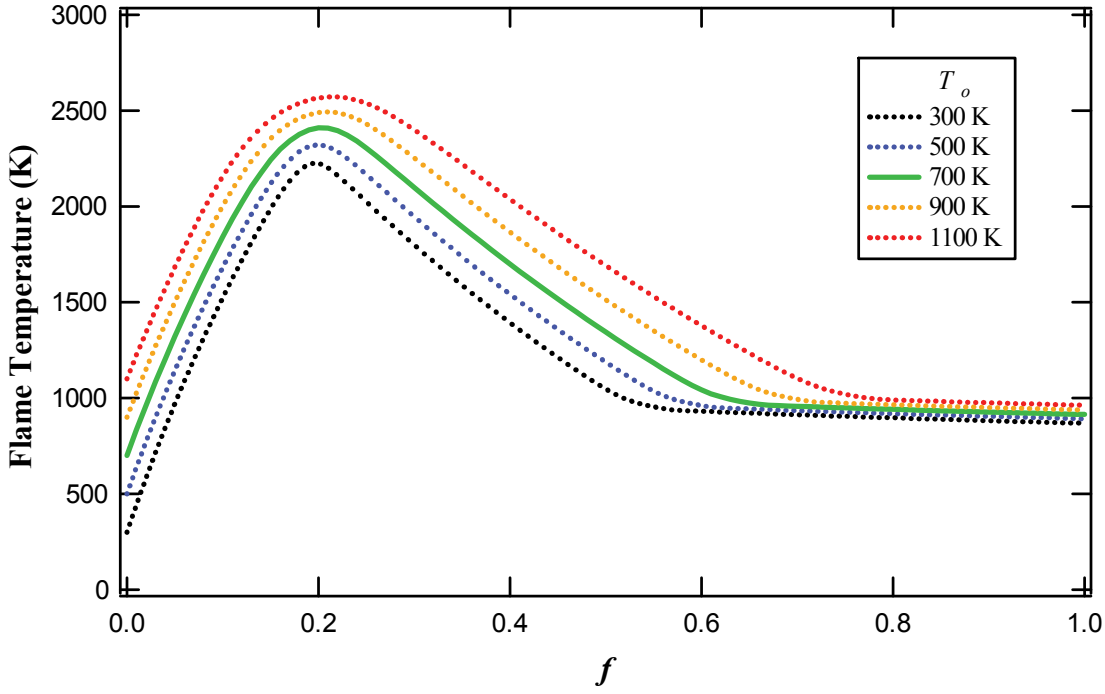

Figure 5-5. Equilibrium flame temperatures as a function of mixture fraction for the reactive gas mixture at different values of T_o.

Another approach would be to remove the necessity of assuming an initial gas temperature by solving the energy equation in terms of overall enthalpy, and obtaining a more accurate estimation of the local enthalpy of the reacting mixture. Gas properties would then be a function of initial conditions (i.e., 298 K), and residual enthalpy (explained previously in the literature review discussion of the mixture fraction PDF approach). This is also a suggestion for future work.

One of the advantages of this mixture-fraction-based model is the ability to predict product species mass fractions. The previous FIRETEC models used simplified chemistry models that could only predict oxygen concentration and hydrocarbon gas concentration. Histories of average oxygen and hydrocarbon mass fractions, plotted together with potential temperature, are shown in Figure 5-6 and Figure 5-7. Histories of

the mixture fraction of the reacting mixture, f_r, and equilibrium product species predictions of CO_2 and CO from the sub-grid pocket combustion model, are shown in Figure 5-8 and Figure 5-9. These history data were extracted from a 12 $m \cdot s^{-1}$ ambient wind grassfire simulation at a point located at the surface in the center of the domain and within the fuel bed (i.e. computational cell number [80,80,1] out of a domain of 160x160x41 cells.) Figure 5-6 shows that as the fire front approaches the cell of interest, the potential temperature increases sharply, the oxygen mass fraction decreases to a minimum. Figure 5-7 shows the hydrocarbons mass fraction increasing to a maximum as the fire front approaches and passes over the point. This occurs as combustible hydrocarbons are produced via pyrolysis, and then subsequently react in the gas phase. In Figure 5-8 and Figure 5-9 it can be seen that as the fire front approaches the cell of interest, the sub-grid pocket combustion model begins to predict CO_2 and CO as equilibrium combustion products. Note that the peaks in the product mass fraction of CO correspond with the peaks in the mixture fraction. As was shown in Figure 4-2*a*, CO production is generally enhanced under fuel-rich conditions (i.e. higher values of the mixture fraction.) For this reason, as the mixture fraction reaches a maximum, the CO equilibrium product mass fraction also reaches a maximum. It should be noted that the mixture fraction of the reacting gases never reached a value greater than 0.6, and no C(solid) was predicted in the equilibrium products. Therefore, relying on the prediction of C(solid) production as a soot precursor was not useful in this case. However, it might be possible to correlate soot predictions with mixture fraction rather than C(s).

These data serve to illustrate a modeling capability that is unique amongst wildfire computational fluid dynamics models. To the author's knowledge, no other

landscape-scale wildfire CFD model in the public literature yields any estimation of the production of various product chemical species, including CO and CO_2. This is a unique capability added to FIRETEC by the implementation of the mixture-fraction-based thermodynamic equilibrium model. However, having pointed out this new, unique capability, the astute reader will exercise caution when interpreting these model results. One must understand that these data not are real data. They are simulated data which have not been validated by experimental measurements. More experimental data are needed from wildfire research before this model can be validated, meaning that model predictions are demonstrated to be consistent with a significant volume of experimental observations. Unfortunately, the computational modeling capabilities of today beg for advances in experimental measurement techniques, which could be applied in the field of wildfire research.

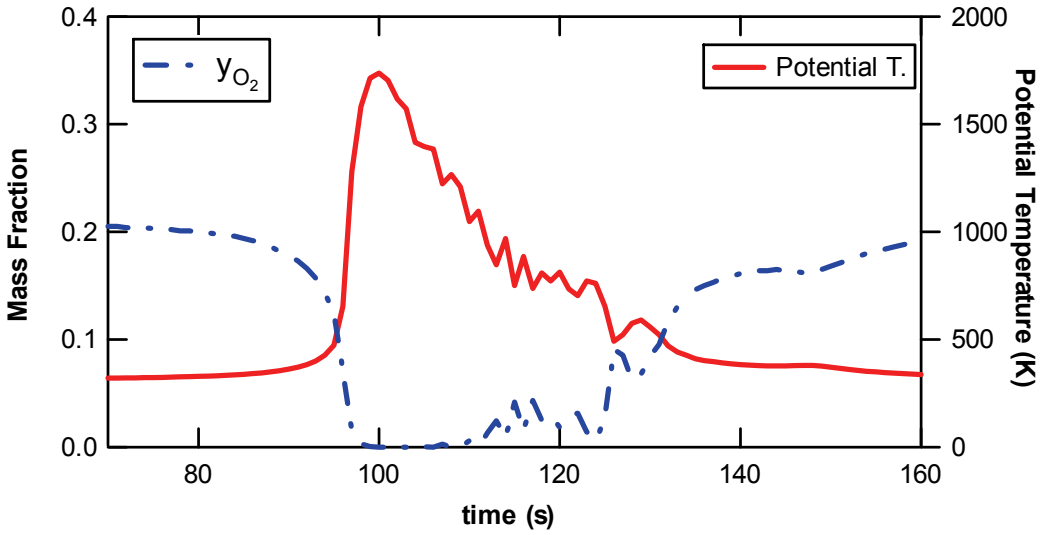

Figure 5-6. History of y_{O2} (left-hand ordinate) and potential temperature (right-hand) ordinate) for one point located in the fuel bed and in the center of the domain of the long fire-line grass fire simulation at 12 m·s^{-1} inlet wind velocity.

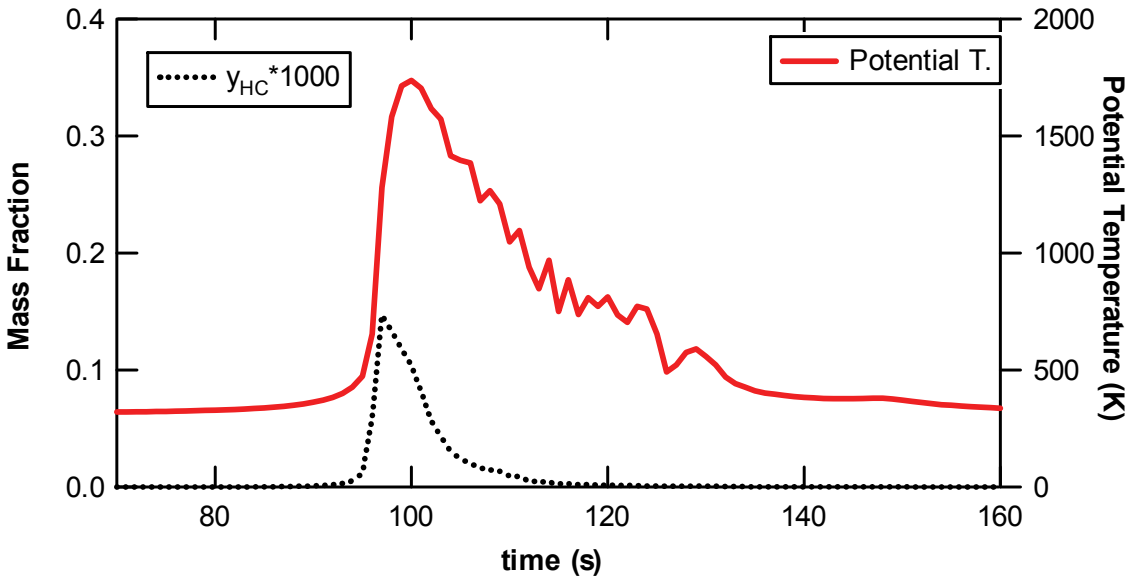

Figure 5-7. **History of y_{HC} (left-hand ordinate) and potential temperature (right-hand) ordinate) for one point located in the fuel bed and in the center of the domain of the long fire-line grass fire simulation at 12 m·s^{-1} inlet wind velocity.**

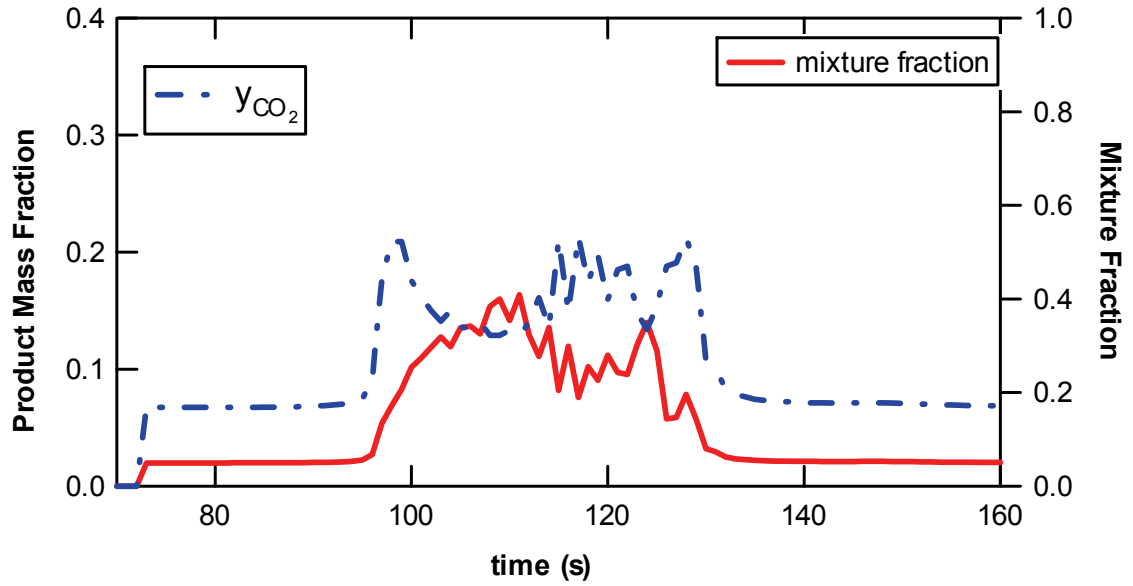

Figure 5-8. **History of y_{CO2} (left-hand ordinate) and mixture fraction (right-hand) ordinate) for one point located in the fuel bed and in the center of the domain of the long fire-line grass fire simulation at 12 m·s^{-1} inlet wind velocity.**

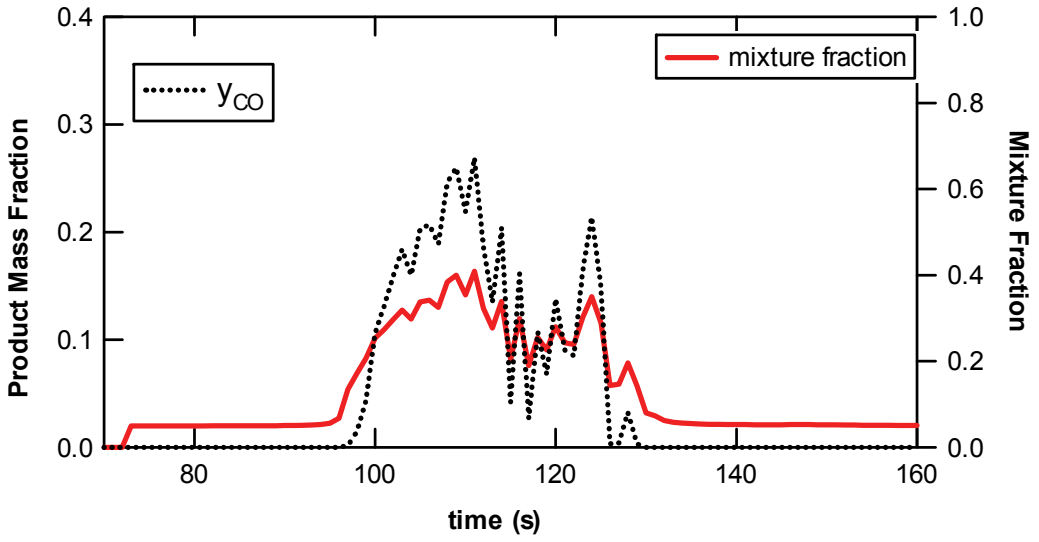

Figure 5-9. History of yCO2 (left-hand ordinate) and mixture fraction (right-hand) ordinate) for one point located in the fuel bed and in the center of the domain of the long fire-line grass fire simulation at 12 m·s-1 inlet wind velocity.

5.2.5 Chaparral and Ponderosa Fire Simulations

Figure 5-10 and Figure 5-11 show plots of downwind spread distance and lateral spread distance for chaparral and Ponderosa pine simulations preformed using the mixture fraction model. Steady downwind and lateral spread were observed in all four chaparral simulations. Even though the fuel moisture content was high (130%) the fires in the chaparral fuel beds are able to spread consistently throughout the simulation. This is an effect of the bulk density of the chaparral, which was higher than the bulk density of grass used in this study. Thus, with a higher bulk density, there was more available fuel for combustion. Upon combustion of the higher density chaparral, more energy is released than in the grassfire cases, and therefore there is sufficient heat release to maintain a propagating fire line, even though the fuel was quite moist.

In contrast, in the Ponderosa pine simulations, continuous downwind and lateral spread was only observed in the higher inlet wind velocity cases at 6 and 12 $m \cdot s^{-1}$. In the 3 $m \cdot s^{-1}$ inlet wind velocity simulation, the fire propagated downwind, but became narrower with time. The same behavior was observed in the 1 $m \cdot s^{-1}$ inlet wind velocity simulation, except in that case, the narrowing caused the fire to quickly become extinguished.

Little to no crowning occurred in the Ponderosa pine simulations. The limited crowning of the fire, and the limited lateral spread were perhaps due in part to the high moisture content (130%) specified for the canopy fuels. The high fuel moisture content means more energy is consumed by the vaporization of water in the solid fuel, which can prevent sustained ignition of the canopy fuels. This assumption was verified by running another simulation with the canopy moisture content specified at 80%. For the comparison simulations, the fuel bed distribution, wind speed, and ignition were identical in both cases. The ambient wind speed was set to 6 $m \cdot s^{-1}$. A graphical representation of the simulation results at 100 seconds of simulated time is shown in Figure 5-12 for the 130% moisture content case, and in Figure 5-13 for the 80% moisture content case. The solid fuel density is colored from green to black based on fuel density, with green representing unburned fuel to black representing areas where the fuel has been consumed. The “flame” is red isosurface indicating a gas temperature of 1000 K. The “smoke” is represented by a transparent black isosurface indicating a reduced oxygen concentration. As is readily observed in Figure 5-12 and Figure 5-13, the reduced moisture content in the canopy fuels resulted in crowning of the fire into the canopy. The crowning led to a consumption of the canopy fuels and a more intense flame front.

(a)

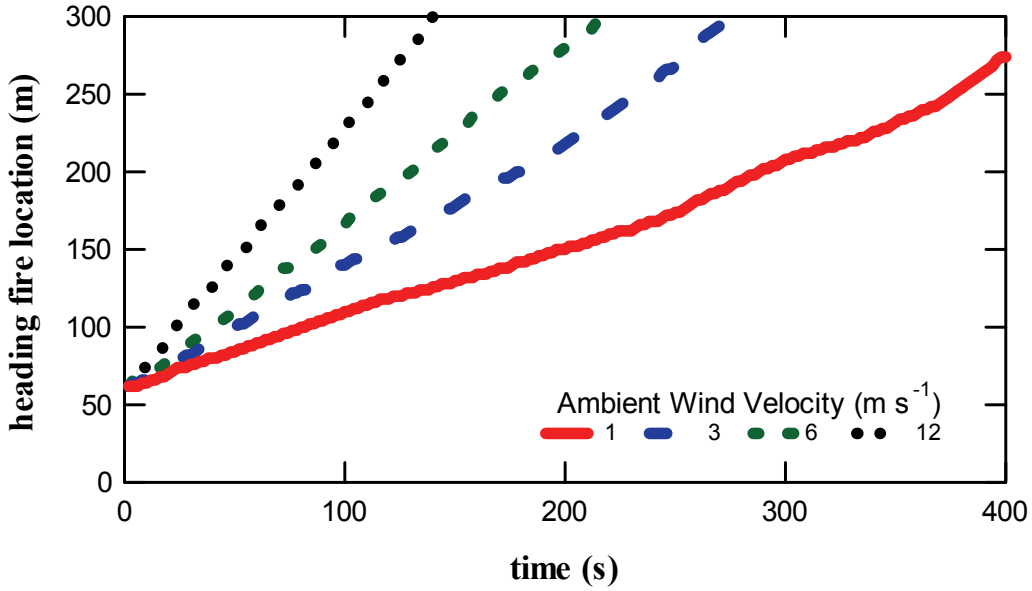

(b)

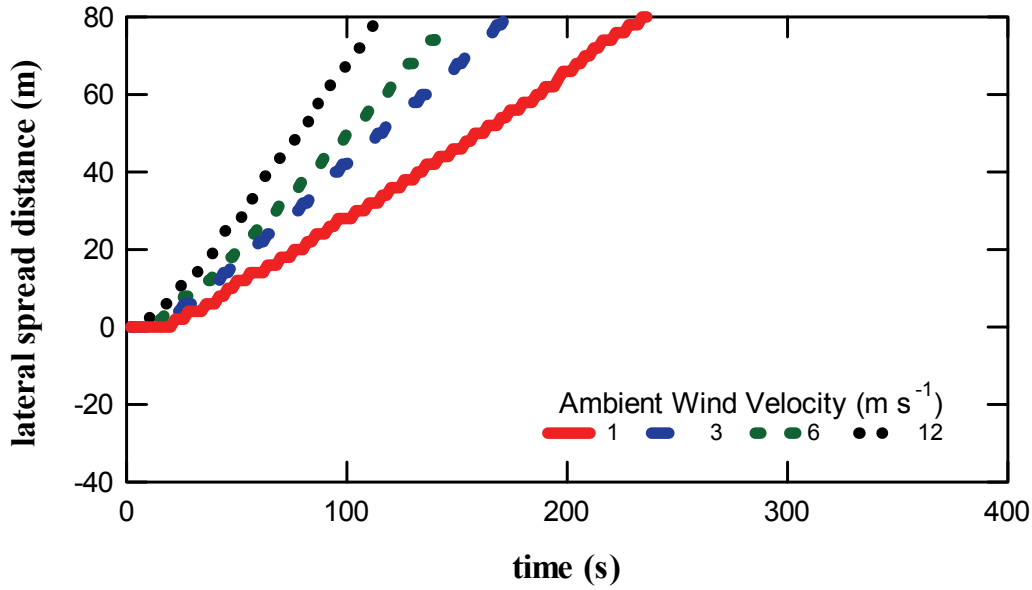

Figure 5-10. ***(a)*** **Downwind spread distance vs. time from simulated chaparral fires.** ***(b)*** **Lateral spread distance vs. time from simulated chaparral fires.**

(a)

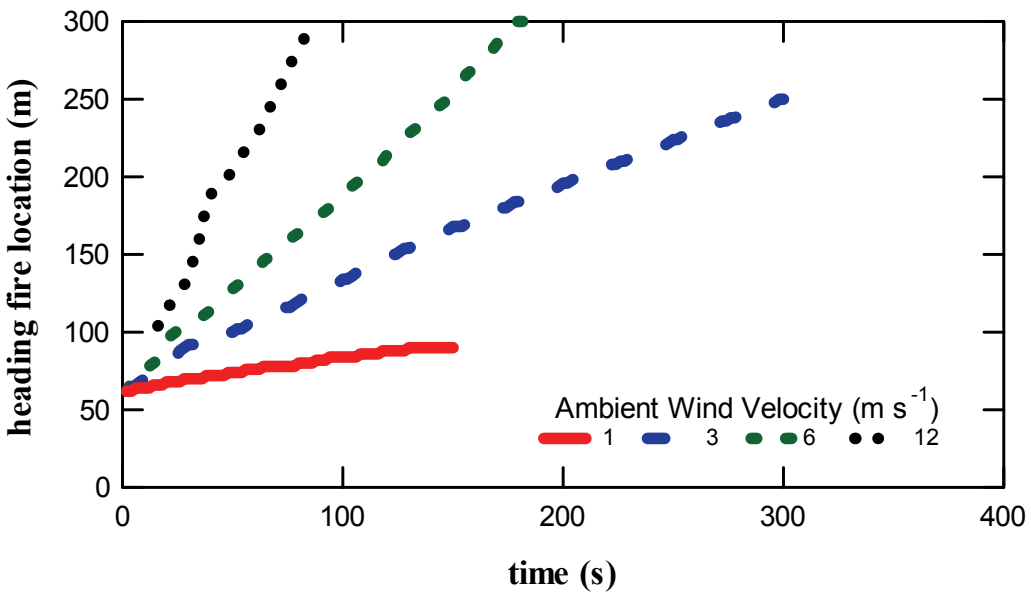

(b)

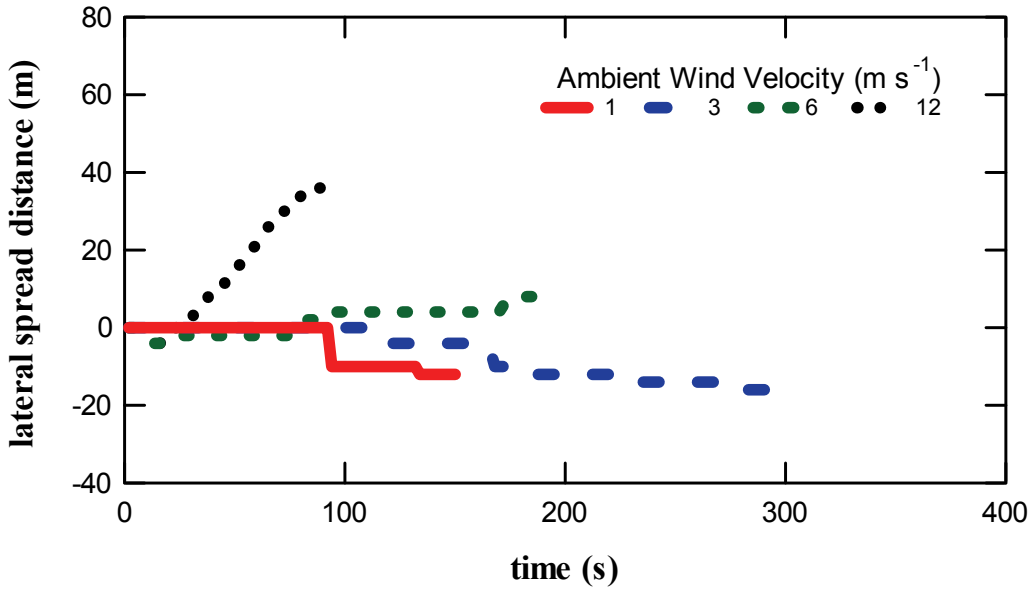

Figure 5-11. ***(a)*** **Downwind spread distance vs. time from simulated Ponderosa pine fires.** ***(b)*** **Lateral spread distance vs. time from simulated Ponderosa pine fires.**

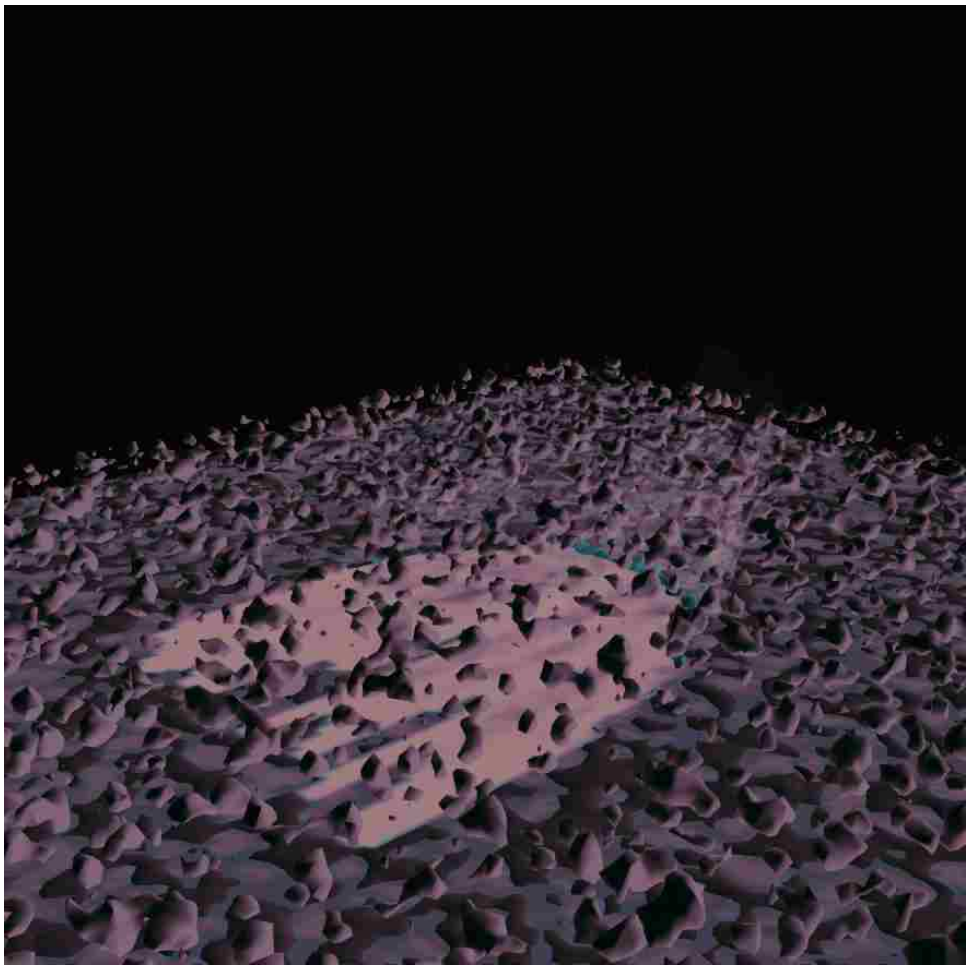

Figure 5-12. A plot from the 130% moisture content simulation, at 100 s of simulated time, showing little-to-no crowning of the fire.

5.2.6 Grassfire Short and Long Fire-Line Grassfire Simulations

After completing the full suite of simulations for grass, chaparral, and Ponderosa pine fuel beds, a number of modifications were introduced to the FIRETEC code by collaborators at Los Alamos National Laboratory. Some of these modifications to the FIRETEC code included significant changes to the radiative heat transfer model subroutines to correct discrepancies between the computer code and the theoretical equations, and also to fix an error in the iterative solution technique used in the radiation

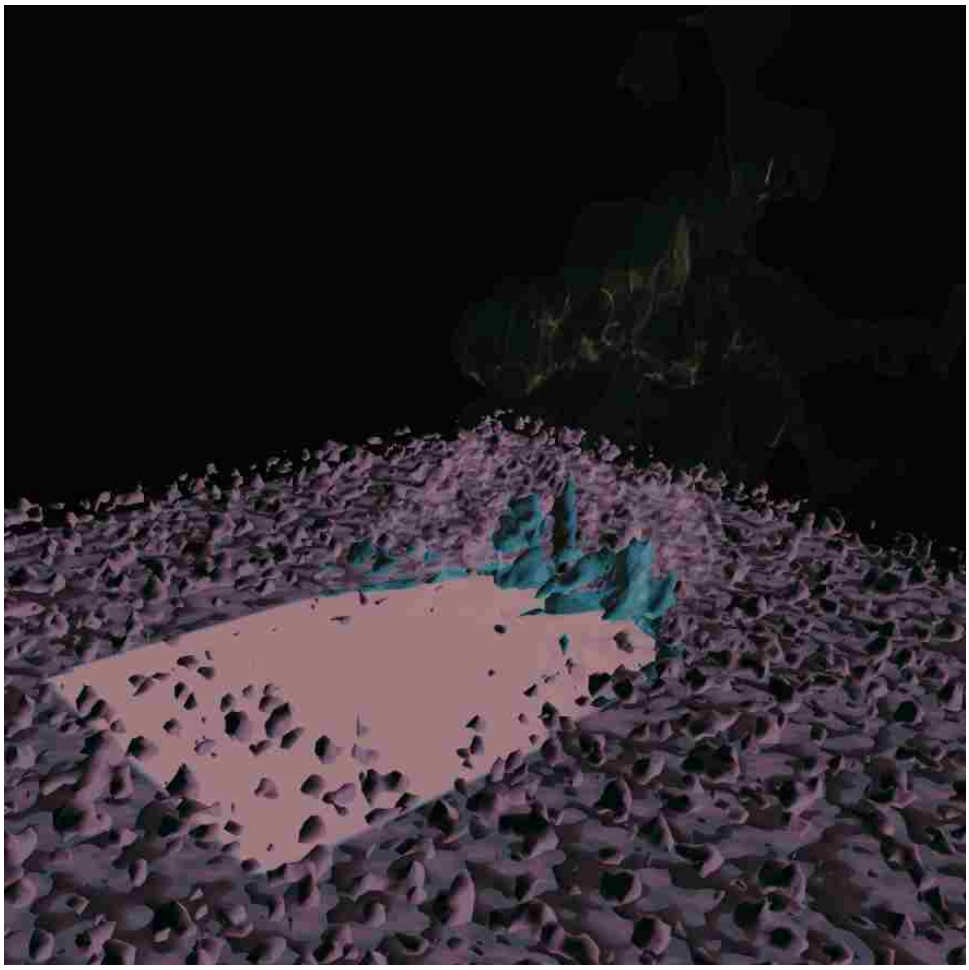

Figure 5-13. A plot from the 80% canopy moisture content simulation, at 100 s of simulated time, showing significant crowning of the fire.

subroutine. Due to these developments in the computer code, another suite of simulations was performed.

In the second suite of simulations the fuel bed consisted of the same type of tall grass described previously and used in the first suite of simulation. The inlet wind velocities were again 1, 3, 6, and 12 $m \cdot s^{-1}$. However, for the second simulation suite, two different lengths of fire-line ignitions were tested, a longer initial fire line, and a shorter initial fire line. The longer fire-line was a 4 meter by 100 meter strip, centered in the crosswind direction, and 60 meters downwind from the inlet boundary. The shorter

ignited fire-line was a 4 meter by 16 meter strip, located in the same crosswind and downwind position as the longer fire line. These two different lengths of ignited fire-lines were used in previously published FIRETEC simulations by Linn and Cunningham (2005).

Figure 5-14 shows results from the short fire line simulations. Forward spread distance is shown in Figure 5-14*a*, and lateral spread distance is shown in Figure 5-14*b*. All four simulations performed with the short fire line ignition resulted in consistent forward and lateral fire spread. Figure 5-15 shows the results from the long fire line simulations, and again, all four simulations resulted in consistent forward spread, and lateral spread as well. The fire line in the 1 $m \cdot s^{-1}$ case does not spread laterally much, until around 250 seconds of simulated time, whereupon it begins to spread rapidly in the lateral direction. The reason for this lateral spread behavior is not readily apparent, and elucidating the precise model components that contributed to this behavior is well beyond the scope of this particular work, though it is suggested as a topic of future study. The purpose of these figures is to demonstrate the feasibility of utilizing the sub-grid pocket model in FIRETEC.

Figure 5-16 summarizes the spread rates for all eight simulations performed in the second suite (red diamonds and black crosses), including a comparison to spread rates from the grass fire runs in the first suite of simulations (blue squares). Results from the first suite of simulations were presented at the 2nd Fire Behavior and Fuels Conference in Destin, FL, on March 28, 2007 (Clark et al., 2007 submitted), denoted herein as FBFC results. The FBFC runs were all performed with long fire line ignitions (4 m by 100 m),

(a)

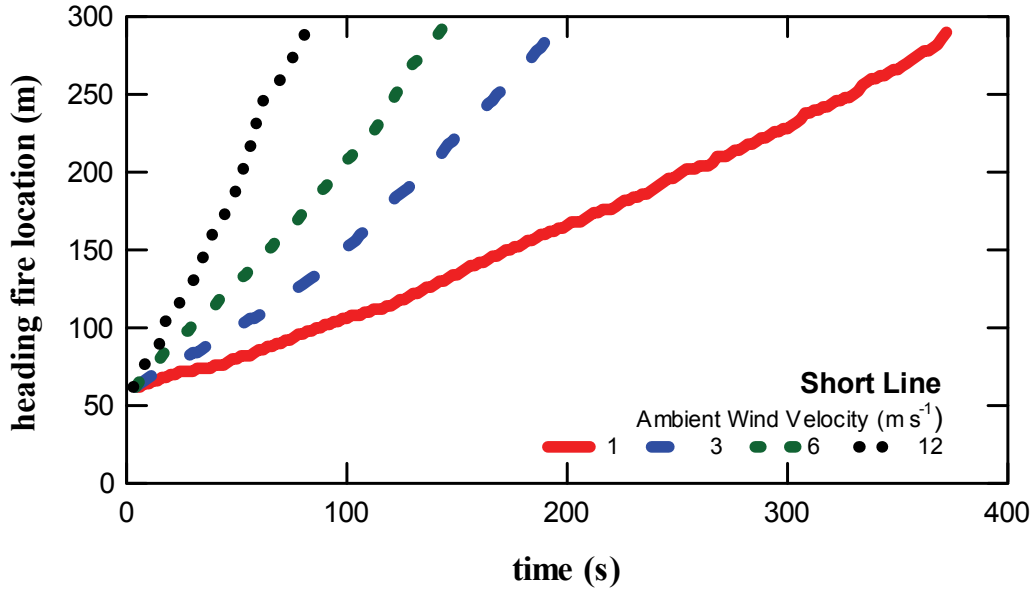

(b)

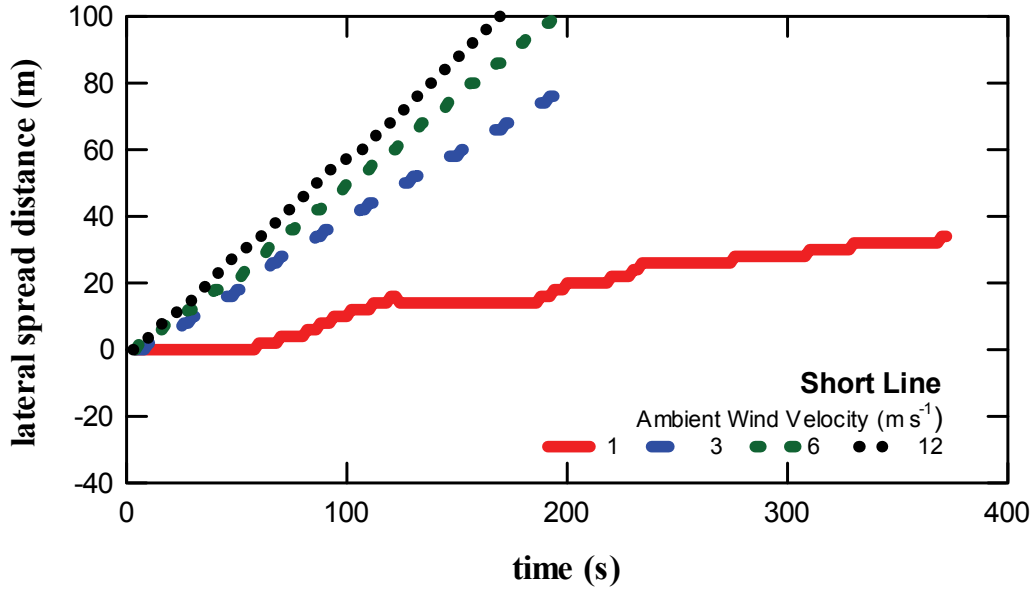

Figure 5-14. Results from simulated grass fires (using the updated FIRETEC) for the short fire line ignition scenarios. (a) Downwind spread distance vs. time (b) Lateral spread distance vs. time.

(a)

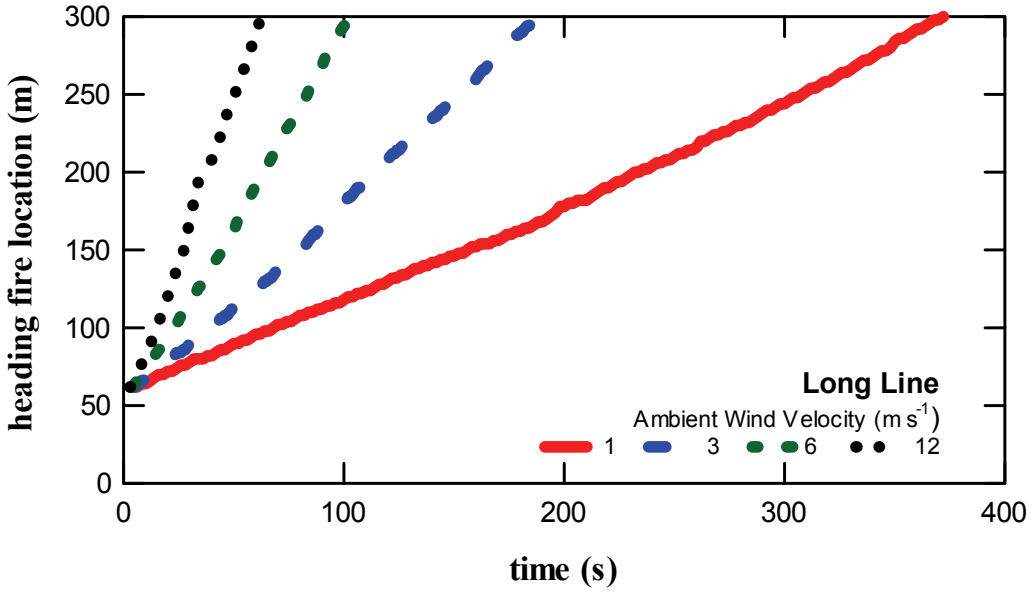

(b)

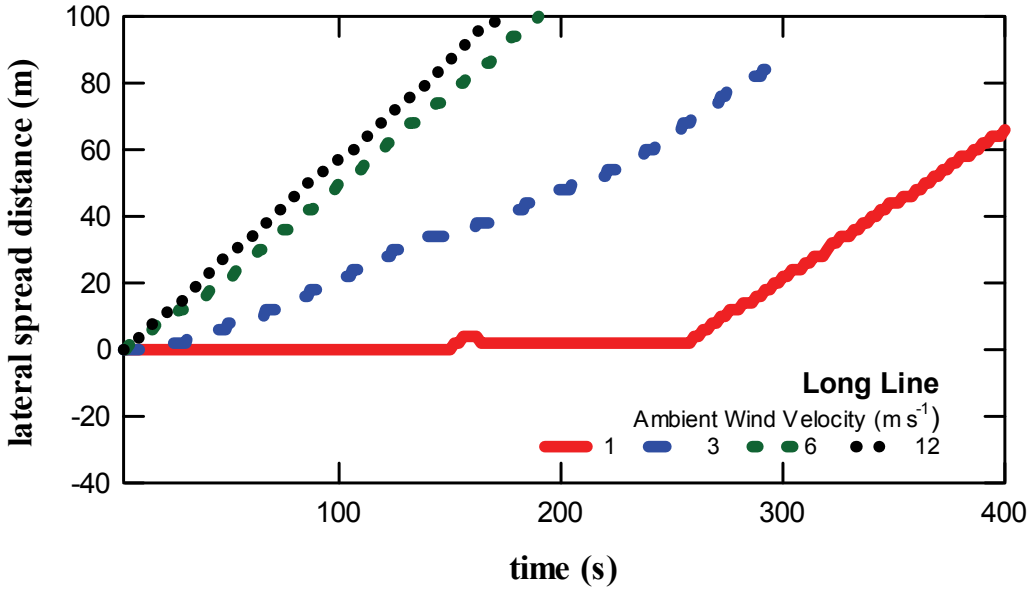

Figure 5-15. Results from simulated grass fires (using the updated FIRETEC) for the long fire line ignition scenarios. *(a)* Downwind spread distance vs. time *(b)* Lateral spread distance vs. time.

and the spread rates from the long line simulations from the second suite of runs were slightly different from the spread rates from the earlier FBFC simulation. These differences are subtle, but the corrections made in the FIRETEC computer code made a difference at all wind speeds. However, the difference is greater at wind speeds of 6 $m \cdot s^{-1}$ or less. At lower wind speeds, one would assume that the process of radiative heat transfer will have a greater overall effect on the spread rate. This is observed in the comparison between the FBFC results (black crosses) and the results of long line wildfire simulations from the second suite of runs (red diamonds), as shown in Figure 5-16.

Also shown in Figure 5-16 are results from short line wildfire simulations conducted in the second suite of runs. The results from this second suite of simulations illustrate the effect of fire line length on overall rate of spread. The overall gross effect was that rate of spread was decreased with a shorter ignition line, a trend which was observed by Linn and Cunningham in previous FIRETEC grassfire simulations (2005).

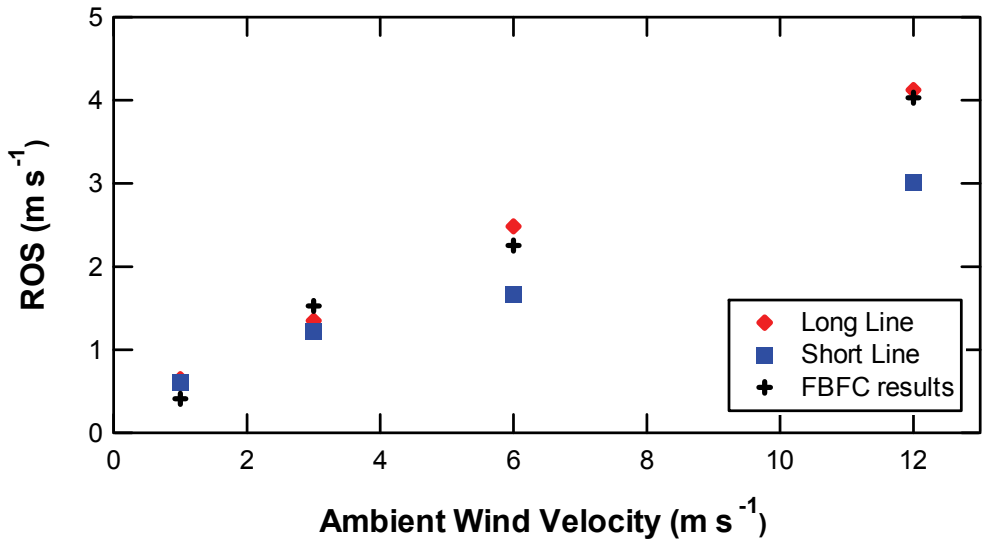

Figure 5-16. Comparison of downwind spread rates in simulated grass fires for both the long and the short fire line tests. Also shown for comparison are the grassfire simulation results reported at the 2nd Fire Behavior and Fuels Conference (Clark et al., 2007 submitted).

In a similar fashion to the histories shown previously in this chapter, histories of oxygen and hydrocarbon mass fractions, plotted together with potential temperature, are shown in Figure 5-17 and Figure 5-18. Histories of mixture fraction, f_r, and equilibrium values of product mass fractions of CO_2 and CO from the sub-grid pocket combustion model are shown in Figure 5-19 and Figure 5-20. These simulated data were taken from the 12 $m \cdot s^{-1}$ inlet wind grassfire simulation at a point located in the center of the domain and within the fuel bed (i.e. computational cell number [80,80,1] out of a domain of 160x160x41 cells.) Figure 5-17 and Figure 5-18 show that as the fire front approaches the cell of interest, the potential temperature increases sharply, the oxygen mass fraction for the cell decreases to a minimum, and the hydrocarbons mass fraction for the cell increases to a maximum. This occurs as combustible hydrocarbons are produced via pyrolysis, and then subsequently react in the gas phase. In Figure 5-19 and Figure 5-20 it can be seen that as the fire front approaches the cell of interest, the sub-grid pocket combustion model begins to predict CO_2 and CO as equilibrium combustion products. Again, peaks in the product mass fraction of CO correspond with the peaks in the mixture fraction, because CO production is enhanced under fuel-rich conditions. Note that these mass fractions of product CO and CO_2 apply only to the mass of reacting material in the pocket mode, not to the total cell volume.

A similar set of histories was also produced for a point located vertically one computational cell above the grass fuel bed. The rectangular coordinates of this point were [80,80,2]. Similar trends that were observed in the previous series of figures (for the point in the fuel bed) are observed in the following figures as well (Figure 5-21, Figure 5-22, and Figure 5-23). Oxygen mass fraction decreases as the flame front approaches

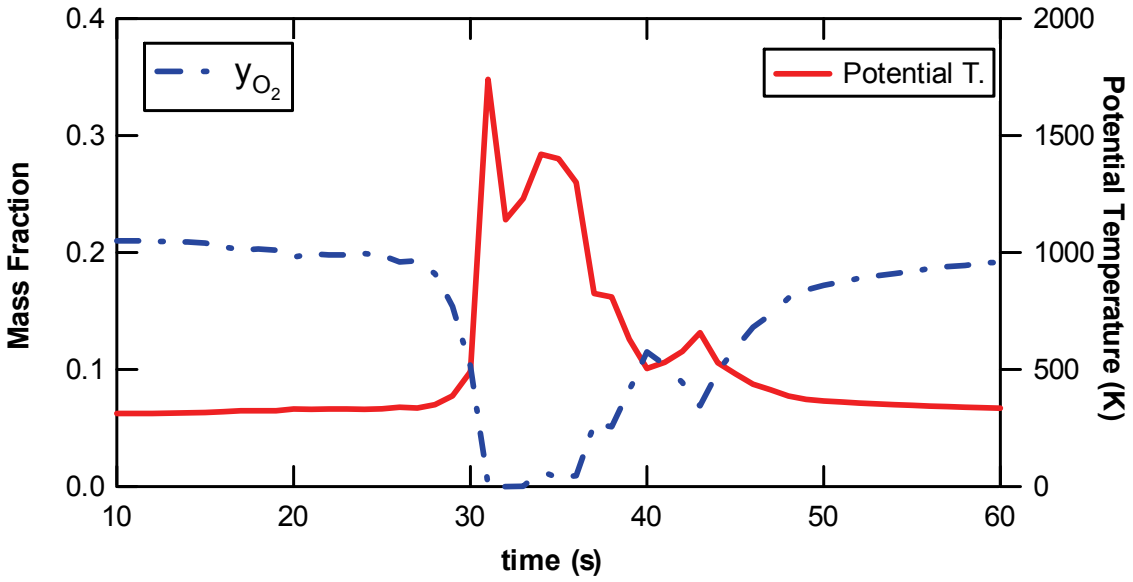

Figure 5-17. History of y_{O2} (left-hand ordinate) and potential temperature (right-hand) ordinate) for one point located in the fuel bed and in the center of the domain of the long fire-line grass fire simulation at 12 m·s^{-1} inlet wind velocity.

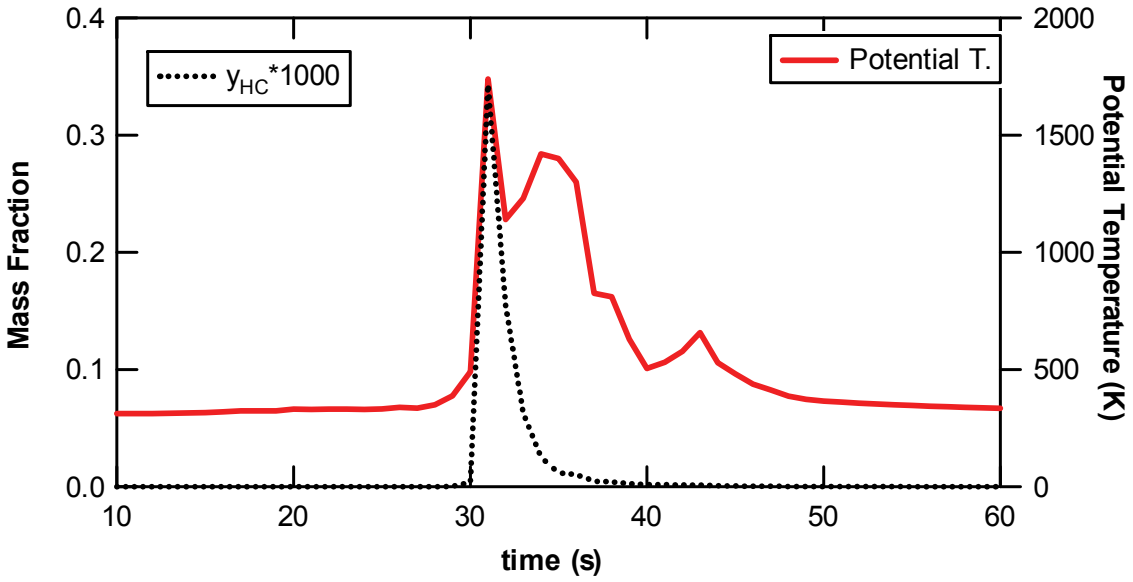

Figure 5-18. History of y_{HC} (left-hand ordinate) and potential temperature (right-hand) ordinate) for one point located in the fuel bed and in the center of the domain of the long fire-line grass fire simulation at 12 m·s^{-1} inlet wind velocity.

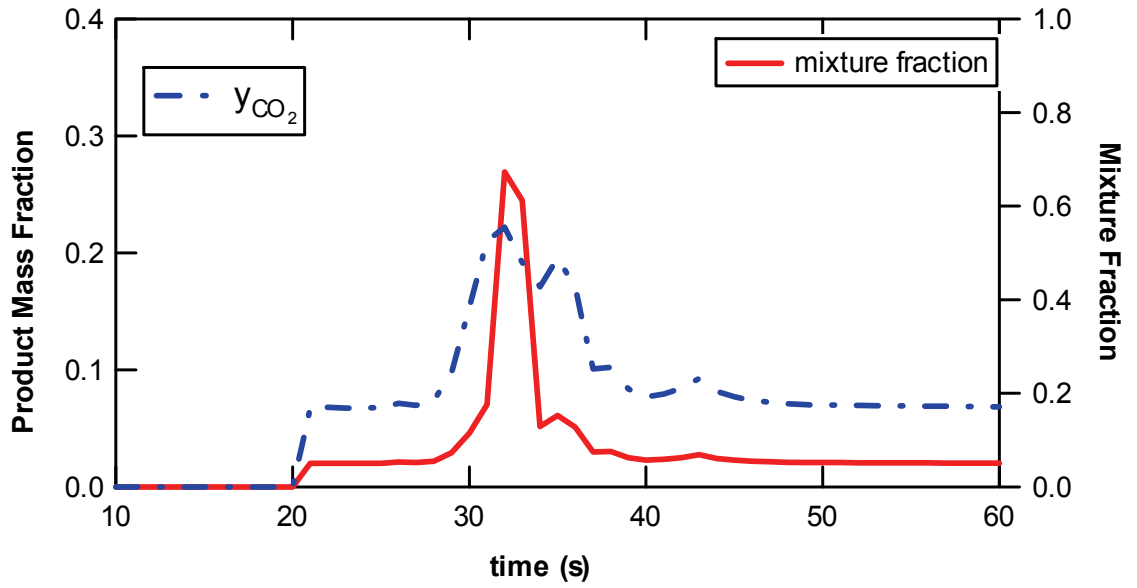

Figure 5-19. History of y_{CO2} (left-hand ordinate) and mixture fraction (right-hand) ordinate) for one point located in the fuel bed and in the center of the domain of the long fire-line grass fire simulation at 12 m·s^{-1} inlet wind velocity.

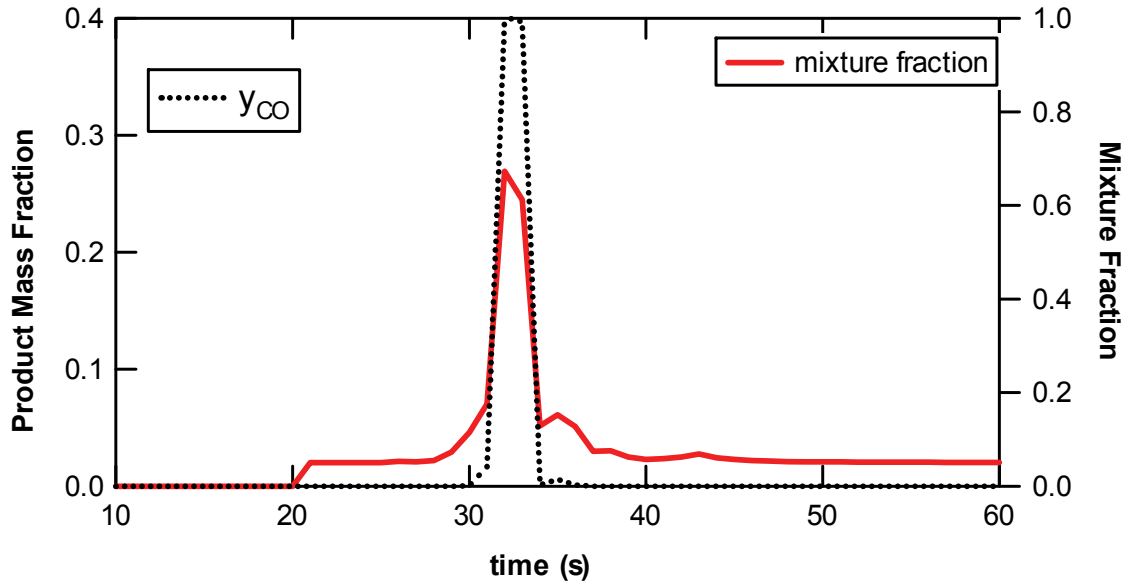

Figure 5-20. History of y_{CO} (left-hand ordinate) and mixture fraction (right-hand) ordinate) for one point located in the fuel bed and in the center of the domain of the long fire-line grass fire simulation at 12 m·s^{-1} inlet wind velocity.

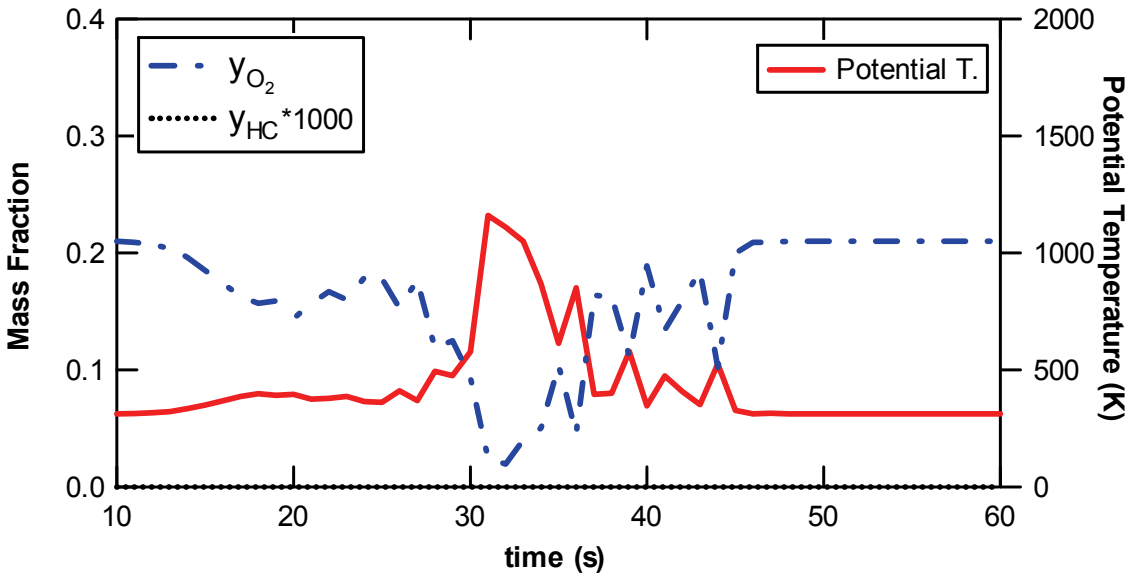

Figure 5-21. History of y_{O2}, y_{HC} (left-hand ordinate), and potential temperature (right-hand) ordinate) for one point located one computational cell above the fuel bed and in the center of the domain of the long fire-line grass fire simulation at 12 m·s^{-1} inlet wind velocity.

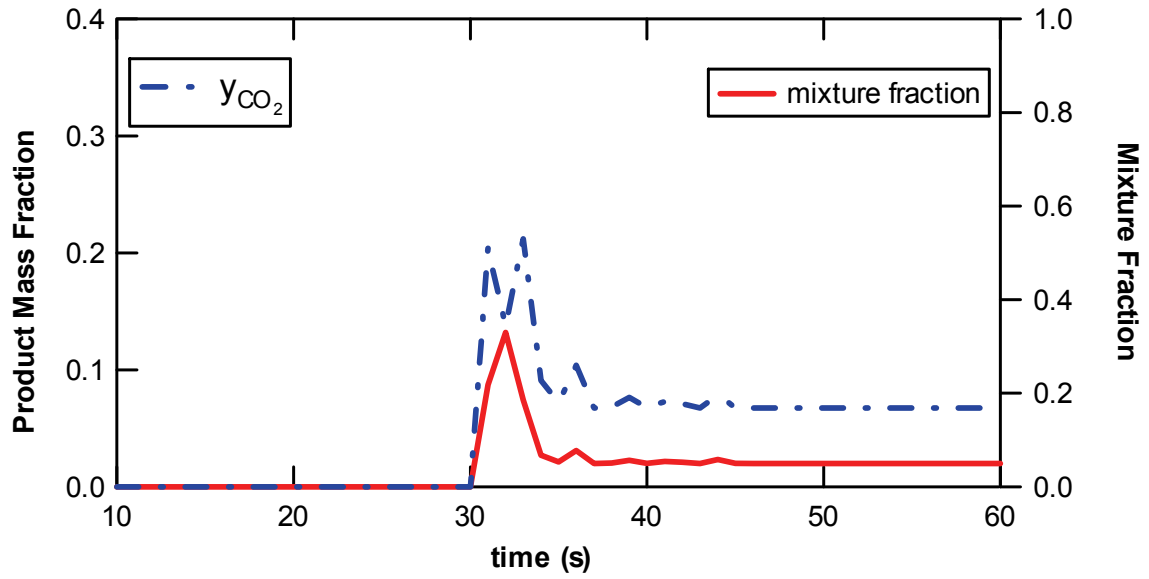

Figure 5-22. History of y_{CO2} (left-hand ordinate), and potential temperature (right-hand) ordinate) for one point located one computational cell above the fuel bed and in the center of the domain of the long fire-line grass fire simulation at 12 m·s^{-1} inlet wind velocity.

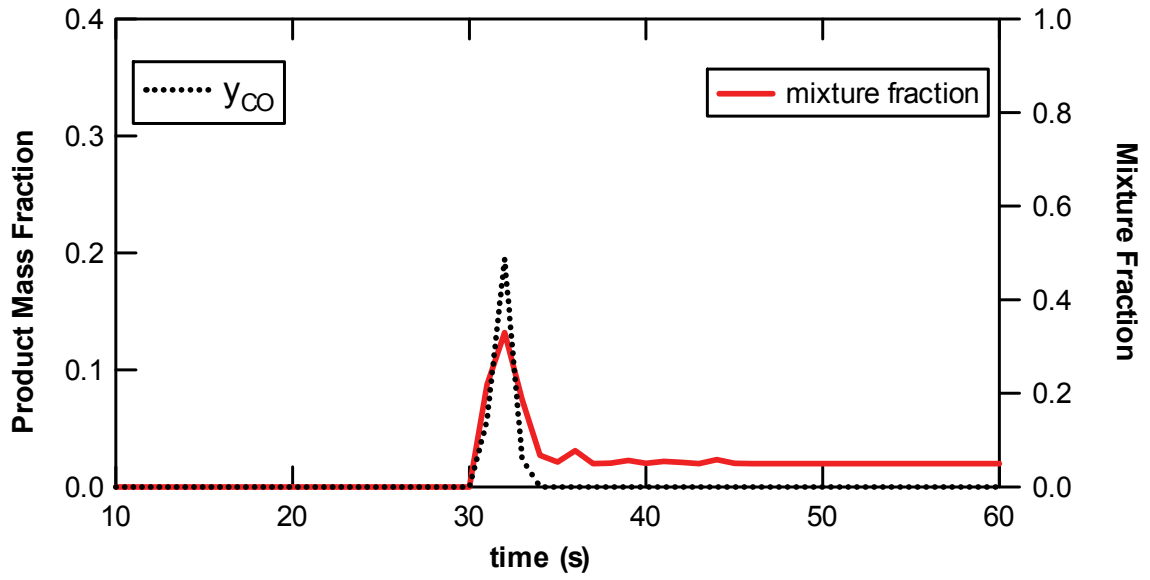

Figure 5-23. History of yCO (left-hand ordinate), and potential temperature (right-hand) ordinate) for one point located one computational cell above the fuel bed and in the center of the domain of the long fire-line grass fire simulation at 12 m·s-1 inlet wind velocity.

and passes, while CO and CO_2 product mass fractions and the mixture fraction all peak. One observation to note is that the hydrocarbon mass fraction in this second vertical cell is not significant. This model result indicates that 'nonlocal' combustion of unburned hydrocarbons is not significant, which is not a result that matches field observations of wildfires, where intermittent flame heights can be observed above the height of the fuel bed.

Figure 5-24 shows a history of the net heating of solid material in the node of interest. The net heating is broken up into a radiative heating component, and a convective heating component, which are modeled within FIRETEC. The simulation results are consistent with expected trends. As the flame front approaches the solid fuel, there occurs a period of net convective heating. As the fuel temperature increases, a radiative flux from the fuel results in a heat loss due to radiative heat transfer. Finally, as

the temperature of the fuel increases about 1500 K, the convective heat transfer results in a net cooling of the fuel, since the fuel temperature becomes larger than the average gas temperature of the computational cell at the location.

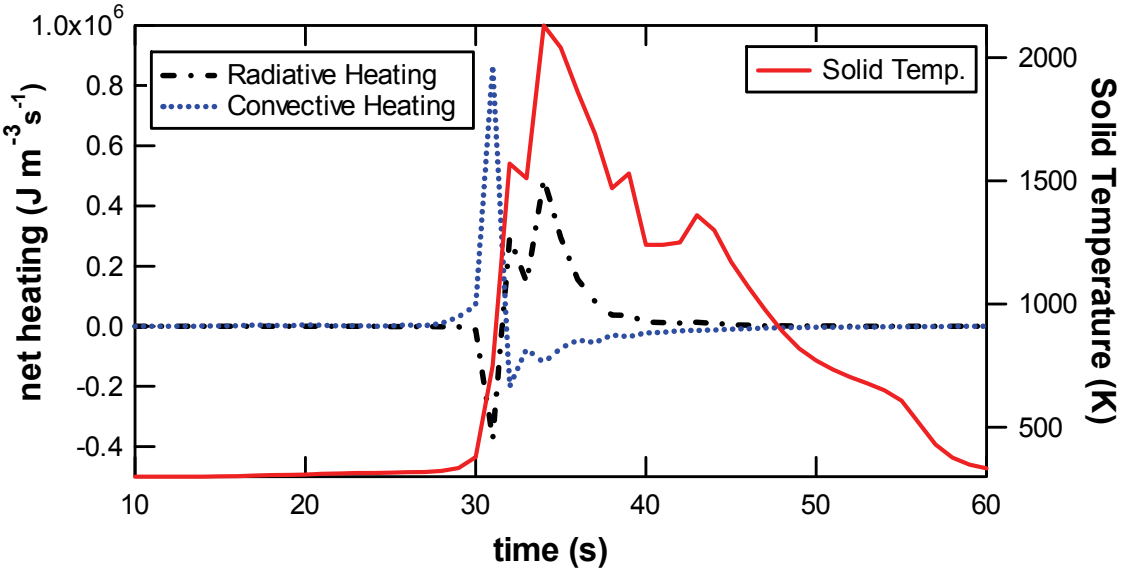

Figure 5-24. History of convective and radiative heating (left-hand ordinate), and potential temperature (right-hand) ordinate) for one point located within the fuel bed and in the center of the domain of the long fire-line grass fire simulation at 12 m·s^{-1} inlet wind velocity.

5.3 Summary

A first-generation mixture-fraction-based sub-grid pocket model was implemented in FIRETEC in order to utilize thermodynamic equilibrium to model gas-phase combustion. This first-generation pocket model was demonstrated successfully in simulations performed for three types of fuel beds (grass, chaparral and Ponderosa pine), and for ambient wind velocities of 1, 3, 6 and 12 m·s^{-1}. Plots of forward and lateral spread, species and temperature histories, and a comparison of forward rate of spread predictions from the sub-grid pocket model, the 'local' model and the 'nonlocal' model

simulations were shown. Overall simulated fire spread rates for the grass fuel bed using the pocket model were 25-100% greater than the simulated spread rates for the same grass fuel bed using the 'local' and 'nonlocal' FIRETEC models. Results of combustion product species compositions from pocket-model FIRETEC simulations included significant fractions of CO and CO_2 in the vicinity of the flame front, but the local mixture fraction was never sufficiently high to yield carbon solid as an equilibrium product.

The first-generation model increased the overall computational time required to perform FIRETEC simulations by approximately 7%. These simulations demonstrated the utility of the mixture-fraction-based sub-grid pocket model, with product species compositions being an important advancement of the mixture-fraction-based model over the 'local' and 'nonlocal' models. However, the higher rates of fire spread observed in the mixture-fraction-based sub-grid pocket model grassfire simulations, as compared to the Cheney experimental correlation for grassfire rate of spread, indicates that fine-tuning of the model will be required to improve the comparison of the mixture-fraction-based FIRETEC simulations to experimental data. This might be accomplished by tuning the pocket model parameters and/or other FIRETEC modeling constants (such as c_F), improving the approximation of the heat of reaction term, improving the method of calculating the initial reactant enthalpy, or solving the energy equation in terms of total enthalpy.

6 Second-Generation Sub-Grid Mixture Fraction Model

A sub-grid model which allowed for a variable flame sheet area was desired. The intention was to attempt to model sub-grid flame sheets by still using the pocket model concept, but allowing for the radius of the hydrocarbon pockets to vary dynamically. Two approaches were developed: (1) a single pocket, variable radius model, and (2) a variable radius transport model. The development of each model is outlined in this section, and simulation results are then discussed.

6.1 Single Pocket, Variable Radius Model Development

The single pocket, variable radius model is based on the same assumed spherical hydrocarbon pocket concept explained in the previous discussion regarding the constant radius pocket model, as illustrated in Figure 5-1. However, rather than assuming a constant radius, the radius is allowed to vary depending on the mass of unburned hydrocarbons present in a computational cell. Furthermore, it is assumed in this model that all unburned hydrocarbons are contained within a single pocket in the cell.

Again, assuming gases are ideal, the volume of unburned hydrocarbons is given by

$$V_{HC,total} = m_{HC,total}\hat{V}_{HC} = \frac{\overline{\rho}_{HC} V_{cell} R T_{HC}}{\overline{P} M_{HC}} \quad . \qquad \textbf{(6-1)}$$

Assuming that all unburned hydrocarbons are concentrated within a single spherical pocket,

$$V_{HC,total} = \frac{4}{3}\pi r^3 \quad \textbf{(6-2)}$$

The radius of the hydrocarbon pocket is solved from the equality of these two expressions.

$$\frac{4}{3}\pi r^3 = \frac{\overline{\rho}_{HC} V_{cell} R T_{HC}}{\overline{P} M_{HC}} \quad \textbf{(6-3)}$$

$$r = \left(\frac{3}{4\pi} \frac{\overline{\rho}_{HC} V_{cell} R T_{HC}}{\overline{P} M_{HC}} \right)^{1/3} \quad \textbf{(6-4)}$$

The volume of the reacting mixture is the sum of the volumes of reacting hydrocarbons and air, just as it was in the constant radius pocket model (see Equation 5-5).

$$V_{mixed} = \frac{4}{3}\pi\left[(3l + 3al)r^2 + (3a^2l^2 - 3l^2)r + (1 + a^3)l^3\right] \quad \textbf{(6-5)}$$

Relying on the ideal gas assumption, the masses of reacting hydrocarbons and air in a computational cell can be calculated.

$$m_{HC,r} = \frac{V_{HC,r}}{\hat{V}_{HC}} = \frac{\overline{P} M_{HC}}{R T_{HC}} \frac{4}{3}\pi\left(3lr^2 - 3l^2 r + l^3\right) \quad \textbf{(6-6)}$$

$$m_{air,r} = \frac{V_{air,r}}{\hat{V}_{air}} = \frac{\overline{P} M_{air}}{R T_{air}} \frac{4}{3}\pi\left(3alr^2 - 3a^2l^2 r + a^3l^3\right) \quad \textbf{(6-7)}$$

The masses of reacting hydrocarbons and air are then divided by the volume of the computational cell in order to convert them to a mass per cell volume density.

$$\rho_{HC,r} = \frac{m_{HC,r}}{V_{cell}} \quad \textbf{(6-8)}$$

$$\rho_{air,r} = \frac{m_{air,r}}{V_{cell}} \tag{6-9}$$

Next, the mixture fraction in a computational cell is calculated,

$$\bar{f}_{cell} \equiv \frac{\bar{\hat{\rho}}_p}{\bar{\hat{\rho}}_p + \bar{\hat{\rho}}_s}, \tag{6-10}$$

as well as the mixture fraction of "air" in the cell

$$f_{air} = \frac{\rho_{p,air}}{\bar{\rho} - \bar{\hat{\rho}}_{HC}} = \frac{\bar{f}_{cell}\bar{\rho} - \bar{\hat{\rho}}_{HC}}{\bar{\rho} - \bar{\hat{\rho}}_{HC}}, \tag{6-11}$$

which again is the mass fraction of reacted primary elements that reside in the air outside of the pure hydrocarbon pockets. Finally, the mixture fraction of the reacting gas mixture is calculated:

$$f_r = \frac{f_{HCpocket}\rho_{HC,r} + f_{air}\rho_{air,r}}{\rho_{HC,r} + \rho_{air,r}}. \tag{6-12}$$

6.1.1 Challenges to Implementation

The single pocket, variable radius model was implemented, but did not yield successful fire spread simulations. The concept and approach appeared very reasonable, and after successful implementation of the constant radius pocket model, a very similar approach, it was surprising and frustrating that the single pocket, variable radius model did not work. Despite much thought and effort, the exact reason for the failure of this method was never determined. However, a second variable radius pocket modeling approach was also developed and successfully implemented, as discussed in the next section.

6.2 Transported Variable Radius Pocket Model Development

A second approach was developed to model sub-grid hydrocarbon pockets with a variable radius, with an attempt to derive a transport equation to model changes in pocket radius due to convection in the flow field, as well as combustion sources and sinks. The development of this approach is now given.

To develop a transport equation for the pocket radius, the species continuity equation for hydrocarbons is multiplied by the normalized pocket radius. The assumption is that the variation in pocket radius due to transport is correlated to the transport of hydrocarbons, i.e.,

$$R_p\left(\frac{\partial \rho_{HC}}{\partial t}+\frac{\partial \rho_{HC} u_i}{\partial x_i}=\sum S_{HC}\right) \tag{6-13}$$

$$R_p\frac{\partial \rho_{HC}}{\partial t}+R_p\frac{\partial \rho_{HC} u_i}{\partial x_i}=R_p\sum S_{HC} \tag{6-14}$$

where the normalized pocket radius is defined as $R_p=\frac{r}{r_o}$.

A simple equation of change for pocket radius is proposed by analogy to transport equations

$$\frac{\partial R_p}{\partial t}+\frac{\partial R_p u_i}{\partial x_i}=\sum S_{R_p}\text{ ,} \tag{6-15}$$

and this equation is then multiplied by the density of hydrocarbons.

$$\rho_{HC}\left(\frac{\partial R_p}{\partial t}+\frac{\partial R_p u_i}{\partial x_i}=\sum S_{R_p}\right) \tag{6-16}$$

$$\rho_{HC}\frac{\partial R_p}{\partial t}+\rho_{HC}\frac{\partial R_p u_i}{\partial x_i}=\rho_{HC}\sum S_{R_p} \tag{6-17}$$

Note that in HIGRAD/FIRETEC, all velocities are assumed to be explicitly resolved. At the resolution of the FIRETEC model, it is assumed that transport by molecular diffusion is negligible. Equations (6-14) and (6-17) are summed, combining terms by making use of the reverse product rule for partial derivatives.

$$\frac{\partial R_p \rho_{HC}}{\partial t} + \frac{\partial R_p \rho_{HC} u_i}{\partial x_i} + R_p \rho_{HC} \frac{\partial u_i}{\partial x_i} = \rho_{HC} \sum S_{R_p} + R_p \sum S_{HC} \qquad \textbf{(6-18)}$$

From this point, a Reynolds averaging approach could be taken, substituting the mean and fluctuating components in for each variable in equation (6-18), and averaging the entire equation. This would result in a transport equation containing Reynolds-stress-like correlation terms. However, at this point it is simply assumed that these turbulence-related terms are all negligible; the estimation of the contribution of any such turbulence terms in a wildfire transport modeling scenario is beyond the scope of this dissertation.

6.2.1 Simulation Results

Grassfire simulations were performed with the transported variable radius pocket model. All fuel bed, ignition, and ambient wind characteristics were set identical to previously run simulations. A summary of downwind rates of spread obtained from the simulations using the transported variable radius pocket model is shown in Figure 6-1. The results from the 'local' model and the constant radius pocket model are also shown in this figure. The results show no clear advantage to using this more complex, variable radius pocket model over the constant radius pocket model. Both versions of the pocket model over-predict the flame front rate of spread, and would require tuning for greater accuracy.

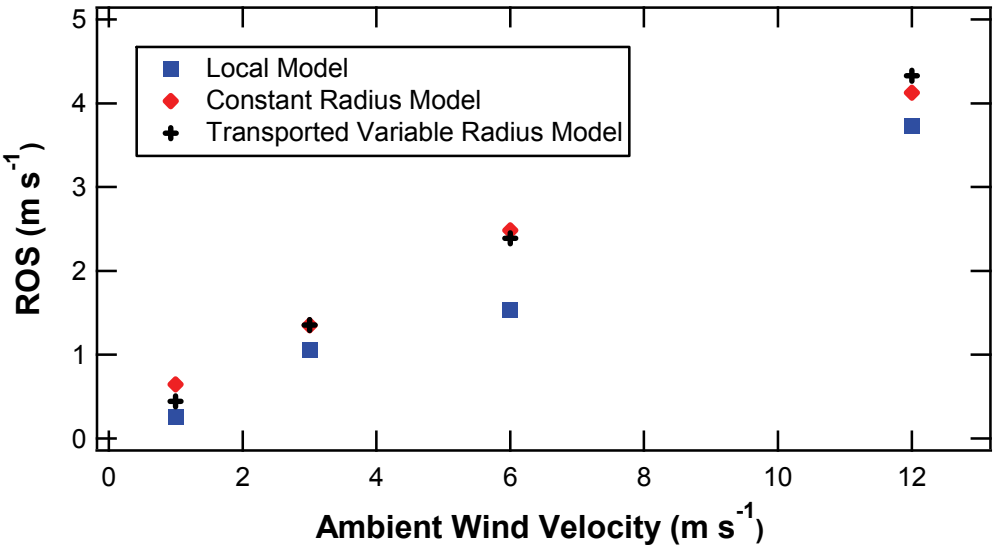

Figure 6-1. Comparison of downwind spread rates in simulated grass fires from the 'local' model, constant radius pocket model, and transported variable radius pocket model.

For the variable radius pocket model, histories of average oxygen and hydrocarbon mass fractions, plotted together with potential temperature, are shown in Figure 6-2 and Figure 6-3. Histories of the mixture fraction of the reacting mixture, f_r, and equilibrium product species predictions of CO_2 and CO from the sub-grid pocket combustion model, are shown in Figure 6-4 and Figure 6-5. As in previous history plots at a point of interest, these history data were extracted from a 12 $m \cdot s^{-1}$ ambient wind grassfire simulation at a point located at the surface in the center of the domain and within the fuel bed (i.e. computational cell number [80,80,1] out of a domain of 160x160x41 cells.) Figure 6-2 shows that as the fire front approaches the cell of interest, the potential temperature increases sharply, the oxygen mass fraction decreases to a minimum. Figure 6-3 shows the hydrocarbons mass fraction increasing to a maximum as the fire front approaches and passes over the point. In Figure 6-4 and Figure 6-5 it can be seen that as the fire front approaches the cell of interest, the sub-grid pocket combustion

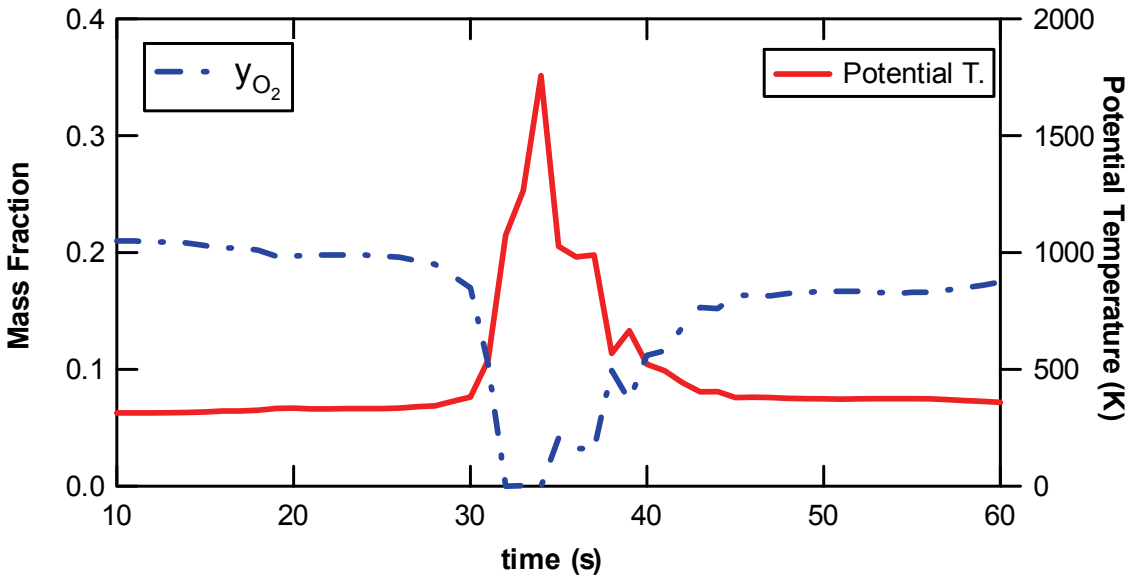

Figure 6-2. **History of yO2 (left-hand ordinate) and potential temperature (right-hand) ordinate) for one point located in the fuel bed and in the center of the domain of the long fire-line grass fire simulation at 12 m·s-1 inlet wind velocity.**

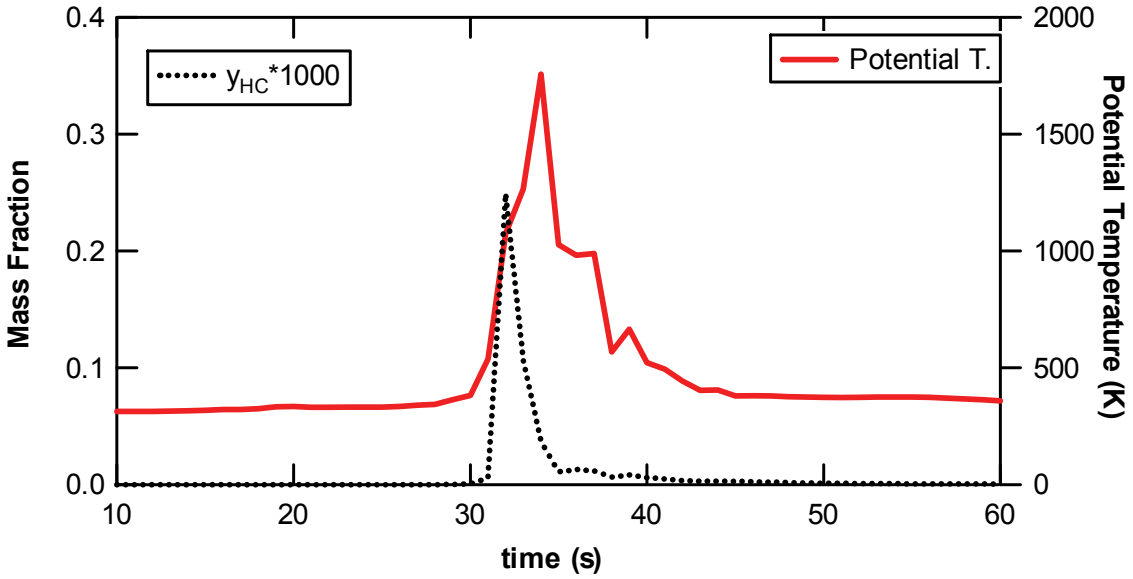

Figure 6-3. **History of y_{HC} (left-hand ordinate) and potential temperature (right-hand) ordinate) for one point located in the fuel bed and in the center of the domain of the long fire-line grass fire simulation at 12 m·s^{-1} inlet wind velocity.**

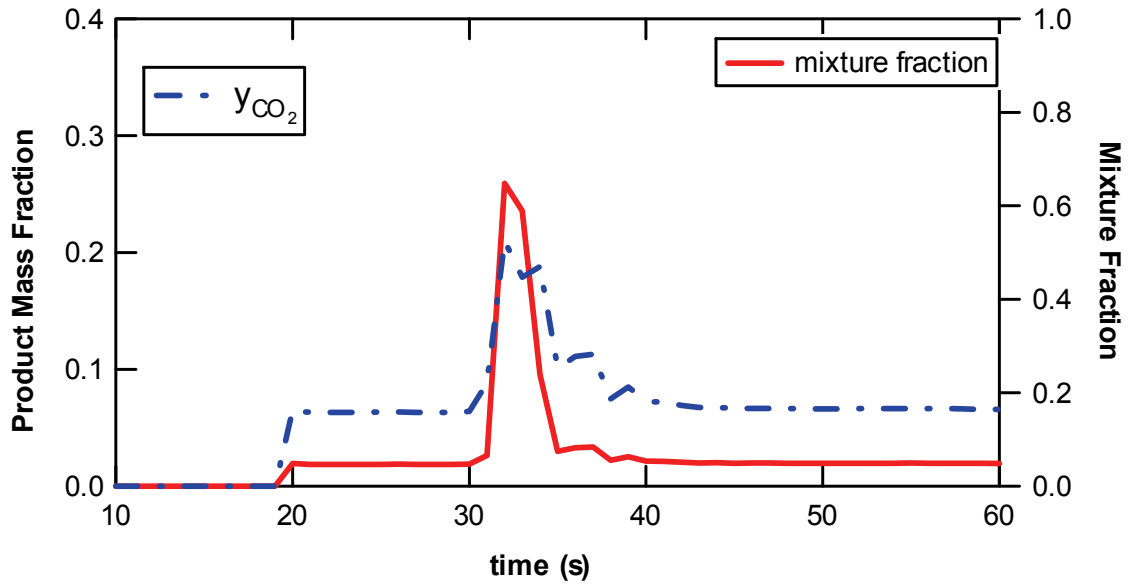

Figure 6-4. **History of y_{CO2} (left-hand ordinate) and mixture fraction (right-hand) ordinate) for one point located in the fuel bed and in the center of the domain of the long fire-line grass fire simulation at 12 m·s^{-1} inlet wind velocity.**

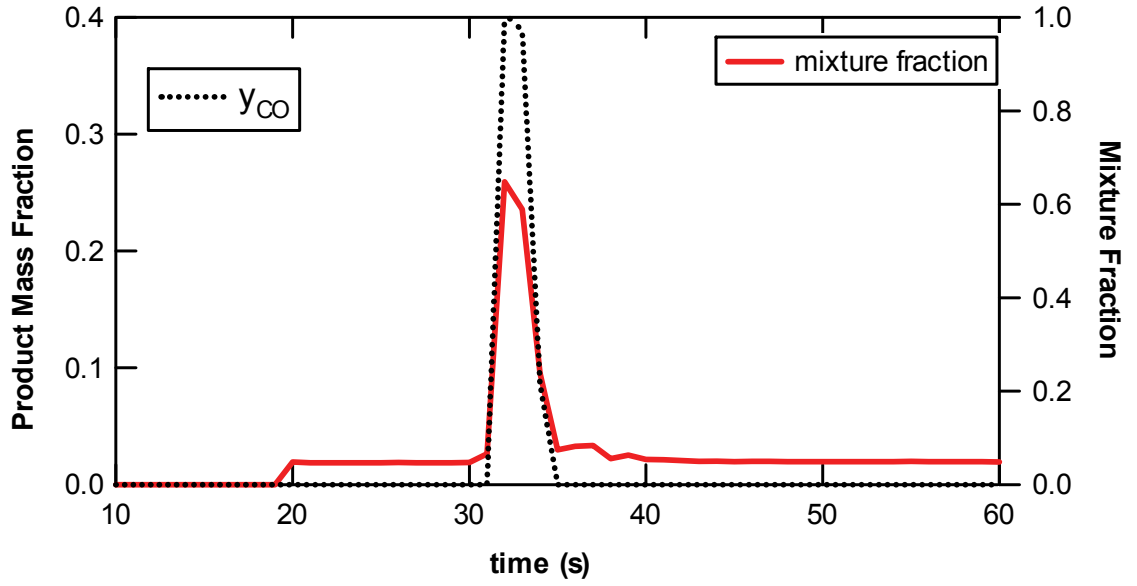

Figure 6-5. **History of y_{CO} (left-hand ordinate) and mixture fraction (right-hand) ordinate) for one point located in the fuel bed and in the center of the domain of the long fire-line grass fire simulation at 12 m·s^{-1} inlet wind velocity.**

model begins to predict CO_2 and CO as equilibrium combustion products. Compared to the history plots shown for the constant radius pocket model (Figures 5-6 thru 5-9), the history plots for the variable radius pocket model show qualitatively similar results. These histories, along with the comparison between the variable radius and constant radius pocket models for the fire rate of spread do not exhibit any significant differences between the two approaches.

6.3 Summary

A second-generation sub-grid mixture fraction model was implemented in FIRETEC, in an effort to extend the pocket model concept with a variable pocket radius. A transport equation was developed for the pocket radius. The motivation for the development of this second-generation pocket model was the desire for the pocket model to simulate variability in the average pocket radius within a computational cell. Conceptually, such variability in the average pocket radius would result from the changing dynamics of pyrolysis, gas-phase combustion, and hydrocarbons transport in the wildfire simulation. The motivation for this extended development to the pocket model seemed clear and reasonable. However, the fire spread rates from simulations using the transported variable radius pocket model showed no distinct improvement over the constant radius pocket model presented in Chapter 5. Nevertheless, the second-generation model is included in this dissertation, since it may be of value for future work.

7 Summary and Conclusions

The purpose of this dissertation research was to develop and implement a new approach for modeling gas-phase combustion physics in FIRETEC, a landscape-scale wildland fire model developed at Los Alamos National Laboratory (LANL). This new approach for modeling gas-phase combustion in FIRETEC was based on existing combustion modeling theory, namely applying a thermodynamic equilibrium model, a concept taken from the mixture fraction probability density function (PDF) model. By adapting and applying a thermodynamic equilibrium model, a gas-phase combustion model was developed for FIRETEC (the PDF for the mixture fraction was not applied). A sub-grid pocket model was conceived and developed to provide a method for implementing this mixture-fraction-based thermodynamic equilibrium combustion model in FIRETEC. This sub-grid pocket model provided a method for modeling the mixture fraction in flame sheets at the sub-grid level.

Simulation results from the mixture-fraction-based thermodynamic equilibrium pocket model were produced for grass, California chaparral, and Ponderosa pine fuel beds. These results demonstrated the feasibility of the new mixture-fraction-based pocket model, which was implemented in FIRETEC. This new gas-phase equilibrium combustion model produced predictions of flame temperature and product species compositions that were more detailed than previous combustion models implemented in

FIRETEC. In particular, the histories of product species predictions indicated the production of CO and CO_2 as the flame front passed over a point in the fuel bed. Simulation results showed limited 'nonlocal' combustion occurring in grid cells above the fuel bed for grassfires. In the test simulations, the mixture fraction of the reacting gases in the pocket model was never sufficiently high to yield carbon solid as an equilibrium product. Carbon solid had been thought of as a potential soot-precursor species for use in future development of a soot production model. However, it could still be possible to correlate soot production with mixture fraction if there is motivation to develop a soot production model in FIRETEC.

For grassfire simulations, the fire spread rates from the mixture-fraction-based pocket model were between 25-100% higher than the fire spread rates from previous FIRETEC models. This was true for the results of both the constant radius pocket model and the transported, variable radius pocket model. Based on the similarity of the results of the constant radius pocket model and the variable radius pocket model there was no distinct advantage to using the more complex variable radius pocket model instead of the constant radius pocket model. Regardless of which pocket model approach is used in future work, fine-tuning of pocket model parameters and other FIRETEC parameters would be required to achieve more accurate results using the mixture-fraction-based thermodynamic equilibrium pocket model. Also, a more accurate method for choosing T_o and estimating the initial enthalpy of the reacting mixture would hopefully improve the calculation of equilibrium flame temperatures in the pocket model, and thereby improve the accuracy of the modeled fire spread rates.

7.1 Limitations

The implementation of the new gas-phase combustion model into FIRETEC was complicated due to constraints on grid resolution. Whereas most contemporary combustion CFD modeling techniques resolve flame sheets at cm to mm scales, the FIRETEC grid resolution was on the order of one meter. In order to implement modeling concepts from the mixture fraction PDF approach, it was necessary to conceive and develop a sub-grid model. Furthermore, the implementation was complicated by the existing formulation of the energy equation in FIRETEC. Consistent with conventions of atmospheric science, the energy equation was cast in terms of potential temperature. This precluded a thermodynamically consistent method for calculating the total gas enthalpy. To do so would require modeling the transport of all important chemical species, a task that would defeat the purpose of implementing a computationally efficient equilibrium model. For this reason, some assumptions were made in order to estimate the enthalpy of mixture reactants in the gas phase and the heat of reaction produced by combustion of the reactants.

The primary objective of this dissertation research was to develop and implement a thermodynamic equilibrium model into FIRETEC. This objective was only achieved through the conception of a sub-grid pocket model. The feasibility of this approach was demonstrated by a series of model simulations which covered a range of fuel types, and ambient wind conditions. A significant amount of effort was required to find pocket model parameters which yielded reasonable spread rates for the constant radius sub-grid pocket model. Though a set of parameters was found to yield reasonable spread rates, optimization or tuning of these pocket model parameters and other FIRETEC parameters

was not done. Considering the enormous computational cost of each simulation, the quantity of data produced from each simulation (which must be analyzed), and the number of parameters subject to variation in the model, it is left to future work for any such optimization and tuning to be conducted. Furthermore, another suggested area of improvement may eliminate the need for tuning of pocket model parameters. Modifying the HIGRAD/FIRETEC model to solve the energy equation in terms of total enthalpy would likely lead to a more accurate method of estimating the enthalpy of the reactant mixture, and improve the prediction of local flame temperatures. Rather than expend the effort to optimize a variety of pocket model parameters, it would perhaps be more advantageous to explore this option in the future.

7.2 Recommendations

Based on the challenges encountered in this dissertation research, a few recommendations are provided for future development on FIRETEC. First, it is strongly recommended that the energy equation be recast in terms of enthalpy rather than potential temperature. Enthalpy is the thermodynamic quantity that is common across the fields of chemistry and transport phenomena. Potential temperature may have advantages in solving momentum and energy transport equations in the field of atmospheric science; however, it limited the application of the thermodynamic equilibrium model in this work. If the energy equation were to be cast in terms of enthalpy, there would likely be a more convenient and thermodynamically consistent approach to calculate the enthalpy of the reactant mixture without assuming a near-flame initial temperature (as was assumed in this work). Also, the thermodynamic equilibrium approach could possibly be

implemented without the type of sub-grid pocket modeling approach used in this work. This would hopefully lead to more accurate predictions of local flame temperatures without the need for extensive tuning of the model.

It is astounding to observe the phenomenal growth in computational power that has become available to the scientific community. This computational power has provided scientists the opportunity to develop a huge variety of numerical models, including wildfire computational fluid dynamics models. Notwithstanding the remarkable computing power available today, there are still computational limits to landscape-scale wildfire CFD models. Limited grid resolution requires creative methods for modeling sub-grid physics and prohibits the application of complex kinetic mechanisms.

A more glaring limitation is the deficiency of field-scale experimental data for model comparison and evaluation. There is a great need in the wildfire computational fluid dynamics community to establish an approach to validation of these complex computational models. The gap must be bridged between the limited availability of measured data in the field and the massive amount of simulated data generated by three-dimensional computational fluid dynamics models. Until then, computing power will grow, and computational models will become more refined, but the question of model validation remains open. However, the key benefit of wildfire CFD models, such as FIRETEC, must be emphasized: these simulation tools allow one to investigate the dynamics of combustion and transport phenomena in ways that would be far too costly to study by conducting large-scale experiments. Thus, development and improvement of wildfire CFD models is of value to the scientific community. In this spirit it is hoped that the development of the gas-phase wildfire combustion model in this dissertation research

has generated new avenues and ideas for future improvement of wildfire CFD simulation tools.

8 References

"PCGC-3: Pulverized Coal Gasification and Combustion - 3D," Provo, UT, Advanced Combustion Engineering Research Center, Brigham Young University (1999).

"BehavePlus," USDA Forest Service (2004).

"Fiscal Year 2007 President's Budget Overview," United States Department of Agriculture Forest Service**:** 66 (2006a).

"FARSITE," USDA Forest Service (2006b).

Andrews, P. L., "BEHAVE: fire behavior prediction and fuel modeling system- BURN subsystem, Part 1," USDA Forest Service**:** 130 (1986).

Andrews, P. L. and C. D. Bevins, "BehavePlus fire modeling system, version 2.0: overview," Proceedings of the Second International Wildland Fire Ecology and Fire Management Congress and Fifth Symposium on Fire and Forest Meteorology, Orlando, FL, American Meteorological Society(2003).

Andrews, P. L., C. D. Bevins and R. C. Seli, "BehavePlus fire modeling system, version 2.0: User's Guide," Ogden, UT, USDA Forest Service, Rocky Mountain Research Station**:** 132 (2003).

Bernard, P. S. and J. M. Wallace, Turbulent Flow: Analysis, Measurement, and Prediction, Hoboken, New Jersey, John Wiley & Sons, Inc. (2002).

Bilger, R. W., "Conditional moment closure for turbulent reacting flow," *Physics of fluids. A, Fluid dynamics,* **5**(2), 436-44 (1993).

Butler, B. W., J. M. Forthofer, R. D. Stratton, M. A. Finney and L. S. Bradshaw, "Fire growth simulations of the Price Canyon, Thritymile and Storm King Mountain fires using high resolution wind simulation tools and FARSITE," Sixth Symposium on Fire and Forest Meteorology and the 19th Interior West Fire Council Meeting, Canmore, Alberta, Canada, American Meterological Society(2005).

Cheney, N. P. and J. S. Gould, "Fire growth in grasslands fuels," *The International journal of wildland fire,* **5**(4), 237-247 (1995).

Cheney, N. P., J. S. Gould and W. R. Catchpole, "Prediction of Fire Spread in Grasslands," *International Journal of Wildland Fire,* **8**(1), 1-13 (1998).

Clark, M. M., T. H. Fletcher and R. R. Linn, "A Sub-Grid, Mixture-Fraction-Based Thermodynamic Equilibrium Model for Gas Phase Combustion in FIRETEC: Development and Results," *International Journal of Wildland Fire,* (2007 submitted).

Clark, T. L., J. Coen and D. Latham, "Description of a coupled atmosphere-fire model," *International Journal of Wildland Fire,* **13**(1), 49-63 (2004).

Colman, J. J. and R. R. Linn, "Separating combustion from pyrolysis in HIGRAD/FIRETEC," Sixth Symposium on Fire and Forest Meteorology and the 19th Interior West Fire Council Meeting, Canmore, Alberta, Canada, American Meterological Society(2005).

Colman, J. J. and R. R. Linn, "Separating combustion from pyrolysis in HIGRAD/FIRETEC," *International Journal of Wildland Fire,* **16**(4), 493-502 (2007).

Cunningham, P. and R. R. Linn, "Numerical simulations of grass fires using a coupled atmosphere-fire model: Dynamics of fire spread," *Journal of Geophysical Research,* **112** (2007).

Ertesvag, I. S. and B. F. Magnussen, "The eddy dissipation turbulence energy cascade model," *Combustion science and technology,* **159**, 213-235 (2000).

Finney, M. A., "FARSITE: Fire area simulator--model development and evaluation," United States Department of Agriculture, Forest Service, Rocky Mountain Research Station**:** 1-47 (1998).

Glickman, T. S., "Glossary of Meteorology," American Meteorological Society (2000).

Gordon, S. and B. J. McBride, "Computer Program for Calculation of Complex Chemical Equilibrium Compositions and Applications: I: Analysis," Cleveland, OH, National Aeronautics and Space Administration**:** 58 (1994).

Hajaligol, M. R., J. B. Howard, J. P. Longwell and W. A. Peters, "Product compositions and kinetics for rapid pyrolysis of cellulose," *Industrial and engineering chemistry process design and development,* **21**(3), 457-465 (1982).

Incorpera, F. P. and D. P. DeWitt, Fundamentals of Heat and Mass Transfer, John Wiley and Sons (1985).

Janicka, J., A. Sadiki and B. Naud, "Large eddy simulation of turbulent combustion systems," *Proceedings of the Combustion Institute,* **30**(1), 537-547 (2005).

Klimenko, A. Y., "Multicomponent diffusion of various admixtures in turbulent flow," *Fluid dynamics,* **25**(3), 327-334 (1990).

Larini, M., F. Giroud, B. Porterie and J. C. Loraud, "A multiphase formulation for fire propagation in heterogeneous combustible media," *International Journal of Heat and Mass Transfer,* **41**(6-7), 881-897 (1998).

Linn, R., J. Winterkamp, C. Efminster, J. Colman and M. Steinzig, "Modeling interactions between fire and atmosphere in discrete element fuel beds,"(2003).

Linn, R. R., "A transport model for prediction of wildfire behavior," Ph. D., Department of Mechanical Engineering, New Mexico State University (1997).

Linn, R. R. and F. H. Harlow, "Mixing-limited transport model used for description of wildfires," Proceedings of the 1998 ASME/JSME Joint Pressure Vessels and Piping Conference, Jul 26-30 1998, San Diego, CA, USA, ASME, Fairfield, NJ, USA(1998).

Linn, R. R. and P. Cunningham, "Numerical simulations of grass fires using a coupled atmospheric-fire model: Basic fire behavior and dependence on wind speed," *Journal of Geophysical Research,* **110** (2005).

Linn, R. R., J. Winterkamp, J. Colman, C. Edminster and J. D. Bailey, "Modeling interactions between fire and atmosphere in discrete element fuel beds," *International Journal of Wildland Fire,* **14**, 37-48 (2005).

Magnussen, B. F. and B. H. Hjertager, "On Mathematical Modeling of Turbulent Combustion With Special Emphasis on Soot Formation and Combustion," *Symp (Int) on Combust, 16th, MIT, Aug 15-20 1976*, 719-729 (1976).

Magnussen, B. F., "The Eddy Dissipation Concept," 11th Task Leaders Meeting, IEA Working Party on Energy Conservation in Combustion, Orenas, Glumslov, Sweden(1989).

Mardini, J. A. and A. S. Lavine, "Heat and mass transfer in green wood during fires," Proceedings of the 1995 ASME International Mechanical Engineering Congress and Exposition. Part 2 (of 2), Nov 12-17 1995, San Francisco, CA, USA, ASME, New York, NY, USA(1995).

Mardini, J. A., A. S. Lavine and V. K. Dhir, "Heat and mass transfer in wooden dowels during a simulated fire: an experimental and analytical study," *International Journal of Heat and Mass Transfer,* **39**(13), 2641-2651 (1996).

McBride, B. J. and S. Gordon, "Computer Program for Calculation of Complex Chemical Equilibrium Compositions and Applications: II. Users Manual and Program Description," Cleveland, OH, National Aeronautics and Space Administration**:** 178 (1996).

McGrattan, K., "Fire Dynamics Simulator (Version 4) Technical Reference Guide," K. McGrattan, Washington D.C., National Institute of Standards and Technology**:** 94 (2005).

Mell, W., J. J. Charney, M. A. Jenkins, P. Cheney and J. Gould, "Numerical simulations of grassland fire behavior from the LANL - FIRETEC and NIST -WFDS models," EastFIRE Conference, George Mason University, Fairfax, VA(2005).

Mell, W., M. A. Jenkins, J. Gould and P. Cheney, "A physics-based approach to modelling grassland fires," *International Journal of Wildland Fire,* **16**(1), 1-22 (2007).

Mizobuchi, Y., J. Shinjo, S. Ogawa, T. Takeno, F. A. Williams, H. Pitsch, N. Peters and K. Luo, "A numerical study on the formation of diffusion flame islands in a turbulent hydrogen jet lifted flame," *Proceedings of the Combustion Institute,* **30**(1), 611-619 (2005).

Morvan, D. and J. L. Dupuy, "Modeling of fire spread through a forest fuel bed using a multiphase formulation," *Combustion and Flame,* **127**(1-2), 1981-1994 (2001).

Morvan, D. and J. L. Dupuy, "Modeling the propagation of a wildfire through a Mediterranean shrub using a multiphase formulation," *Combustion and Flame,* **138**(3), 199-210 (2004).

Nunn, T. R., J. B. Howard, J. P. Longwell and W. A. Peters, "Product compositions and kinetics in the rapid pyrolysis of milled wood lignin," *Industrial & engineering chemistry process design and development,* **24**(3), 844-852 (1985).

Pickett, B., Provo, UT, Brigham Young University (2007).

Pitsch, H., "LARGE-EDDY SIMULATION OF TURBULENT COMBUSTION," *Annual Review of Fluid Mechanics,* **38**(1), 453-482 (2006).

Pope, S. B., "Monte Carlo Method for the PDF Equations of Turbulent Reactive Flow," *Combustion Science and Technology,* **25**(5-6), 159-174 (1981).

Pope, S. B., "PDF Methods for Turbulent Reactive Flows," *Progress in Energy and Combustion Science,* **11**(2), 119-192 (1985).

Reisner, J., S. Wynne, L. Margolin and R. Linn, "Coupled Atmospheric-Fire Modeling Employing the Method of Averages," *Monthly Weather Review,* **128**(10), 3683-3691 (2000).

Rothermel, R. C., "A mathematical model for predicting fire spread in wildland fuels," Ogden, Utah, Intermountain Forest and Range Experiment Station, Forest Service, U.S. Department of Agriculture**:** 40 (1972).

Smagorinsky, J., "General circulation experiments with the primative equations," *Monthly Weather Review,* **91**(3), 99-164 (1963).

Smith, N. S. A., R. W. Bilger and J. Y. Chen, "Modelling of nonpremixed hydrogen jet flames using a conditional moment closure method," *Symposium (International) on Combustion*, 263-269 (1992).

Smith, W. S., R. R. Linn, J. Sauer, J. Canfield and J. Winterkamp, "HIGRAD/FIRETEC Wildfire Model: Description of Basic Model Theory and Numerics," Los Alamos, NM, Los Alamos National Laboratory (2007). unpublished report (contact Rodman R. Linn).

Smoot, L. D. and P. J. Smith, Coal combustion and gasification, New York, Plenum Press (1985).

Spalding, D. B., "Mixing and Chemical Reaction in Steady Confined Turbulent Flames," 13th Symposium on Combustion, Pittsburgh, PA, The Combustion Institute(1971).

Stocks, B. J., M. E. Alexander, B. M. Wooton, C. N. Stefner, M. D. Flannigan, S. W. Taylor, N. Lavoie, J. A. Mason, G. R. Hartley, M. E. Maffey, G. N. Dalrymple, T. W. Blake, M. G. Cruz and R. A. Lanoville, "Crown fire behaviour in a northern jack pine - black spruce forest," *Canadian Journal of Forest Research,* **34**, 1548-1560 (2004).

Turns, S. R., An Introduction to Combustion: Concepts and Applications, McGraw-Hill (2000).

Vaz, G. C., J. C. S. Andre and D. X. Viegas, "Fire spread model for a linear front in a horizontal solid porous fuel bed in still air," *Combustion Science and Technology,* **176**(2), 135-182 (2004).

Viegas, D. X., "A mathematical model for forest fires blowup," *Combustion Science and Technology,* **177**(1), 27-51 (2005).

Weise, D. R., T. H. Fletcher, S. Smith, S. Mahalingam, X. Zhou and L. Sun, "Correlation of mass loss rate and flame height for live fuels," Sixth Symposium on Fire and Forest Meteorology and the 19th Interior West Fire Council Meeting, Canmore, Alberta, Canada, American Meterological Society(2005).

Westbrook, C. K., Y. Mizobuchi, T. J. Poinsot, P. J. Smith and J. Warnatz, "Computational combustion," *Proceedings of the Combustion Institute,* **30**(1), 125-157 (2005).

White, F. M., Viscous fluid flow, New York, McGraw-Hill (2006).

Zhou, X. and S. Mahalingam, "Evaluation of reduced mechanism for modeling combustion of pyrolysis gas in wildland fire," *Combustion Science and Technology,* **171**(1), 39-70 (2001).

Zhou, X., S. Mahalingam and D. Weise, "Modeling of marginal burning state of fire spread in live chaparral shrub fuel bed," *Combustion and Flame,* **143**(3), 183-198 (2005a).

Zhou, X., D. Weise and S. Mahalingam, "Experimental measurements and numerical modeling of marginal burning in live chaparral fuel beds," *Proceedings of the Combustion Institute,* **30**(2), 2287-2294 (2005b).

Zhou, X. Y. and J. C. F. Pereira, "Multidimensional model for simulating vegetation fire spread using a porous media sub-model," *Fire and Materials,* **24**(1), 37-43 (2000).

Appendix A

Computer code was written in the Fortran programming language for this dissertation work. All relevant subroutines (or portions thereof) developed for this dissertation are included in this appendix.

From compress.f:

```
! mmc 9/2006 Read in mftable, a table of stored thermo-chemical
! equilibrium solutions
      if (isubgridgas==1) then
        open
(unit=155,file='cea2mftable',status='old',form='unformatted',action='re
ad')
        read (155) fsize
        if (mpi_rank==0) print*,'fsize=',fsize
        read (155) hsize
        if (mpi_rank==0) print*,'hsize=',hsize
        read (155) hmax
        if (mpi_rank==0) print*,'hmax=',hmax
        read (155) zdim
        if (mpi_rank==0) print*,'zdim=',zdim
        read (155) num_species
        if (mpi_rank==0) print*,'num_species=',num_species
```

```
        allocate (ceaproducts(num_species))
        read (155) (ceaproducts(i),i=1,num_species)
        if (mpi_rank==0) print*,'Product species=
',(ceaproducts(i),i=1,num_species)
        if (mpi_rank==0) print*,'CHI=',chi
        read (155) charscratch
!        read (155) priHSUB0
!        read (155) secHSUB0
!        if (mpi_rank==0) print*,'secHSUB0=',secHSUB0
        allocate (mftable((-hsize)/2:hsize/2,0:fsize,zdim))
        do i=(-hsize)/2,hsize/2
          do j=0,fsize
            read(155) (mftable(i,j,k),k=1,zdim)
          end do
        end do
        close(155)
      end if
```

From fuelnonlocal.f

```
! Mixture fraction model
!
         elseif (isubgridgas==1.and.k<10) then
           allocate (equil_sols(num_species+1))
           if (ivarr==1) then
             rpocket(i,j,k)=xv(i,j,k,11)/xv(i,j,k,8)
             rpkt=rpocket(i,j,k)
             lf=.70*rpkt
             chi = (3.*rpkt**2 - 3.*rpkt*lf + lf**2) /   &
     & ((3.+3.*af)*rpkt**2 + (3.*af*af*lf-3.*lf)*rpkt    &
     & +(1.+af**3)*lf**2)
           end if

           rhohc = xv(i,j,k,8)
           rho_hc_r(i,j,k) = chi*rhohc*( (3.*lf+3.*af*lf)*rpkt**2  &
  &              + (3.*af*af*lf*lf-3.*lf*lf)*rpkt + (1.+af**3)*lf**3 )&
  &              / (rpkt**3)
           rho_air_r(i,j,k) = (1.-chi)*rhohc*( (3.*lf+3.*af*lf)*rpkt**2
&
  &              + (3.*af*af*lf*lf-3.*lf*lf)*rpkt + (1.+af**3)*lf**3 )&
  &              / (rpkt**3)
           mf_air = (xv(i,j,k,9)-mfhc*rhohc)/(xv(i,j,k,nv)-rhohc)

           mfmix = (mfhc*rho_hc_r(i,j,k)+mf_air*rho_air_r(i,j,k))  &
  &                / (rho_hc_r(i,j,k)+rho_air_r(i,j,k))
           mfmix_save(i,j,k)=mfmix !MMC 11/17/06 for
debugging/evaluation only
           gastemp = xv(i,j,k,4)/xv(i,j,k,nv)*(pr(i,j,k)*1.0e-
5)**(rg/cp)
           temp_save(i,j,k)=gastemp !MMC 11/17/06 for
debugging/evaluation only
           hr=0.0
           hr_save(i,j,k)=hr     11/17/06 for debugging/evaluation only

           call equilinterp (mfmix,hr,equil_sols)
           do ii=1,num_species
```

```
              combustionproducts(ii,i,j,k)=equil_sols(ii+1)
            end do
            deltatemp(i,j,k)=equil_sols(1)-gastemp
            tflame_save(i,j,k)=equil_sols(1) !MMC 11/17/06 for
debugging/evaluation only
            deltah(i,j,k)=cp*deltatemp(i,j,k)
            if (deltatemp(i,j,k)<0.) thetasolid(i,j,k)=0.    !MMC 2/1/07
Avoid pulling energy out of solid phase during occasional endothermic
gas phase reactions
            fg(i,j,k)=(rho_hc_r(i,j,k)+rho_air_r(i,j,k))/dtp
            sootfracprod(i,j,k)=equil_sols(num_species+1)          &
                                +equil_sols(num_species)           &
                                +equil_sols(num_species-1)
!MMC 1/23/07 C(s) is output by CEA2 in three segments... I think
! by temperature range (perhaps due to crystal states or something????)
!            if(k==2.and.xv(i,j,k,8)>1.E-12) print*,'hc=',xv(i,j,k,8)
            deallocate (equil_sols)
          end if !end of isubgridgas if-construct
```

From convection.f:

```
                  if (isubgridgas==1) then
                reactht=(thetasolid(i,j,k)*ff(i,j,k)*dtp/xvb(i,j,k,8))
     &                     *deltah(i,j,k)*fg(i,j,k)+hfsolid*ff(i,j,k)
                  else
```

From subgridgas.f90:

```
module subgridgas
  implicit none
  save
  integer :: hsize,fsize,zdim,num_species
  character(len=15),allocatable,dimension(:) :: ceaproducts
  character(len=1) :: charscratch
  real(kind=selected_real_kind(4)),allocatable,dimension(:,:,:) ::
mftable
  real(kind=selected_real_kind(8)) :: hmax
  real,parameter :: rpkt1=0.01    ! radius of a combustible gas pocket
  real :: rpkt=rpkt1
  real :: lf=.67369*rpkt1
  real,parameter :: lf1=.67369*rpkt1     ! flame thickness parameter
  real,parameter :: af=2.5        ! multiplication factor for lf
  real :: chi = (3.*rpkt1**2 - 3.*rpkt1*lf1 + lf1**2) / &
 & ((3.+3.*af)*rpkt1**2 + (3.*af*af*lf1-3.*lf1)*rpkt1   &
 & +(1.+af**3)*lf1**2)
  real,parameter :: mfhc=1.
  real :: rinitial=0.1
  real,allocatable,dimension(:,:,:) :: deltatemp,deltah
  real,allocatable,dimension(:,:,:) :: rho_hc_r,rho_air_r
  real,allocatable,dimension(:,:,:) :: fmf,fmfb,fsoot,fsootb
  real,allocatable,dimension(:,:,:) :: frpocket,frpocketb
 !arrays used for global storage, for debugging/evaluation purposes
  real,allocatable,dimension(:,:,:) :: tflame_save,mfmix_save
  real,allocatable,dimension(:,:,:) :: temp_save,hr_save
  !mass fraction of soot produced in a time step
  real,allocatable,dimension(:,:,:) :: sootfracprod
  real,allocatable,dimension(:,:,:,:) :: combustionproducts
  real,allocatable,dimension(:,:,:) :: rpocket
  real :: priHSUB0,secHSUB0

  contains
```

```
! subroutine equilinterp    mmc 9/14/06
!
! Equilinterp is a subroutine that does 4-point interpolation
! on a stored table of thermodynamic equilibrium solutions to
! return values of T and yi for a given mixture fraction (mfmix)
! and residual enthalpy (hr)
!
! from pcgc3 code: mftable--the array of stored therm. equil. solutions
! stored as: mftable(hr,mf,(phi,rho,cpsum,rgas,MW,T,or y(i)))
!   **check tablesetup.f to verify the storage arrangement
!     of mftable!!**
! from cea2 code: cea2mftable
! stored as mftable(hr,mf,T,Y(i),i=1,num_species)
!   **check cea2firetecpreprocess.f90 to verify the storage
!     arrangement of mftable!!**
! hr-------the residual enthalpy of reacting material (J/kg)
! fsize----number of elements of mftable in second dimension
! hsize----number of elements of mftable in first dimension
! zdim-----number of elements of mftable in third dimension, where
! phi,rho,cpsum,rgas,MW,T,y(i) are stored for each (hr,mf)
! num_species--number of species considered in the system for which
!        y(i) is calculated and stored in mftable
! hmax---------maximum value of hr in mftable, cannot interpolate
!              above hmax, or below -hmax
! Arguments are:
!  mfmix----the mixture fraction of reacting material
!  equil_sols----------1 dimensional array to store interpolated
!                      values of T & y(i) to pass back to the
!                      calling program unit
!
  subroutine equilinterp(mfmix,hr,equil_sols)
  implicit none

  real,intent(inout) :: mfmix,hr
  real, dimension(num_species+1), intent(out) :: equil_sols
  real :: hrlow,hrhigh,hr_frac,mflow
  real :: mfhigh,mf_frac,interpy1,interpy2
  integer :: jlow,jhigh,ilow,ihigh
```

```
  integer :: i,imax

  imax=size(equil_sols,1)
  jlow=int(fsize*mfmix)
  jhigh=jlow+1
  if (hr>0.) then
    ilow=int(hr*real(hsize/2)/hmax)
    ihigh=ilow+1
  else
    ihigh=int(hr*real(hsize/2)/hmax)
    ilow=ihigh-1
  end if

! Below is the interpolation scheme. To prevent array over-runs at the
! edges of mftable, special cases are handled if:
!       mfmix == 1 and hr ==  hmax
!   or  mfmix == 1 and hr == -hmax
!   or  mfmix == 1 and -hmax < hr < hmax
!   or  0 <= mfmix < 1 and hr ==  hmax
!   or  0 <= mfmix < 1 and hr == -hmax
!
!   else
!       0 <= mfmix < 1 and -hmax < hr < hmax
!
!   A simple 4-point interpolation is done, where
!    (x,y) lies inside (x1,y1) (x1,y2) (x2,y1) (x2,y2).
!
!   The interpolated solutions are stored in equil_sols(i)
  if (jlow==fsize) then
    if (ilow==hsize/2) then
      do i=1,imax
        equil_sols(i)=mftable(ilow,jlow,i+2)
      end do
    elseif (ilow<(-hsize)/2) then
      do i=1,imax
        equil_sols(i)=mftable(ihigh,jlow,i+2)
      end do
    else
```

```
      do i=1,imax
        hrlow=mftable(ilow,1,1)
        hrhigh=mftable(ihigh,1,1)
        hr_frac=(hr-hrlow)/(hrhigh-hrlow)
        interpy1=mftable(ilow,jlow,i+2)
        interpy2=mftable(ihigh,jlow,i+2)
        equil_sols(i)=hr_frac*(interpy2-interpy1)+interpy1
      end do
    end if
  else
    if (ilow==hsize/2) then
      do i=1,imax
        mflow=mftable(1,jlow,2)
        mfhigh=mftable(1,jhigh,2)
        mf_frac=(mfmix-mflow)/(mfhigh-mflow)
        equil_sols(i)=mf_frac                    &
&            *(mftable(ilow,jhigh,i+2)           &
&            -mftable(ilow,jlow,i+2))            &
&            +mftable(ilow,jlow,i+2)
      end do
    elseif (ilow<(-hsize)/2) then
      do i=1,imax
        mflow=mftable(1,jlow,2)
        mfhigh=mftable(1,jhigh,2)
        mf_frac=(mfmix-mflow)/(mfhigh-mflow)
        equil_sols(i)=mf_frac                     &
&             *(mftable(ihigh,jhigh,i+2)          &
&             -mftable(ihigh,jlow,i+2))           &
&             +mftable(ihigh,jlow,i+2)
      end do
    else
      do i=1,imax
        mflow=mftable(1,jlow,2)
        mfhigh=mftable(1,jhigh,2)
        hrlow=mftable(ilow,1,1)
        hrhigh=mftable(ihigh,1,1)
        mf_frac=(mfmix-mflow)/(mfhigh-mflow)
        hr_frac=(hr-hrlow)/(hrhigh-hrlow)
```

```
        interpy1=mf_frac*(mftable(ilow,jhigh,i+2)   &
 &                -mftable(ilow,jlow,i+2))           &
 &                +mftable(ilow,jlow,i+2)
        interpy2=mf_frac*(mftable(ihigh,jhigh,i+2)  &
 &                -mftable(ihigh,jlow,i+2))          &
 &                +mftable(ihigh,jlow,i+2)
        equil_sols(i)=hr_frac*(interpy2-interpy1)+interpy1
      end do
    end if
  end if
  return
  end subroutine equilinterp
end module subgridgas
```

The thermodynamic equilibrium table used for this dissertation research was generated using the NASA Chemical Equilibrium with Applications computer program. This program was adapted to generate a series of equilibrium solutions for mixture fractions between 0 and 1, at intervals of 0.01.

The Chemical Equilibrium with Applications code can be downloaded from: http://www.grc.nasa.gov/WWW/CEAWeb/.